



UNIVERSITÀ POLITECNICA DELLE MARCHE

FACOLTÀ DI INGEGNERIA

Corso di Laurea Magistrale in Biomedical Engineering

**Development of a Procedure for
Sound Quality Evaluation based on
Electroencephalography and
Assessment Analysis**

Relatore:

Prof.ssa Milena Martarelli

Tesi di Laurea di:

Alessandro Bini

Correlatore:

Prof. Gianmarco Battista

A.A. 2022/2023

ABSTRACT

The evaluation of sound quality is certainly one of the topics of major scientific research in recent years. In particular, trying to obtain a classification for certain types of sounds or environments based on the study of brain waves can guide and, at the same time, help companies in the development of particular components so as to reduce as much as possible sounds that can be annoying, stressful, and in some cases even harmful to human beings. The development of sound quality should be integrated into the overall design process, with test methods serving as a vital component of the decision-making process to ensure product suitability [1]. One of the big challenges in the XXI century, as an essential part of human brain analysis procedures, is the determination of mathematical models capable to explain and forecast the relationships between human activities and electroencephalography (EEG) signals. EEG signals produce data organized in temporal sequences with a structured behaviour and have been used for different purposes, from seizure detection and epilepsy diagnosis, to automatic detection of abnormal EEG, and recognition of Alzheimer's disease brain activity, the detection of awareness, or the use of brain-computer interfaces (BCI) [28]. This thesis aims to carry out in parallel two pre-processing methods for the automatic removal of bad channels and portions of the signal with many artifacts, including the data filtering part as well, to finally try to figure out with which of the two methods better results could be expected for the study of brain waves subjected to different types of sound stimuli. The first approach was to use EEGLAB, a toolbox that can be used in MATLAB, while the second approach was to use AUTOREJECT, a library to automatically reject bad trials and repair bad sensors in magneto-electroencephalography (M/EEG) data. Signals from 43 healthy volunteers (22 males and 21 females) were acquired for the experiment using a commercially available wearable device: the Interaxon MUSE headband. The data acquisition process involved utilizing the MUSE application, which was paired with a smartphone via Bluetooth Low Energy (BLE) technology. After applying the 2 approaches and filtering the raw data, the data were processed by calculating the various power spectra densities and then the outliers were removed. After that, an analysis on the normal distribution of the data and a parametric ANOVA statistical test were conducted. The results show that six of the forty-three subjects analysed with EEGLAB were discarded as not having enough data to

pursue this type of study. Differently, the AUTHOREJECT approach was able to retain all forty-three subjects. Regarding outliers removal, the two methods behaved almost the same with a 51.35 percent rejection rate. As far as Gaussianity analysis conducted with the Shapiro-Wilk Test is concerned, the two approaches also appear to be robust, with a slight advantage of the EEGLAB method (92.65%) over AUTOREJECT (85.22%). Even in the alpha frequency range this trend seems to be confirmed with EEGLAB (94.70%) surpassing the AUTOREJECT method (90.91%). The results of the ANOVA test show how data processed with the two approach for TP9-TP10 channels have a relatively high F-statistic, standing for a gap between the groups means (4.29 ± 1.17) while a decrease in F-statistic values can be observed in alpha frequency range (1.73 ± 0.47). Consistent results are also confirmed by the α values showing in the whole frequency range, for both EEGLAB and AUTOREJECT, similar behave, with p-values much less than 0.05 ($4.9e-3 \pm 7.6e-3$). An opposite trend as obtained for the F-statistic occurs for the alpha frequency range (0.16 ± 0.08). A better acoustic physiological response was obtained analysing the Relative Alpha Band Power with the AUTOREJECT (F-statistic = 2.95 ± 1.33 , $\pm = 0.042 \pm 0.056$) method and EEGLAB method (F-statistic = 1.62 ± 0.06 , $\pm = 0.16 \pm 0.02$).

In conclusion, despite the presence of some limiting factors such as data integrity, data quantity, device choice and others, is possible to say that due to the three analyses conducted in this thesis, the EEGLAB method and the AUTOREJECT method are very similar in terms of outliers removal and normality analysis of the data. While with regard to the ANOVA statistical test, nothing statistically significant could be stated in the characterization between one sound and another. Differently, we noticed how the AUTOREJECT method seems to perform better in the range of relative alpha power than the EEGLAB approach.

CONTENTS

1. INTRODUCTION	4
1.1. The Sound	4
1.1.1. Sound Quality.....	8
1.2. The Brain	10
1.2.1. Neurons.....	14
1.2.2. Auditory System.....	17
1.3. EEG Signal	21
1.3.1. History of EEG.....	25
1.3.2. EEG Devices.....	26
1.3.3. EEG Patterns.....	29
1.3.4. Time-Frequency Analysis.....	32
2. MATERIALS AND METHODS	36
2.1. Experimental Setup	36
2.1.1. Participants.....	36
2.1.2. EEG Measurement Device.....	36
2.1.3. Data Collection.....	38
2.2. Data Pre-Processing	40
2.2.1. EEGLAB.....	41
2.2.2. AUTOREJECT.....	47
2.3. Data Processing	50
2.4. Statistical Analysis	53
3. RESULTS	59
3.1. Outliers Removal	59
3.2. Gaussian Data Analysis	69
3.2.1. All Frequency Band.....	69
3.2.2. Alpha Frequency Band.....	73
3.3. Statistical Test: One-Way ANOVA	77
3.3.1. All Frequency Band.....	78
3.3.2. Alpha Frequency Band.....	81
3.3.3. Relative Alpha Frequency Band.....	85
4. CONCLUSIONS AND FUTURE DEVELOPMENTS	90
FIGURE LIST	95
TABLE LIST	99
BIBLIOGRAPHY	100
APPENDIX 1	104

1. INTRODUCTION

The evaluation of sound quality is certainly one of the topics of major scientific research in recent years. In particular, trying to obtain a classification for certain types of sounds or environments based on the study of brain waves can guide and, at the same time, help companies in the development of particular components so as to reduce as much as possible sounds that can be annoying, stressful, and in some cases even harmful to human beings.

In general, most definitions of sound quality encompass the notion of how well a product's sound aligns with the user's expectations and preferences. Within industries such as automotive and audio, sound quality testing holds significant importance as a design concept. Marketing studies in these fields have shown a correlation between sound and non-auditory factors like luxury, power, speed, safety, and expense, underscoring the significance of sound as a crucial design consideration. The development of sound quality should be integrated into the overall design process, with test methods serving as a vital component of the decision-making process to ensure product suitability [1].

That is why we decided to conduct this study, which allows us to investigate and classify a given subject's physiological reaction, specifically the brain's EEG waves, in response to acoustic stimuli so that we can evaluate and understand which brain wave characteristics are associated with pleasant sounds or, conversely, annoying sounds.

1.1. The Sound

In physics, sound is a vibration that propagates as an acoustic wave, through a transmission medium such as a gas, liquid or solid. In human physiology, sound is the reception of such waves and their perception by the brain [2].

To understand sound, it is crucial to examine the characteristics of sound waves. Sound waves can be categorized into two fundamental types: transverse and longitudinal, based on their propagation method. In a transverse wave, exemplified by a wave formed when one end of a stretched rope is moved back and forth, the motion composing the wave occurs perpendicular to the direction of wave movement along the rope. Electromagnetic sources like light or radio generate a significant group

of transverse waves, where the electric and magnetic fields oscillate at right angles to the direction of wave propagation. In contrast, sound travels through air or other media as a longitudinal wave, wherein the mechanical vibrations constituting the wave align with the direction of wave propagation. One can create a longitudinal wave in a coiled spring by compressing several turns together and then releasing them, allowing the compression to traverse the spring's length. Air can be likened to layers akin to these coils, with a sound wave propagating as layers of air compress and expand, much like the compression moving down the spring. Thus, a sound wave consists of alternating compressions and rarefactions, representing regions of high pressure and low pressure respectively, which move at a specific velocity. Alternatively, it can be described as a periodic variation of pressure, oscillating or vibrating around the equilibrium pressure prevailing at a particular time and location [3].

During the process of propagation, waves have the ability to undergo reflection, refraction, or attenuation when interacting with the medium they traverse. The behaviour of sound propagation is influenced by three key factors [4]:

- The density and pressure of the medium: the relationship between density and pressure, influenced by temperature, determines the speed of sound within the medium.
- Motion of the medium: if the medium is in motion, the absolute speed of the sound wave can be either increased or decreased depending on the direction of the medium's movement. If the sound and wind are moving in the same direction, the speed of sound propagation will be augmented by the wind speed. Conversely, if the sound and wind move in opposite directions, the speed of the sound wave will be reduced by the wind speed.
- The viscosity of the medium: viscosity of the medium affects the rate at which sound is attenuated. In many media like air or water, the impact of attenuation due to viscosity is negligible.

In situations where sound travels through a medium with varying physical properties, it may experience refraction, resulting in dispersion or focusing of the sound wave [4].

The variations in pressure within a sound wave exhibit a repeating pattern in space, which is characterized by a specific distance known as the wavelength of the sound, typically measured in meters and denoted as λ . As the wave travels through the air, it takes a certain time period, represented as T and measured in fractions of a second, for one complete wavelength to pass a given point in space. Furthermore, within each one-second interval, a specific number of wavelengths pass through that point. This quantity is referred to as the frequency of the sound wave, measured in hertz or kilohertz, and denoted as f . Figure 1 shows those types of parameters.

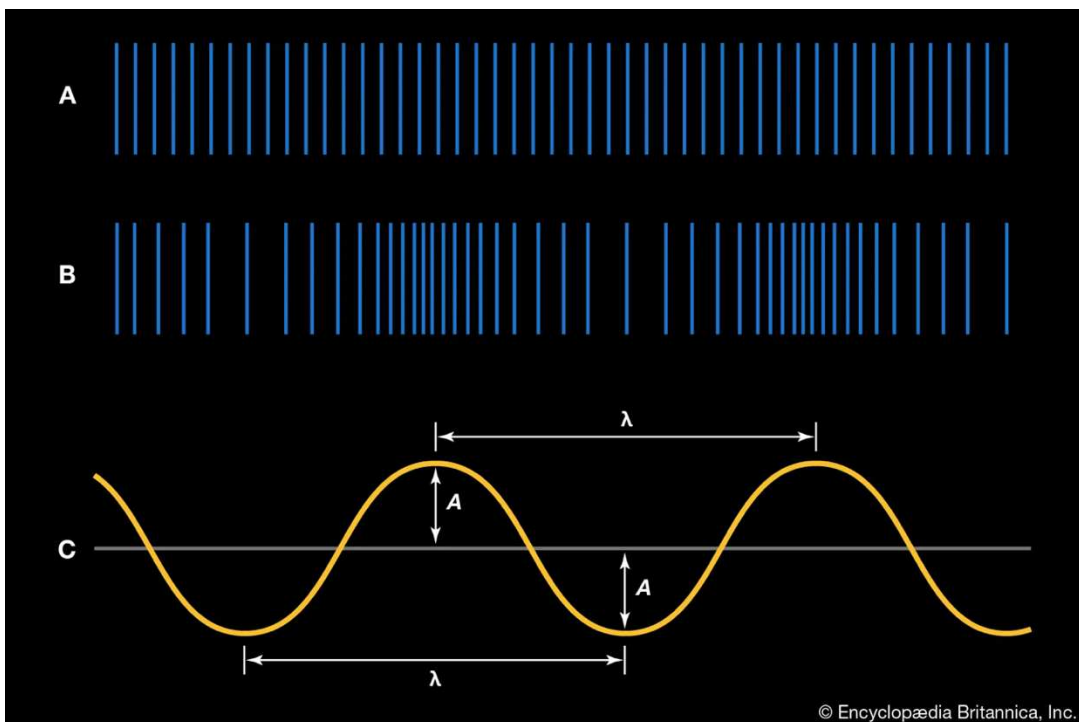


Figure 1: Graphic representations of a sound wave: (A) air at equilibrium, in the absence of a sound wave; (B) compressions and rarefactions that constitute a sound wave; and (C) transverse representation of the wave, showing amplitude (A) and wavelength (λ) [3].

There exists an inverse relationship between the frequency and period of a wave, as expressed by the following equation [3]:

$$f = \frac{1}{T} \quad (1.1)$$

This relationship implies that sound waves with higher frequencies exhibit shorter periods, while those with lower frequencies have longer periods. For instance, a sound wave with a frequency of 20 hertz would correspond to a period of 0.05 seconds (i.e., $20 \text{ wavelengths/second} \times 0.05 \text{ seconds/wavelength} = 1$), whereas a sound wave with a frequency of 20 kilohertz would have a period of 0.00005 seconds ($20,000 \text{ wavelengths/second} \times 0.00005 \text{ seconds/wavelength} = 1$). The range of frequencies between 20 hertz and 20 kilohertz encompasses the audible frequency range for human hearing. The physical property of frequency is perceptually associated with pitch, meaning that higher frequencies are perceived as higher pitches. Additionally, there exists a relationship between the wavelength, frequency or period, and the speed of a sound wave (c), as follows [3], [5]:

$$c = f\lambda = \frac{\lambda}{T} \quad (1.2)$$

The velocity of sound is influenced by the medium through which the waves propagate and is considered an essential characteristic of the material involved. The initial notable attempt to measure the speed of sound was conducted by Isaac Newton. Newton hypothesized that the speed of sound within a specific substance could be calculated by taking the square root of the pressure exerted on it and dividing it by the substance's density:

$$c = \sqrt{\frac{p}{\rho}} \quad (1.3)$$

Where c represents the sound velocity, p the pressure and ρ the density of the medium [5].

The ear mechanism possesses the capability to detect and respond to pressure waves of both small and high amplitudes due to its nonlinear nature. It exhibits higher sensitivity to sounds with small amplitudes compared to sounds with large amplitudes. Given the significant nonlinearity of the ear in perceiving pressure waves, it is convenient to utilize a nonlinear scale for describing the intensity of sound waves.

This scale is represented by the sound intensity level, also known as the decibel level, which is quantified by the equation [3]:

$$L = 10 \log \left(\frac{I}{I_0} \right) \quad (1.4)$$

In the given context, the variable L represents decibels, which serve as a measure for the intensity I of a sound wave expressed in watts per square meter. The reference intensity I_0 , corresponding to a level of 0 decibels, is approximately equivalent to the intensity of a 1,000 hertz frequency wave at the threshold of hearing, which is about 10^{-12} watt per square meter. A key characteristic of this logarithmic scale is that each increment on the decibel scale corresponds to a constant multiplicative factor in absolute intensity. Therefore, an increase in absolute intensity from 10^{-12} to 10^{-11} watt per square meter corresponds to a 10-decibel increase, just as an increase from 10^{-1} to 1 watt per square meter also corresponds to a 10-decibel increase [3].

1.1.1. Sound Quality

Sound perception is a key aspect in many industrial applications where the acoustic comfort of the final user is relevant [6]. The sound quality and its acoustic characteristics have an impact on the emotions that we sense in everyday life. In fact, sound is a fundamental element determining how people feel and react to circumstances [7]. When considering activities like driving a car, it becomes apparent that the overall quality of the driving experience is influenced by the sound of the engine as perceived by the driver [8]. This is just one factor contributing to why brands are now placing significant emphasis on sound as a key element in maximizing user experience and influencing behaviour. It is well recognized that sound has the ability to impact people's mood and even modify consumer behaviours [9]–[11].

Consequently, acoustic comfort holds paramount importance in various industrial applications, primarily driven by two distinct reasons. The first reason relates to acoustic pollution, as evidenced by studies conducted by the European Union. Noise has been identified as one of the most hazardous pollutants affecting public

health, leading to significant discomfort and an associated increase in cardiac issues [12]. Consequently, it becomes crucial to mitigate the annoyance and acoustic energy of environmental noise pollution. The second reason is important in the case of products that are purchased by private customers. Intuitively, a potential customer may discard a product not considered satisfying enough. This aspect leads engineers to specifically address the concept of product sound quality, recognizing its importance in meeting customer expectations [13]. In this context, the significance of acoustic comfort cannot be overstated, and it presents several challenges. Firstly, sound quality generally needs a detailed description of the acoustic problem. In engineering applications, this description can pose a significant challenge for designers due to the inherent complexity involved. Even without considering non-linearity, analytical descriptions may encounter insurmountable difficulties due to intricate geometries, boundaries, constraints, material properties, and inhomogeneity that are commonly encountered in engineering problems. To address these challenges, numerical methods are often employed as a means to overcome these complexities [6].

Extensive research has been conducted on sound quality, often utilizing psychoacoustic metrics such as loudness, sharpness, roughness, fluctuation strength, and tonality. Additionally, the articulation index (AI), which measures the extent to which background noise hinders human speech, is widely employed as a decisive parameter for evaluating sound quality, particularly in the automotive industry. In the development of sound quality models for specific products like vehicles and household appliances, studies commonly utilize one or multiple psychoacoustic metrics through methods such as multiple linear regression (MLR) or nonlinear approaches like artificial neural networks (ANN). With the increasing emphasis on user experience and the heightened quality expectations, household appliances now need to go beyond their fundamental functions.

Everyday objects such as handheld hairdryers can often generate undesirable high levels of noise, causing interference with communication, discomfort, and potential risks to hearing health [14].

As a result, classifying sounds and emotions based on experiential, physiological, and behavioural responses is a relevant field of study [7].

1.2. The Brain

The human brain is an extraordinary organ and complex structure composed of various regions, each with unique functions and interconnected networks. Understanding the intricate details of brain anatomy is crucial in comprehending the complexity of its functions. The vertebrate central nervous system (CNS) consists of the brain and the spinal cord. The first is in turn subdivided in three compartments: forebrain, midbrain, and hindbrain. Beyond these three basic sections, brain anatomy subdivides those in further compartments, with their specific structures and functions. Forebrain consists of the cerebrum and the diencephalon; the hindbrain consists of the cerebellum, the pons, and the medulla oblongata. The midbrain (or mesencephalon) has no further subdivisions. The term brainstem is referred to the posterior part of the brain, adjoining and structurally continuous with the spinal cord. In the human brain the brainstem includes the midbrain, the pons, and the medulla oblongata (sometimes also the diencephalon is included). The brain is encased within the cranium (or skull) and the spinal cord runs through a canal in the vertebral column. Nerves of the peripheral nervous system enter and leave the spinal cord by passing through notches between the stacked vertebrae. Three layers of membrane, collectively called meninges, lie between the bones and the tissues of the CNS. These membranes help stabilize the neural tissue and protect it from bruising against the bones of the skeleton. Starting from the bones and moving toward the neural tissue, the membranes are: the dura mater, the arachnoid membrane, and the pia mater. An adult human brain has a mass of about 1400 g and contains an estimated 10^{12} neurons. The brainstem, located at the base of the brain, acts as a bridge between the brain and the spinal cord. It is responsible for many essential functions that regulate our body, including breathing, heart rate, blood pressure, and basic survival reflexes like swallowing and coughing. The brainstem is divided into three regions: the medulla oblongata, pons, and midbrain. Each region has specific roles in relaying sensory and motor information, regulating sleep and wake cycles, and controlling autonomic functions [15], [16]:

- Medulla oblongata: frequently called just the medulla, is the transition from the spinal cord into the brain proper. Its white matter includes ascending somatosensory tracts that bring sensory information to the brain, and descending corticospinal tracts that convey information from the cerebrum to the spinal cord. About 90% of the corticospinal tracts cross the midline to the opposite side of the body in a region of the medulla known as the pyramids. This crossover is called decussation, so that each hemisphere of the brain controls the opposite side of the body.
- Pons: it is a bulbous protrusion on the ventral side of the brainstem above the medulla and below the midbrain. Because its primary function is to act as a relay station for information transfer between the cerebellum and the cerebrum, the pons is often grouped with the cerebellum. The pons also coordinates the control of breathing along with centers in the medulla.
- Midbrain: it is the third region of the brainstem, and is a relatively small area that lies between the lower brain stem and the diencephalon. The primary function of the midbrain is control of eye movement, but also relays signals for auditory and visual reflexes.

The cerebellum is the second largest structure in the brain. It is located inside the base of the skull, just above the nape of the neck. Most of the nerve cells in the brain are in the cerebellum. The cerebellum plays an important role in motor control, and it may also be involved in some cognitive functions such as attention and language as well as in regulating fear and pleasure responses. Its specialized function is to process sensory information and coordinate the execution of movement. In fact, the cerebellum does not initiate movement, but contributes to coordination, precision, and accurate timing, refining the response elaborated by the higher brain by integrating it with sensorial inputs, received from somatic receptors in the periphery of the body and from receptors for equilibrium and balance located in the inner ear. Cerebellar damage produces disorders in fine movement, equilibrium, posture, and motor learning in humans. Moving up from the brainstem, there are the structures of the forebrain, which is composed by the cerebrum and the diencephalon. The diencephalon is interposed between the brainstem and the cerebrum, and is composed of two main sections, the thalamus and the hypothalamus, and two endocrine

structures, the pituitary gland and pineal gland. Most of the diencephalon is occupied by many small nuclei that make up the thalamus, the major relay station of the brain: there, informations are conveyed from the optic tract, ears, and spinal cord as well as motor information from the cerebellum. It projects fibers to the cerebrum, where the information is processed. The thalamus is often described as a relay station because almost all sensory information from lower parts of the CNS passes through it. Like the spinal cord, the thalamus can modify information passing through it, making it an integrating center as well as a relay station. The hypothalamus lies beneath the thalamus. Although the hypothalamus occupies less than 1% of the total brain volume, it is the center for homeostasis and contains centers for various behavioural drives, such as hunger and thirst. Output from the hypothalamus also influences many functions of the autonomic division of the nervous system, as well as a variety of endocrine functions. The hypothalamus receives input from multiple sources, including the cerebrum, the reticular formation, and various sensory receptors. Output from the hypothalamus goes first to the thalamus and eventually to multiple effector pathways. Finally, there are the pituitary gland, subdivided in the posterior pituitary (neurohypophysis) and the anterior pituitary (adenohypophysis), and the pineal gland: these are concerned hormones and are involved in the endocrine system. The cerebrum is the largest and most distinctive part of the human brain and fills most of the cranial cavity. It is composed of two hemispheres connected primarily at the corpus callosum, a distinct structure lying upon the thalamus and formed by axons passing from one side of the brain to the other. This connection ensures that the two hemispheres communicate and cooperate each other. Each cerebral hemisphere is divided into four lobes, named for the bones of the skull under which they are located: frontal, parietal, temporal, and occipital. Each lobe has specific functions. For example, the frontal lobe is involved in decision-making, planning, and personality, while the parietal lobe processes sensory information and spatial awareness. The surface of the cerebrum has a furrowed, walnut-like appearance, with grooves called sulci dividing convolutions called gyri. During development, the cerebrum grows faster than the surrounding cranium, causing the tissue to fold back on itself to fit into a smaller volume. The degree of folding is directly related to the level of processing of which the brain is capable (less-advanced mammals, such as rodents, have brains with a relatively smooth surface). Grey matter of the cerebrum can be divided into

three major regions: the cerebral cortex, the basal ganglia, and the limbic system. The cerebral cortex is the outer layer of the cerebrum, only a few millimeters thick. The cerebral cortex is the place wherein the higher brain functions arise. The second region of cerebral grey matter consists of the basal ganglia (basal nuclei), which are involved in the control of movement. The third region of the cerebrum is the limbic system, which surrounds the brainstem. The limbic system represents probably the most primitive region of the cerebrum. It acts as the link between higher cognitive functions, such as reasoning, and more primitive emotional responses, such as fear. The major areas of the limbic system are the amygdala and circulate gyrus, which are linked to emotion and memory, and the hippocampus, which is associated with learning and memory. On a microscopic level, the brain consists of billions of neurons, which are the building blocks of the nervous system. Neurons communicate with each other through specialized connections called synapses, forming complex neural circuits that underlie our thoughts, emotions, and behaviours. The brain also contains glial cells, which provide support and nourishment to neurons, as well as play a role in neural signalling and defence against pathogens [15]–[17]. Figure 2 shows the major structures of the brain described earlier.

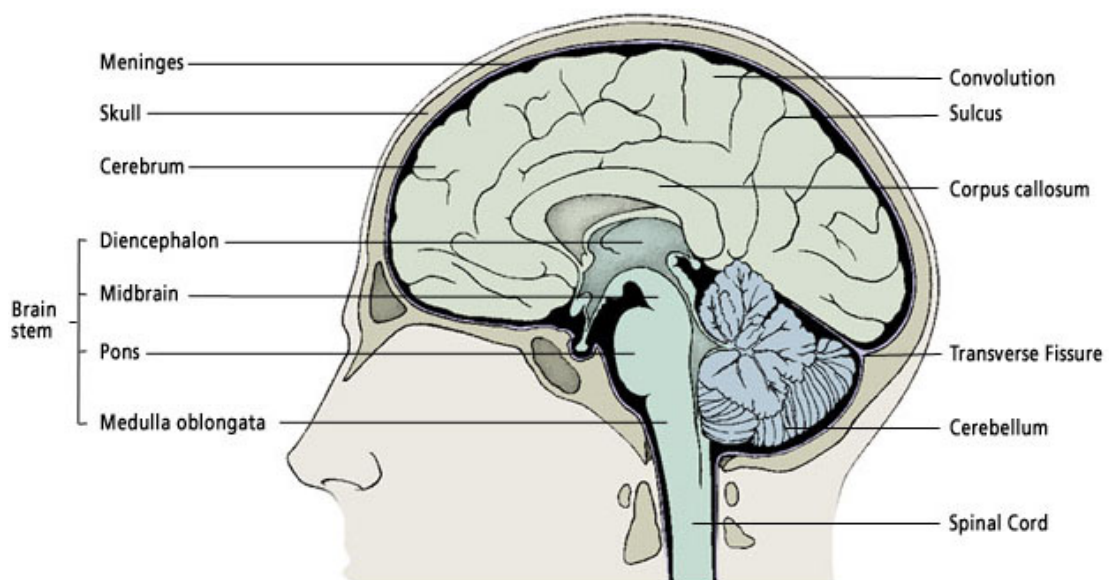


Figure 2: Structure of the brain [18].

1.2.1. Neurons

The nervous system is composed primarily of two cell types: neurons, the basic signalling units of the nervous system, and support cells known as glial cells (or glia or neuroglia). The neuron, or nerve cell, is the functional unit of the nervous system and are responsible for transmitting electrical and chemical signals throughout the body. Neurons, the fundamental building blocks of the nervous system, can be structurally divided into three main parts: the cell body (soma), dendrites, and axon:

- **Cell Body (Soma):** The cell body, also known as the soma, is the main part of the neuron that contains the nucleus and other organelles necessary for its functioning. It integrates incoming signals from dendrites and generates outgoing signals along the axon. The cell body plays a vital role in maintaining the overall metabolic and synthetic functions of the neuron.
- **Dendrites:** Dendrites are branching extensions that emanate from the cell body. They receive incoming signals from other neurons and transmit those signals toward the cell body. Dendrites are covered with numerous synaptic connections, allowing them to receive chemical signals (neurotransmitters) released by neighbouring neurons. The structure of dendrites increases the surface area available for receiving and processing synaptic inputs, enabling the integration of multiple signals.
- **Axon:** The axon is a long, slender projection that carries outgoing signals away from the cell body. It can extend over varying distances, ranging from a few millimeters to more than a meter in length. The axon is specialized for transmitting electrical impulses, known as action potentials, from the neuron's cell body to other neurons, muscles, or glands. Axons are covered by a fatty insulating layer called the myelin sheath, which is formed by specialized cells called oligodendrocytes in the central nervous system (CNS) or Schwann cells in the peripheral nervous system (PNS). The myelin sheath helps to increase the speed and efficiency of signal propagation along the axon. At the end of the axon, multiple branches called axon terminals form specialized junctions called

synapses, where the neuron communicates with target cells by releasing neurotransmitters.

It is important to note that the structural diversity of neurons is vast, and their shapes and sizes can vary significantly depending on their location and functions within the nervous system. Some neurons have a single, short dendrite, while others may have numerous dendrites branching from the cell body. Similarly, axons can differ in length and branching patterns. These structural variations allow neurons to perform specialized functions in transmitting and processing information throughout the complex neural networks of the brain and body. Figure 3 shows the different structural part that forms a neuron cell.

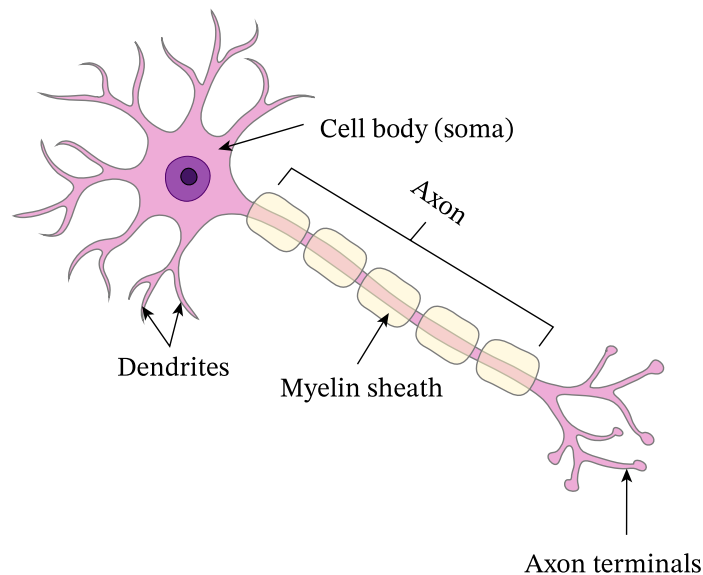


Figure 3: Typical structure of a neuron cell [19].

Thus, by means of dendrites and axons, neurons can communicate with other cells or between their selves, forming networks. The region where an axon terminal meets its target cell is called a synapse. The neuron that delivers a signal to the synapse is known as the presynaptic cell, and the cell that receives the signal is called postsynaptic cell. The narrow space between the two cells is called synaptic cleft, and is filled with extracellular matrix whose fibers hold the presynaptic and postsynaptic cells in position. The shape, number and length of axons and dendrites vary from one neuron to the next, but these structures are an essential

feature that allows neurons to communicate with one another and with other body's cells. Neurons can be classified either structurally or functionally. Structurally, neurons are classified by the number of processes that originate from the cell body, as summarized in Figure 4; in particular, based on the dendrites and the axon presented by them [20], [21]:

- Bipolar: this type of neurons has a single axon and a single dendrite coming off the cell soma. The processes are two relatively equal fibers extending off the central cell body.
- Multipolar: these neurons have many dendrites and branched axons.
- Unipolar: these neurons have the cell body located off one side of one unique long process that is called the axon, which comprises also the dendrite that during development has become a part of it.
- Anaxomic: these neurons lack an identifiable axon but have numerous branched dendrites.

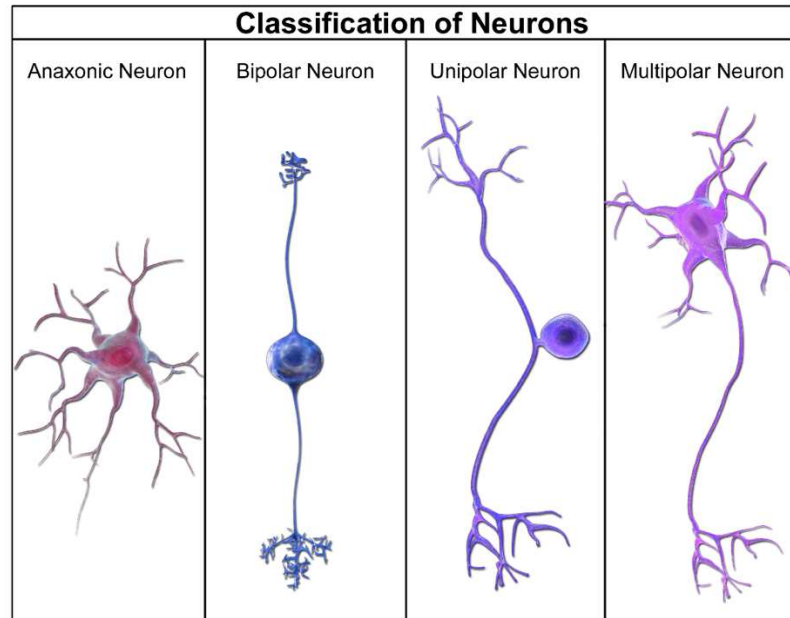


Figure 4: Classification of neurons [22].

Because physiology is concerned chiefly with function, neurons were classified also according to their functions: afferent neurons (sensory neurons), interneurons, and efferent (somatic, motor and automatic) neurons. Afferent neurons carry information about temperature, pressure, light, and other stimuli from sensory receptors to the CNS. Peripheral sensory neurons (almost entirely belonging to the PNS) are pseudo-unipolar, with cell bodies located in the dorsal ganglia of the spinal cord and very long processes that extend out to receptors in the limbs and internal organs. In these sensory neurons, the cell body is out of the direct path of signals passing along the axon. In contrast, sensory neurons in the nose and eye are much smaller bipolar neurons. Interneurons (short for interconnecting neurons) form the dense neuronal networks mainly which lie entirely inside the CNS and they come in a variety of forms but often have quite complex branching processes that allow them to communicate with many other neurons. They are devoted to the integration of all the information coming from the outside, generating an appropriate response and coordinating the whole-body functioning; in addition, they are thought to be responsible of the emergent properties of each individuals known as cognitive functions. Efferent neurons, both somatic, motor and autonomic, have the task of conveying the response produced by the CNS to the target. They have enlarged axon terminals, and many autonomic neurons have enlarged regions along the axon called varicosities. Both axon terminals and varicosities store and release neurotransmitters [21].

The human brain alone contains an estimated 86 billion neurons, each capable of forming connections with thousands of other neurons. This intricate network of interconnected neurons forms the basis of neural circuits and enables the complex processes underlying perception, memory, learning, and behaviour [20].

1.2.2. Auditory System

The human auditory system is a remarkable physiological system responsible for the perception of sound, Figure 5. It comprises a complex network of structures and processes that allow us to detect, analyse, and interpret auditory stimuli. The journey of sound begins with the outer ear, which consists of the pinna (the visible part of the ear) and the ear canal. The pinna helps in collecting sound waves and

directing them into the ear canal, which leads to the eardrum (tympanic membrane). When sound waves reach the eardrum, they cause it to vibrate. These vibrations are then transmitted to the middle ear, which consists of three small bones called ossicles: the malleus (hammer), incus (anvil), and stapes (stirrup). The ossicles amplify the vibrations and transmit them to the inner ear. The inner ear is a complex structure that contains the cochlea, a spiral-shaped organ responsible for converting sound vibrations into electrical signals that can be interpreted by the brain. The cochlea is filled with fluid and is divided into three fluid-filled compartments. When the ossicles transmit the vibrations to the oval window, it creates pressure waves in the fluid of the cochlea. These pressure waves cause movement of the basilar membrane, which is lined with hair cells. Hair cells are the sensory cells of the auditory system and are responsible for converting mechanical vibrations into electrical signals. When the basilar membrane moves, it causes the hair cells to bend, triggering the release of neurotransmitters that initiate electrical impulses in the auditory nerve fibers. The auditory nerve fibers carry these electrical signals from the hair cells to the brain. The signals then travel through a series of neural pathways, including the cochlear nucleus, superior olivary complex, and inferior colliculus, before reaching the auditory cortex in the temporal lobe of the brain. In the auditory cortex, the electrical signals are decoded and processed, allowing us to perceive and interpret different aspects of sound, such as pitch, loudness, and location. The brain integrates this information with other sensory inputs and past experiences to create a rich and meaningful auditory experience [23], [24].

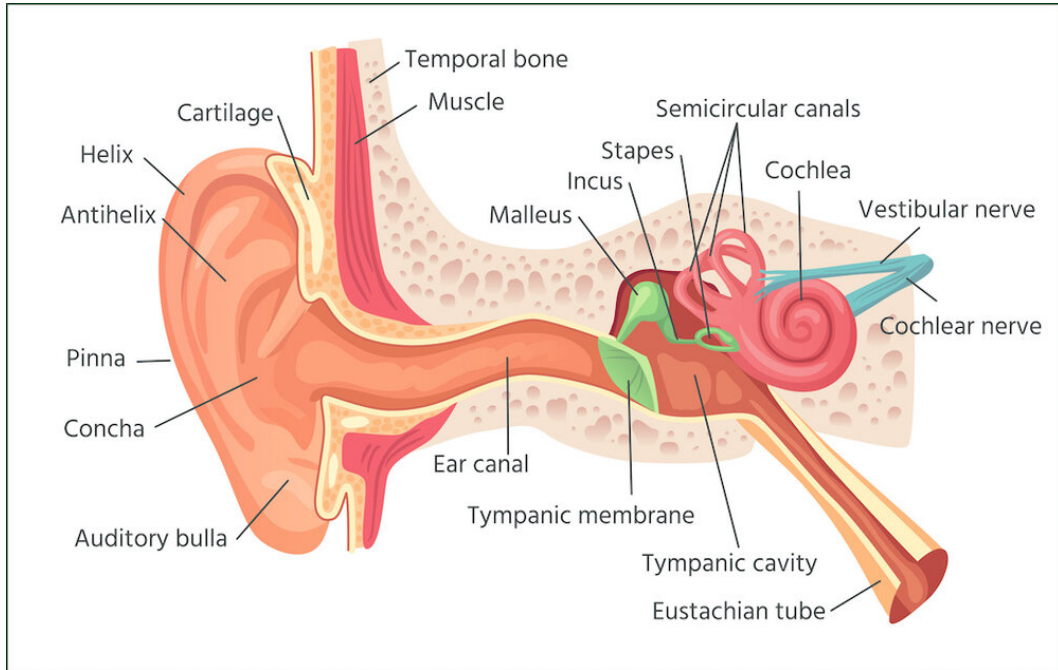


Figure 5: Structure of the auditory system [25].

1.2.2.1 Auditory Cortex

The auditory cortex is a region of the brain located in the temporal lobes, specifically within the superior temporal gyrus. It plays a critical role in processing and interpreting auditory information received from the ears [26]. The auditory cortex serves as the ultimate destination for afferent auditory information. While it comprises several subdivisions, a general division can be made between the primary auditory cortex and the peripheral or belt areas. The primary auditory cortex (A1) is located in the superior temporal gyrus of the temporal lobe and receives precise input from the ventral division of the medial geniculate complex, resulting in a well-defined tonotopic map. In contrast, the belt areas of the auditory cortex receive more diffuse input from the belt areas of the medial geniculate complex, leading to less precise tonotopic organization. The primary auditory cortex (A1) exhibits a tonotopic map that corresponds to the cochlea, similar to the topographical maps found in the primary visual cortex (V1) and primary somatic sensory cortex (S1) for their respective sensory systems. Unlike the visual and somatic sensory systems, the

cochlea has already processed the acoustic stimulus, arranging it tonotopically along the length of the basilar membrane [27]. Consequently, A1 is characterized by a tonotopic map, which is also observed in most auditory structures between the cochlea and the cortex. Additionally, orthogonal to the frequency axis of the tonotopic map, there is a striped arrangement of binaural properties. One stripe consists of neurons that are excited by both ears (referred to as EE cells), while the next stripe consists of neurons excited by one ear and inhibited by the other (known as EI cells). This alternating pattern of EE and EI stripes resembles the arrangement of ocular dominance columns in V1. The specific sensory processes occurring in other divisions of the auditory cortex are not fully understood, but they likely play crucial roles in higher-order processing of natural sounds, including those used for communication. Certain areas may be specialized in processing frequency combinations, while others may specialize in processing amplitude or frequency modulations. Sounds that are particularly relevant for intraspecific communication often possess a highly organized temporal structure. In humans, speech serves as an excellent example of such time-varying signals, where different phonetic sequences are perceived as distinct syllables and words. Behavioural studies involving cats and monkeys have demonstrated the significance of the auditory cortex in processing temporal sequences of sound. When the auditory cortex is removed in these animals, they lose the ability to discriminate between two complex sounds that share frequency components but differ in temporal sequence. Consequently, monkeys lacking the auditory cortex cannot distinguish one conspecific communication sound from another. Studies involving human patients with bilateral damage to the auditory cortex also reveal significant difficulties in processing the temporal order of sounds. Therefore, it is likely that specific regions within the human auditory cortex specialize in processing elementary speech sounds and other acoustical signals with complex temporal characteristics, such as music. Notably, Wernicke's area, a critical region for language comprehension, resides within the secondary auditory area [26], [27].

1.3. EEG Signal

One of the big challenges in the XXI century, as an essential part of human brain analysis procedures, is the determination of mathematical models capable to explain and forecast the relationships between human activities and electroencephalography (EEG) signals. EEG signals produce data organized in temporal sequences with a structured behaviour and have been used for different purposes, from seizure detection and epilepsy diagnosis, to automatic detection of abnormal EEG, and recognition of Alzheimer's disease brain activity, the detection of awareness, or the use of brain-computer interfaces (BCI) [28].

Electroencephalography (EEG) is an electrophysiological method to monitor the electrical activity of the brain. Information about the dynamics of cognitive processes is encoded in complex ways in this electric activity which makes the EEG a powerful tool for cognitive research. Usually, the EEG is measured non-invasively with electrodes recording differences in the electric potential along the scalp. It is widely agreed that these potential differences mainly arise from synchronized synaptic activity in populations of pyramidal neurons which are organized in cortical columns [29]. Figure 6 visualizes in a simplified manner how the electrical activity of the brain can be sensed by an electrode.

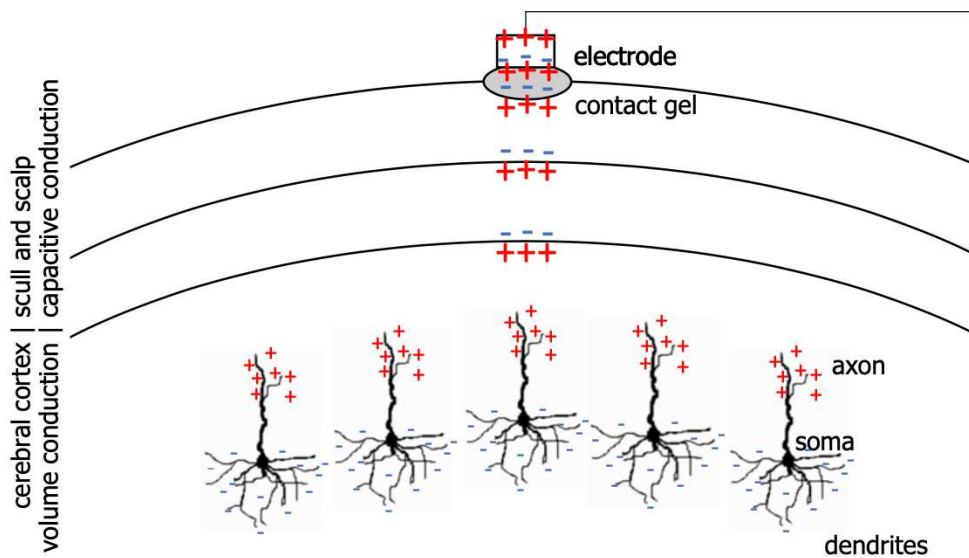


Figure 6: Origin of EEG Signal [29].

Upon excitation by neurotransmitters, the sodium channels at the postsynaptic dendrites of the neuron open. This leads to an inflow of positive Na^+ -ions. The extracellular region near the dendrites becomes more negative than the remaining region along the neuron, which leads to the formation of an electric dipole field. When inhibition by neurotransmitters occurs at the postsynaptic dendrites, the polarity of the dipoles and thus also the measured polarity at the electrode is reversed. As the electric field travels towards the electrode by volume conduction in the brain fluid and capacitive conduction in the poorly conductive biological tissues and the skull, it is weakened significantly. In order to generate a measurable signal at the electrode, many equally oriented neurons have to be activated simultaneously for their electric fields to sum up. The number of neurons required is of magnitude 10^8 . Neuroanatomist Korbinian Brodmann defined regions in the cerebral cortex which have since their definition been correlated to diverse cortical functions. Areas 41, 42 and partly 22 form the auditory cortex, which is shown in pink in Figure 7. This region is related to diverse auditory functions and is therefore of special interest for the study [29].

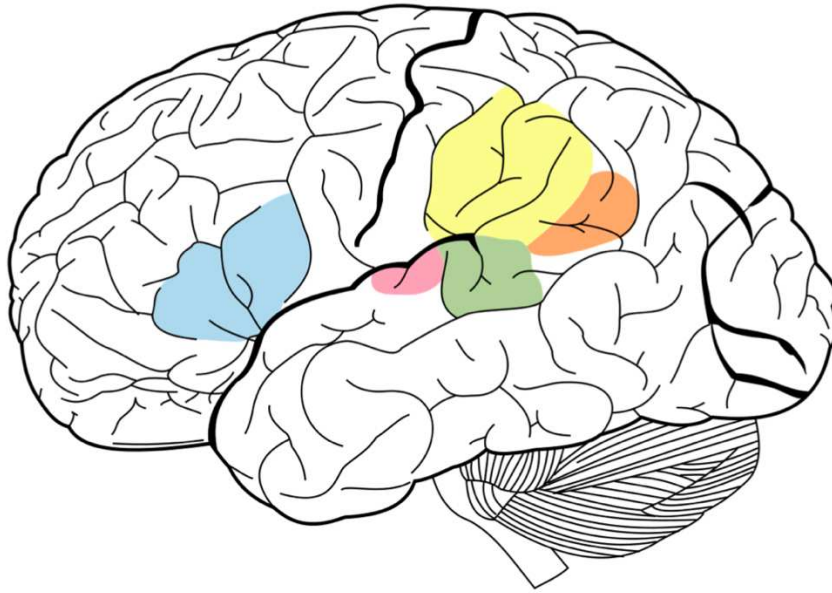


Figure 7: Brodmann Areas: The auditory cortex is highlighted in pink and interacts with the other areas highlighted [29].

EEG signals play a significant role in clinical and research environments, providing valuable insights into brain activity. These signals are captured through scalp-mounted sensors, allowing us to measure the electrical activity generated by large groups of neurons in the brain. By analysing EEG signals, we can gain knowledge about cognitive and emotional states, monitor alertness and mental engagement levels, investigate chronic conditions, and even utilize them for biofeedback or assistive devices. One of the key advantages of EEG signals is their ability to offer multi-dimensional information by processing them in the time, frequency, or spatial domains. This versatility enables us to interpret complex neural patterns and understand brain activities from different perspectives. Additionally, EEG signals are capable of capturing these intricate patterns at a rapid pace, providing real-time insights into brain functioning. Furthermore, EEG holds several practical advantages, making it a reliable, portable, and non-invasive method for measuring brain electrical activity. Its affordability and accessibility contribute to its widespread use in both research and clinical healthcare settings. Overall, EEG stands as a central methodology in the field, offering valuable information for scientific exploration and holding promise as a tool for improving patient care [30].

Figure 8 illustrates the EEG framework, which consists of commonly used modules in EEG analysis.

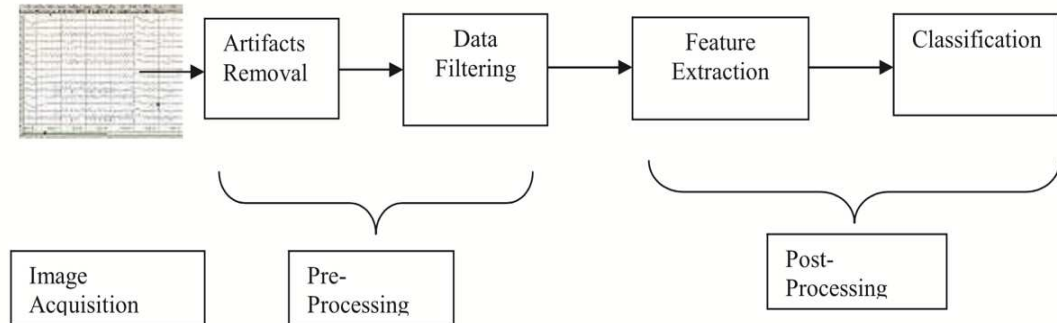


Figure 8: EEG signals processing steps [31].

The first phase, EEG Signal Acquisition, involves directly collecting raw EEG signals from the brain's scalp. The second phase is the pre-processing stage, which includes two processes: artifact removal and data filtering. Identifying and eliminating artifacts present a challenge during signal acquisition and analysis. These artifacts can be caused by factors such as head motion, physical issues with electrodes/channels/leads, or connectivity problems between the head and the device. Such artifacts can distort the frequency and shape of the signals. The next phase in signal analysis is feature extraction, where various signal processing techniques like Fourier Transform, Wavelet, Principal Component Analysis are employed to derive meaningful features (abnormal/normal). Fourier Transform is a popular automated method that categorizes signals into different frequency bands: Delta (<4 Hz), Theta (4-8 Hz), Alpha (8-13 Hz), and Beta (13-30 Hz). However, Fast Fourier Transform (FFT) may not be suitable for EEG signals with high noise ratios. Parametric Spectrum Estimation methods, such as Autoregressive (AR), are used to reduce spectral loss and provide better frequency resolution. It's worth noting that parametric methods may not be suitable for non-stationary signals like EEG. Classification, the subsequent phase, utilizes the extracted features to obtain target observations. Feature extraction and classification are two crucial challenges encountered in time domain analysis [32].

1.3.1. History of EEG

Throughout history, extensive research has been conducted to explore the electrical activity within the brain. As early as 1875, physician Richard Caton conducted experiments on rabbits and monkeys, publishing his findings in the *British Medical Journal*. Adolf Beck furthered this research in 1890 by placing electrodes directly on the surface of a dog and a rabbit brain to investigate sensory stimulation, leading to the discovery of brainwaves and the emergence of EEG as a scientific field. In 1924, Hans Berger, a German physiologist and psychiatrist, made a significant breakthrough by recording the first human EEG brainwaves, Figure 9. Berger's invention of the electroencephalogram revolutionized the field of clinical neurology and was described as a remarkable development by author David Millet in his book "The Origins of EEG." The field of clinical electroencephalography took shape in 1935, inspired by the work of neuroscientist Frederic Gibbs, Hallowell Davis, and William Lennox. Their research focused on epileptiform spikes, interictal spike waves, and clinical absence EEG seizures, leading to the understanding that interictal spikes are a distinctive feature of epilepsy. The first EEG laboratory was established at Massachusetts General Hospital in 1936. In 1947, The American EEG Society, now known as The American Clinical Neurophysiology Society, was founded, and the first International EEG Congress was held. In the 1950s, William Grey Walter introduced EEG topography, a technique for mapping electrical activity across the brain's surface. Although popular in the 1980s, EEG topography did not become widely adopted in mainstream neurology. A significant milestone occurred in 1988 when scientists Stevo Bozinovski, Liljana Bozinovska, and Mihail Sestakov achieved control of a physical object using an EEG machine. This breakthrough showcased the potential of EEG technology. In 2011, EEG entered the consumer market with the launch of EMOTIV by tech entrepreneurs Tan Le and Dr. Geoff Mackellar. Today, EEG technology, including headsets and caps, plays a crucial role in Brain-Computer Interface (BCI) systems. BCI, also known as HMI, MMI, BMI, and DNI, aims to track cognitive performance and enable control over virtual and physical objects through machine learning of trained mental commands. BCI holds promise for various applications, bridging the gap between

the brain and technology. An inspiring demonstration of the capabilities of EEG technology occurred in 2017 when quadriplegic racer Rodrigo Hübner Mendes became the first person to drive a Formula 1 car solely using his brainwaves, made possible by an EMOTIV EEG Headset [33], [34].

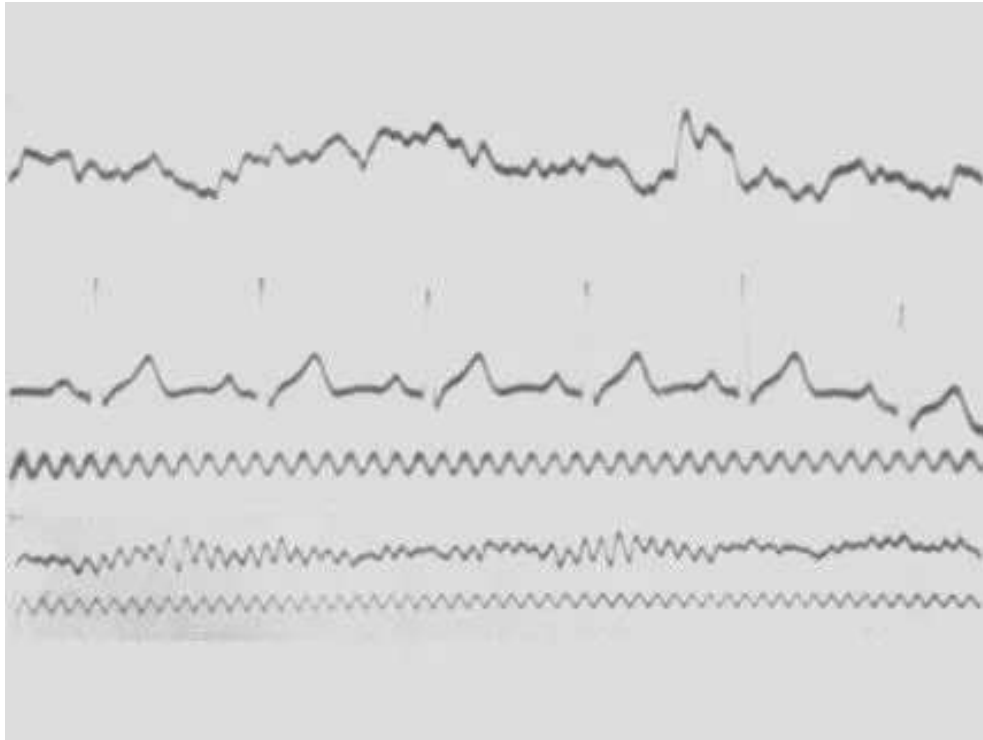


Figure 9: Hans Berger achieved the first-ever recording of human electroencephalography (EEG) in 1924. In his ground-breaking experiment, Berger captured the upper signal representing EEG activity, while the lower signal served as a 10 Hz timing reference [35].

1.3.2. EEG Devices

EEG recording devices, also known as electroencephalography devices, are essential tools used in the field of neuroscience and clinical medicine. These devices are designed to capture and measure the electrical activity of the brain. EEG recording devices consist of electrodes that are placed on the scalp to detect the small electrical signals generated by the neurons in the brain. These electrodes are connected to an amplifier, which amplifies and filters the signals to ensure accurate recording. The recorded EEG signals are then typically digitized and stored for further analysis and interpretation. EEG recording devices come in various forms, ranging from traditional wired systems with multiple electrodes to

more portable and wireless solutions that offer greater flexibility and ease of use. These devices play a crucial role in diagnosing and monitoring various neurological conditions such as epilepsy, sleep disorders, and brain injuries. They are also valuable tools in research settings, enabling scientists to study brain activity and investigate the underlying mechanisms of cognitive processes and disorders. With advancements in technology, EEG recording devices continue to evolve, offering improved signal quality, enhanced comfort for patients, and advanced features for data analysis, making them indispensable instruments in the field of neuroscience and clinical practice [36]. EEG headsets, whether wired or wireless, enable the transmission of data to a computer using different methods:

- **Wired Communications:** Wired headsets utilize cables to establish a connection, offering stability and the ability to transfer larger amounts of data efficiently. Irrespective of the connection type, it's important to note that movement of cables and electrodes can introduce artifacts into the EEG signal, as it can interfere with the electrode-skin connections [37].
- **Wireless Communications:** Wireless headsets employ either wireless or Bluetooth technology to establish a connection, providing users with greater freedom of movement. However, a notable disadvantage of wireless EEG headsets is the potential loss of connectivity during data capture, which may result in data not being recorded [37].

Another classification of the devices is based on the electrode type placed onto the scalp:

- **Soft gel-based:** the electrodes establish a connection with the scalp by applying a conductive gel into the designated pocket of each electrode. Once the experiment is concluded, it is essential to clean the headset by removing the gel and thoroughly cleaning the electrodes. Typically, alcohol is used for this cleaning process due to its evaporative properties [38].
- **Saline solution:** certain EEG headsets utilize a conductive gel to facilitate a low-impedance electrical connection between the skin and the sensor

electrode. In such headsets, electrodes are connected by applying saline solution to each electrode [38].

- Dry: these devices eliminate the need for gel or saline to establish electrode-to-scalp contact, simplifying the process of recording EEG data without requiring the assistance of a trained technician. Moreover, dry devices offer the advantage of significantly reduced setup time compared to their wet headset counterparts [38].
- Others: Some EEG sensor connections types do not fit cleanly into either of these two categories. Conductive solid gel materials, such as those produced by Enobio, have also been used successfully in EEG devices [38].

In January of 2019, researchers at the University of California, The Otto von Guericke University of Magdeburg, and The Hebrew University of Jerusalem performed a comparative analysis of the signal quality of dried wireless and wet wire EEG devices, and concluded that the quality of wireless dry devices is significantly comparable with the wired wet. Although some researchers observed that, for those activities that demand body movement like running/walking, wired wet sensors showed better performance. This seems to indicate that wet sensors may be more resistant to movement artifacts, although more research needs to be conducted to fully understand which technology can provide more reliable data [39].

1.3.2.1. Electrode Placement Standards

Electrode placement in EEG follows standardized systems to ensure accurate and consistent recording of brain activity. One commonly used system is the International 10-20 System, which is based on anatomical landmarks and measurements. This system divides the scalp into regions and assigns specific electrode positions based on percentages of inter-electrode distances. The electrodes are labeled with letters and numbers to indicate their locations, such as Fp (frontopolar), F (frontal), C (central), P (parietal), and O (occipital), followed by numbers to represent the left/right hemisphere and

specific areas within each region. In addition to the 10-20 System, other standards exist, such as the 10-10 System, which includes more electrode positions for higher spatial resolution. The 10-10 System extends the coverage of the scalp by adding additional electrode sites between those of the 10-20 System, resulting in more precise localization of brain activity. This system has become increasingly popular in research and clinical settings for its enhanced accuracy in identifying specific brain regions. Another notable standard is the 10-5 System, which further increases electrode density by adding additional positions between those of the 10-10 System. This system allows for even finer spatial resolution and is particularly advantageous for studies requiring high-density EEG recordings, such as source localization and connectivity analysis. Proper electrode placement is crucial for obtaining reliable and meaningful EEG data. It ensures optimal coverage of brain regions and minimizes the risk of signal distortion or artifacts. Additionally, standardized electrode placement facilitates the comparison and exchange of data across studies and enables accurate localization of brain activity. While the International 10-20, 10-10, and 10-5 Systems are the most widely used standards, variations and adaptations exist to meet specific research or clinical requirements. These standardized systems provide a common language for EEG researchers and clinicians, promoting consistency, reproducibility, and effective communication within the field.

1.3.3. EEG Patterns

The EEG is commonly characterized by its rhythmic activity and transients, which are categorized into frequency bands. Although the division of these bands is somewhat subjective (for example, any rhythmic activity between 8–12 Hz can be referred to as "alpha"), these distinctions emerged due to observed scalp distribution patterns or specific biological implications. Spectral methods such as Welch, available in EEG software like EEGLAB or the Neurophysiological Biomarker Toolbox, are typically employed to extract frequency bands. The computational analysis of EEG data is often referred to as quantitative electroencephalography (qEEG). EEG signals exhibit voltage fluctuations

associated with various mental states, internal conditions of the subject, or pathological disorders. Research on brain waves indicates that distinct cognitive processes are linked to different frequency domains. These waves are generated by synchronized neural activity and are influenced by the subject's internal state. Analysing these fluctuations has revealed the presence of harmonic frequencies ranging from 1 to 100 Hz, with the majority of informative content residing below 40 Hz, while activity beyond this range is likely to be artifacts according to standard clinical recording techniques. Waveforms are further categorized into alpha, beta, theta, delta and gamma bandwidths, which encompass the primary EEG data used in clinical practice [36].

- Delta waves refer to the frequency range below 4 Hz, displaying the highest amplitude and the slowest patterns. In adults, they are typically observed during slow-wave sleep, while in infants, they are also commonly present. Focal occurrences of delta waves may indicate subcortical lesions, while a more widespread distribution can be associated with diffuse lesions, metabolic encephalopathy, hydrocephalus, or deep midline lesions. In adults, delta waves are usually most prominent in the frontal region, whereas in children, they are more noticeable in the posterior region.
- Theta waves encompass the frequency range from 4 Hz to 7 Hz. They are considered normal in young children and can be observed during drowsiness, arousal in older individuals, and even during meditation. However, excessive theta activity for a specific age group may signify abnormal brain function. Focal disruptions of theta waves can be observed in cases of focal subcortical lesions, while a generalized distribution may indicate diffuse disorders, metabolic encephalopathy, deep midline disorders, or certain instances of hydrocephalus. On the contrary, theta waves have also been associated with relaxed, meditative, and creative states.
- Alpha waves are characterized by a frequency range between 8 Hz and 13 Hz. The term "alpha wave" was coined by Hans Berger to describe the initial rhythmic EEG activity he observed. It is known as the "posterior

basic rhythm" or "posterior dominant rhythm," seen in the posterior regions on both sides of the head, with greater amplitude on the dominant side. Alpha waves become more prominent when the eyes are closed and during relaxation, but diminish in intensity with eye opening or mental exertion. In young children, the posterior basic rhythm is actually slower than 8 Hz (technically falling within the theta range). Apart from the posterior basic rhythm, there are other normal alpha rhythms, such as the mu rhythm (alpha activity in the contralateral sensory and motor cortical areas), which emerges when the hands and arms are at rest, as well as the "third rhythm" (alpha activity in the temporal or frontal lobes). Alpha waves can exhibit abnormal patterns, such as diffuse alpha activity in coma that is unresponsive to external stimuli, known as "alpha coma."

- Beta waves span the frequency range from 13 Hz to approximately 30 Hz. They typically appear symmetrically on both sides and are particularly noticeable in the frontal region. Beta activity is closely linked to motor behaviour and tends to diminish during active movements. Low-amplitude beta waves with multiple and varying frequencies are often associated with active, busy, or anxious thinking and focused concentration. Rhythmic beta activity characterized by dominant frequencies can be related to various conditions, including Dup15q syndrome and the effects of certain drugs, especially benzodiazepines. In areas of cortical damage, beta waves may be absent or reduced. They dominate the EEG of individuals who are alert, anxious, or have their eyes open.
- Gamma waves fall within the frequency range of approximately 30 Hz to 100 Hz. They are believed to represent the synchronization of different neuronal populations into networks responsible for specific cognitive or motor functions. Gamma rhythms are associated with the binding of neural circuits together.

Table 1 shows the various brainwave bands with their main characteristics.

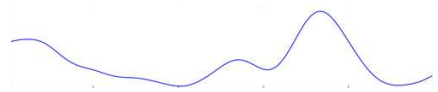

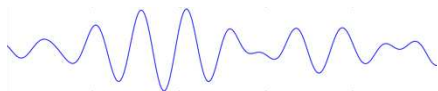


Band	Frequency [Hz]	Brain State	Signal Shape
Delta (δ)	[1,4]	Deep sleep	
Theta (θ)	[4,8]	Meditation Emotional stress Creative inspiration	
Alpha (α)	[8,13]	Closed eyes wakeful state Wakeful relaxation Mental stress	
Beta (β)	[13,30]	Strong mental activity Problem solving Concentration	
Gamma (γ)	[30,100]	Cognitive activity Motor activity	

Table 1: EEG frequency bands.

1.3.4. Time-Frequency Analysis

EEG signals encompass rhythmic activity that arises from variations in the excitability of neuron populations, reflecting neural oscillations. These oscillations possess distinctive characteristics such as frequency, phase, and power, and can be investigated using signal analysis methods. Neural oscillations are categorized into frequency bands with logarithmically increasing center frequencies, a grouping that stems from the underlying neurobiological mechanisms governing these oscillations. This categorization proves useful in discerning different states of the brain, as alterations in the rhythmic patterns of neural oscillations to some extent indicate the neurophysiological manifestation of cognitive functions. The strength of neural oscillations can be quantified by the amount of energy conveyed by their electric fields per unit of time, which correlates with the power of the EEG signal (eq. 1.5-1.6) [29]:

$$P = \lim_{T \rightarrow \infty} \frac{1}{2T} \int_{-T}^T x^*(t)x(t)dt \quad (1.5)$$

or for discrete signals:

$$P = \lim_{N \rightarrow \infty} \frac{1}{2N + 1} \sum_{n=-N}^N x^*[n]x[n] \quad (1.6)$$

In order to specify how the power is distributed in the frequency domain, the power spectral density (PSD) can be used. It is defined as the Fourier transform of the signal's autocorrelation function (eq. 1.7-1.8):

$$PSD = S_{xx}(\omega) = \int_{-\infty}^{+\infty} r_{xx}(\tau)e^{-i\omega\tau} d\tau \quad (1.7)$$

with:

$$r_{xx}(\tau) = \lim_{T \rightarrow \infty} \frac{1}{2T} \int_{-T}^T x^*(t)x(t + \tau)dt \quad (1.8)$$

For time discrete signals, the PSD can be estimated with Welch's method [29]: first, the signal is segmented into K segments $x_k[j]$ of length L, which can also overlap. These segments are then weighted with a window function $w[j]$ to reduce the leakage effect. After that, the Fourier transform is taken (eq. 1.9):

$$A_k[n] = \frac{1}{L} \sum_{j=0}^{L-1} x_k[j]w[j]e^{\frac{2kijn}{L}} \quad (1.9)$$

In a next step, K periodograms I_k are calculated by (eq. 1.10-1.11-1.12):

$$I_k[f_n] = \frac{L}{U} |A_k[n]|^2 \quad (1.10)$$

with:

$$f_n = \frac{n}{L}, n = 0, \dots, \frac{L}{2} \quad (1.11)$$

and:

$$U = \frac{1}{L} \sum_{j=0}^{L-1} w^2[j] \quad (1.12)$$

The estimated PSD is the average of the periodograms (eq. 1.13):

$$PSD = \hat{S}_{xx}[f_n] = \frac{1}{K} \sum_{k=1}^K I_k[f_n] \quad (1.13)$$

Typical EEG signal PSDs are shown in Figure 10.

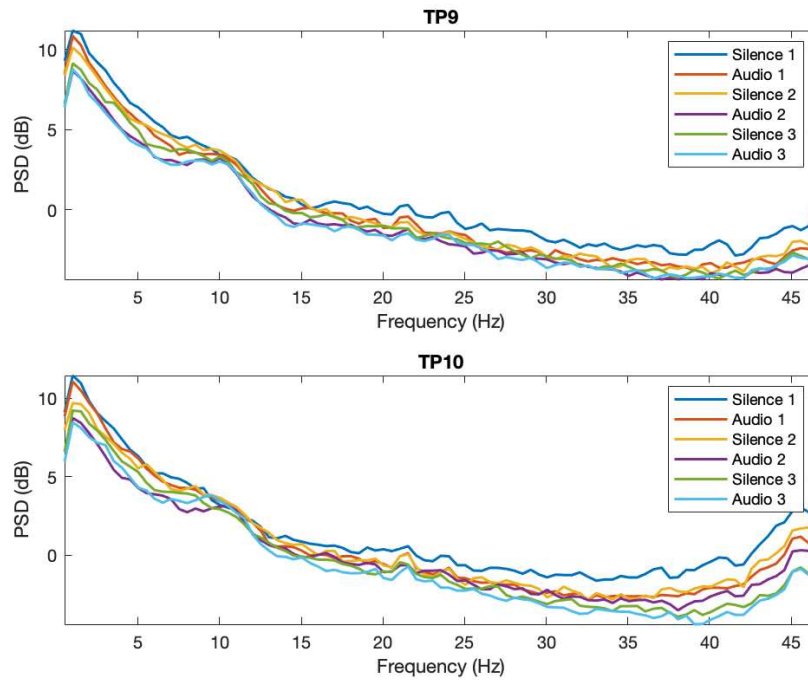


Figure 10: Characteristic PSD of EEG Signals. Data taken from our study. The plots show the averaged PSD across all subject measured both for TP9-TP10 electrodes.

To obtain the band power, the PSD is integrated over the frequency intervals discussed in the previous chapter (eq. 1.14):

$$P_{\text{band}} = \int_{\text{lower limit}}^{\text{upper limit}} \text{PSD}(f)df \quad (1.14)$$

For cross-subject analysis it is helpful to normalise the band power with the total power, which yields the relative band power (eq. 1.15):

$$\tilde{P}_{\text{relative, band}} = \frac{\int_{\text{lower limit}}^{\text{upper limit}} \text{PSD}(f)df}{\int \text{PSD}(f)df} \quad (1.15)$$

Both EEG band power and relative band power are quantities which are widely used for EEG characterisation.

2. MATERIALS AND METHODS

2.1. Experimental Setup

2.1.1. Participants

Signals from 43 healthy volunteers (22 males and 21 females) were acquired for the experiment. All volunteers were local students or employees at the “Università Politecnica delle Marche” of Industrial Engineering and Mathematical Science Department, where the experiment took place.

2.1.2. EEG Measurement Device

In this study, the acquisition of EEG signals was performed using a commercially available wearable device: the Interaxon MUSE headband (Figure 11).

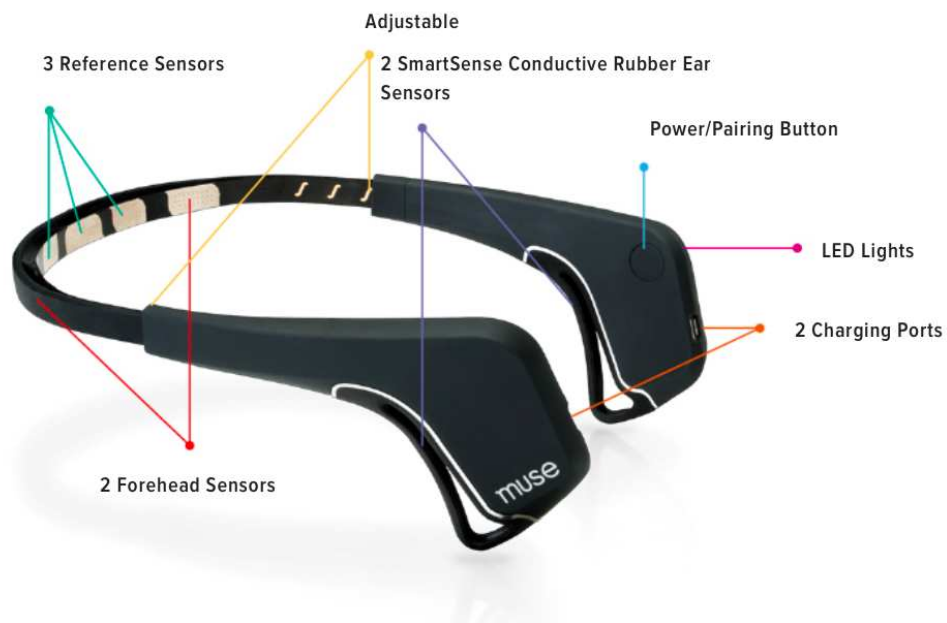


Figure 11: The 2016 Muse EEG system made by InterAxon Inc [40].

The placement of electrodes followed a specific standard: the reference electrode FPz was positioned on the forehead, while the input electrodes consisted of two frontal electrodes (AF7 and AF8) located on the left and right sides of the reference, respectively, made of silver material. Additionally, two posterior electrodes (TP9 and TP10) were placed above each ear using conductive silicone-rubber material (Figure 12). Before positioning the headband on the subject's heads, their skin was cleaned with alcohol swipes at electrode sites, and a thin layer of water was applied with a sponge to the electrodes to improve signal quality. The MUSE device recorded signals at a sampling frequency of 256 Hz.

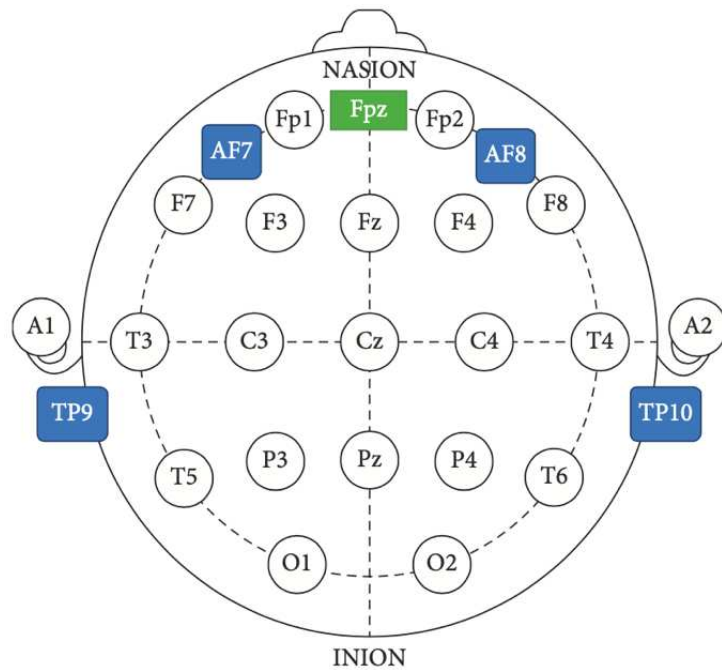


Figure 12: Top-down view of the 10-20 system EEG electrode positions on the subject's head [41].

The data acquisition process involved utilizing the MUSE application, which was paired with a smartphone via Bluetooth Low Energy (BLE) technology. Impedance check was provided by the App (horseshoe symbol) and visually confirmed by the raw signal displayed on the screen in real-time. However, the reliability of the MUSE device may be subject to scrutiny. The limited number of electrodes could hinder the evaluation of multiple brain networks, as it may not provide focused coverage of specific brain areas. Furthermore, the frontal

electrodes are more susceptible to capturing artifacts caused by eye blinks and movements, potentially interfering with the accurate measurement of actual brain waves [42]. The use of dry electrodes could also lead to discomfort over time and a higher risk of misplacement on the forehead, resulting in decreased signal accuracy. Certain factors such as head shape, size, and hairstyles may present challenges in collecting data, as insufficient contact with the head surface may impede proper signal acquisition [43], [44]. Nevertheless, numerous studies have demonstrated the effectiveness of the MUSE device in research settings. For example, Krigolson et al. successfully employed MUSE for Event-Related Potential (ERP) studies [45]. They assessed the reliability of ERP data collected with the MUSE device through resampling analysis, and obtained reliable ERP components (especially the N200) with a limited number of participants. Youssef et al., in their study on lie detection using MUSE, achieved notable success in their experimental objectives [46]. Ratti and colleagues conducted a comparison between EEG medical devices and consumer-grade MUSE portable devices [47]. Their findings showed that the power spectral densities (PSDs) of MUSE were similar to medical-grade systems, albeit with slightly higher variation (power spectral ratios ranging from 1.125 to 1.225 for MUSE, compared to 0.975 to 1.025 for medical equipment). This broader spectrum increase in MUSE data could potentially reflect artifacts in the recordings made by the dry electrodes. Nonetheless, the simplicity and ease of setup, along with the quick applicability (less than 10 minutes), make MUSE highly convenient for self-help applications [47].

2.1.3. Data Collection

The data used in the analysis has been collected from participants wearing the Muse headband and headphones, as shown in Figure 13. The participants were seated in a comfortable chair at a distance of about 70 cm from the screen. They were instructed to sit still, relax their muscles and try to minimize eyes movements during the course of a trial.



Figure 13: Experimental setup of a volunteer during a test.

The headband was adjusted to the comfort of the participant. The experimental protocol and data management were communicated to all the volunteers, ensuring that they were well-informed. Furthermore, the collected data underwent a process of anonymization. Volunteers were asked to sign a privacy information sheet and another one in which we explained why this study was conducted. After that we instructed each subject on how the test would be done, thus preparing them for what they should and should not do. Volunteers were then asked to use their smartphones to scan a QR code that led them to an online questionnaire created with Google Form. Here each subject entered personal information, i.e., first name, last name, age, gender, country of origin, the volume value set on the pc for the test, and a series of questions pertaining to the sounds they would later listen to. Specifically, these were structured into 3 sets of 3 questions to be filled in immediately after the end of each audio they listened to. In particular, each subject was asked how annoying or pleasant, relaxing or stressful, and finally quiet or loud that particular audio was.

The proper test consisted of 3 audios of 1-minute duration preceded by 1 minute of silence. This was done to relax the participant from the effect of the stressed and non-stressed audios. The sequence of the 3 audios reported listening to a car engine under acceleration, a piece of a classical song by Ludovico Einaudi, and finally an extract of noise from car traffic during the day. The user started the test by clicking a point on desktop which led to a “beep” sound, that act both for informing the subject that the test had begun and for synchronization useful for data processing. During the test, the proper coupling between electrodes and the subject's skin and thus the good performance of the test could be monitored live through the Muse Headband app. Bluetooth Low Energy (BLE) technology was used so that the EEG Muse Headband communicates with a paired smartphone. At the end of listening to the 3 audios (about 6 minutes), the test can be considered concluded with an operator stopping the recording. After that, the captured data was automatically transferred to a folder in Google Drive so that it could be reviewed in real time by all operators that worked for this project.

2.2. Data Pre-Processing

EEG recording is susceptible to capturing various sources of noise and physiological artifacts, including eye blinking, movements, and non-physiological artifacts like electrical interference. Consequently, it becomes crucial to employ a pre-processing and denoising techniques on the recorded EEG data. Drawing from the existing literature, a custom code was developed to facilitate the filtration and isolation of the signal of interest.

Data preprocessing was done in MATLAB v2023a. MATLAB (Matrix Laboratory) is a high-level programming language and numerical computing environment used for analyzing, modelling, visualizing large amounts of data and developing algorithms for data processing. This programming environment also has many advanced toolboxes for specific domains, such as signal processing, machine learning and control systems [48].

In particular, we decided to conduct the study in a non-fully traditional way, so no Event Related Potential (ERP) and no Independent Component Analyses (ICA) was performed. Regarding ICA, the reason is definitely related to the fact that with only 4

electrodes it cannot be applied. It is necessary to have a significant number of channels. Since we were dealing with a high number of raw data, to be more precise we had 43 subjects with 6 audios each, we decided to avoid manual pre-processing and use automatic pre-processing. Filtering each dataset with a low-pass filter, a high-pass filter, a notch filter for power line noise removal and then eliminating the portions of the signal corrupted by any kind of artifacts did not seem to us to be the best solution in terms of time. Studies have shown how interesting and robust this approach can be. A. Delorme et al., shown that it is possible to find automated data rejection methods that were not significantly worse than human manual rejections [49]. The performance of their algorithms was likely better than human raters, because their rejections were closer to all human raters than raters' rejections were with each other. It is interesting to note that standard methods for high-density EEG, such as the correlation of neighboring channels, are inefficient with low-density montages. This is because these methods assume a few outliers in a large number of channels. They also tried independent component analysis (ICA) on a few datasets and obtained poor results. ICA performs well on high-density montages, and there is no theoretical reason why it should not perform well with 4 channels, so this requires further investigation.

Therefore, we decided to carry out in parallel two pre-processing methods for the automatic removal of bad channels and portions of the signal with many artifacts, including the data filtering part as well, to finally try to figure out with which of the two methods better results could be expected for the study of brain waves subjected to different types of sound stimuli. The first approach was to use EEGLAB, a toolbox that can be used in MATLAB, while the second approach was to use AUTOREJECT, a library to automatically reject bad trials and repair bad sensors in magneto-electroencephalography (M/EEG) data.

2.2.1. EEGLAB

EEGLAB is an interactive MATLAB toolbox for processing continuous and event-related EEG, MEG and other electrophysiological data incorporating independent component analysis (ICA), time/frequency analysis, artifact rejection, event-related statistics, and several useful modes of visualization of the

averaged and single-trial data. EEGLAB runs under Linux, Unix, Windows, and Mac OS X. EEGLAB provides an interactive graphic user interface (GUI) allowing users to flexibly and interactively process their high-density EEG and other dynamic brain data using independent component analysis (ICA) and/or time/frequency analysis (TFA), as well as standard averaging methods. EEGLAB also incorporates extensive tutorial and help windows, plus a command history function that eases users' transition from GUI-based data exploration to building and running batch or custom data analysis scripts. EEGLAB offers a wealth of methods for visualizing and modeling event-related brain dynamics, both at the level of individual EEGLAB 'datasets' and/or across a collection of datasets brought together in an EEGLAB 'studyset.' For experienced MATLAB users, EEGLAB offers a structured programming environment for storing, accessing, measuring, manipulating and visualizing event-related EEG data. For creative research programmers and methods developers, EEGLAB offers an extensible, open-source platform through which they can share new methods with the world research community by publishing EEGLAB 'plug-in' functions that appear automatically in the EEGLAB menu of users who download them. For example, novel EEGLAB plug-ins might be built and released to 'pick peaks' in ERP or time/frequency results, or to perform specialized import/export, data visualization, or inverse source modeling of EEG, MEG, and/or ECOG data.

In this study, as a consequence of what we said earlier, so that we did not have to load and work with datasets one at a time, we extracted EEGLAB's function for importing data. Specifically, we used the 'pop_musemonitor' function, extracted from a specific open-source plug-in to import data acquired exclusively with Muse Headband. This made it possible for us to be able to create, work with, and customize a script in MATLAB. The '*pop_musemonitor*' function not only allowed us to import data acquired with Muse Headband, but also to do an initial clean-up of the data thanks to the automatic process performed by the plug-in. In particular, several parameters were set: the sampling rate, checkboxes that allowed cleaning bad channels and data corrupted by artifacts with their respective thresholds, and finally a first high-pass filter with frequency 0.5 Hz (Figure 14).

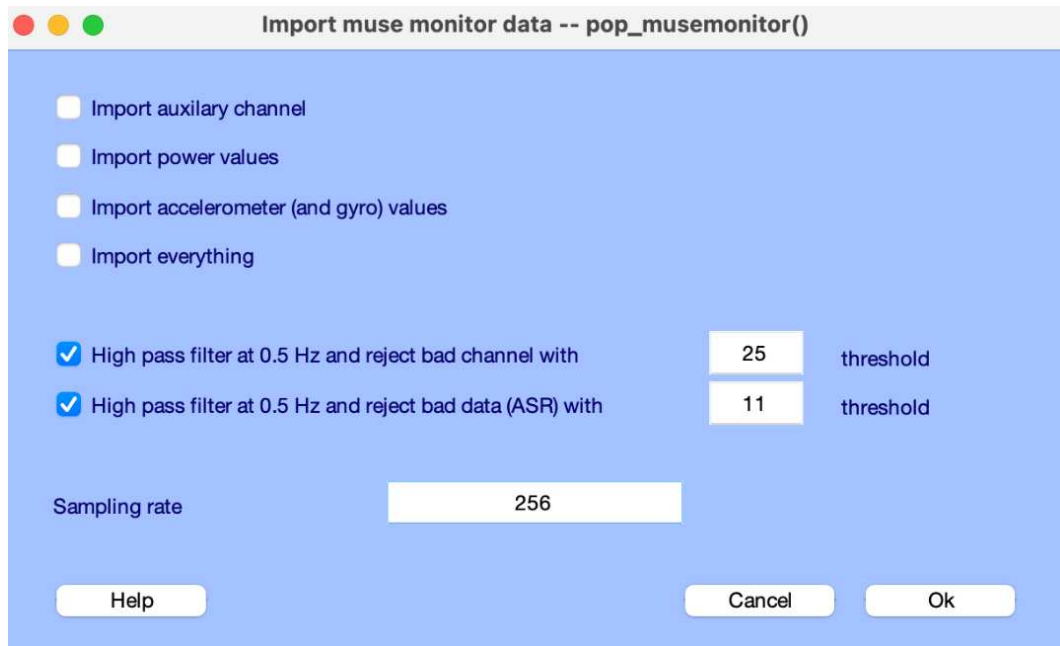


Figure 14: GUI window in EEGLAB Toolbox that allow to import .CSV file recorded with Muse Headband Device.

In order to automate the process, we extracted this function, 'pop_musemonitor', modifying and inserting it into our script in MATLAB. Figure 15 shows the adjustment made. According to the study conducted by A. Delorme et al., we set the parameter thresholds for bad channel removal and bad data removal to 25 and 11, respectively [49].

The first parameter is linked to the Spectral Thresholding Method. This algorithm calculates the log-power spectrum of each channel using the 'pop_spectopo' function of EEGLAB which uses the 'pwelch' function of MATLAB. Then various frequency bands were considered, including 0-5 Hz, 5-15 Hz, 15-25 Hz, 25-35 Hz, 35-45 Hz, 45-55 Hz, 0-55 Hz, 5-55 Hz, and 15-55 Hz. To determine the thresholds for each frequency band, an array of threshold values ranging from 10 to 50 $\log_{10}(\mu V^2)/Hz$ was scanned, with increments of 1. Normalization was disabled, and default values were used for other parameters. Typically, when using a high-density montage, the "pop_rejchan" function normalizes the signals measured across channels, allowing thresholds to be set in terms of the standard deviation of the spectral estimation. However, since there were only 4 channels in this study, normalizing signals across channels to reject outliers was not possible.

Therefore, the absolute spectra values were employed. Whenever a spectra value for a given channel exceeded the threshold, it was labeled for rejection [49].

The second parameter is related to the Artifact Subspace Reconstruction (ASR). For this latter one the ‘*clean_artifact*’ function from the ‘Clean_rawdata v2.5’ plugin of EEGLAB was used. The researchers adjusted the *WindowCriterionTolerances* argument within the range of 5 to 15, with increments of 1. The *WindowCriterion* parameter was set to 0 to automatically discard faulty data segments rather than attempting to correct them. Additionally, all other features, including *BurstRemoval*, were deactivated. The default values for filtering parameters were employed [49].

```
opt = finputcheck(options, { 'aux'      'string'  { 'on' 'off' }  'off';
                          'power'   'string'  { 'on' 'off' }  'off';
                          'acc'     'string'  { 'on' 'off' }  'off';
                          'srate'   { 'string' 'real' } { {} {} } '256'; |
                          'rejchan'  'float'   { }           25;
                          'rejdata'  'float'   { }           11;
                          'importall' 'string'  { 'on' 'off' }  'off' }, 'pop_importmuse');
if isstr(opt), error(opt); end
```

Figure 15: *pop_musemonitor* function parameter adjustment.

After the first pre-processing phase, a second phase was made. This involved the utilization of a notch filter to eliminate power line noise (50 Hz), a high-pass filter set at 0.2 Hz to eliminate DC offset and low-frequency skin potential artifacts, as well as a low-pass filter set at 47 Hz to eliminate high-frequency noise. At this point all the acquired data were cleaned and loaded in structure form into MATLAB. Figure 16 shows how the *clean_dataset* structure was made: 43 subjects in the rows and 6 audios in columns (three one-minute audios each preceded by a minute of silence).

The screenshot shows the MATLAB Variables window for a variable named 'clean_dataset'. It is a 43x6 cell array. The first few rows are visible, showing a grid of 1x1 structures. Each cell contains a 1x1 structure, which is a MATLAB struct. The first row shows a structure with one field, an empty array '[]'. The other rows show structures with multiple fields, though the specific field names and values are not legible in this view.

	1	2	3	4	5	6
1	1x1 struct	[]	1x1 struct	1x1 struct	1x1 struct	1x1 struct
2	1x1 struct	1x1 struct	1x1 struct	1x1 struct	1x1 struct	1x1 struct
3	1x1 struct	1x1 struct	1x1 struct	1x1 struct	1x1 struct	1x1 struct
4	1x1 struct	1x1 struct	1x1 struct	1x1 struct	1x1 struct	1x1 struct
5	1x1 struct	1x1 struct	1x1 struct	1x1 struct	1x1 struct	1x1 struct
6	1x1 struct	1x1 struct	1x1 struct	1x1 struct	1x1 struct	1x1 struct
7	1x1 struct	1x1 struct	1x1 struct	1x1 struct	1x1 struct	1x1 struct
8	1x1 struct	1x1 struct	1x1 struct	1x1 struct	1x1 struct	1x1 struct
9	1x1 struct	1x1 struct	1x1 struct	1x1 struct	1x1 struct	1x1 struct
10	1x1 struct	1x1 struct	1x1 struct	1x1 struct	1x1 struct	1x1 struct
11	1x1 struct	1x1 struct	1x1 struct	1x1 struct	1x1 struct	1x1 struct
12	1x1 struct	1x1 struct	1x1 struct	1x1 struct	1x1 struct	1x1 struct
13	1x1 struct	1x1 struct	1x1 struct	1x1 struct	1x1 struct	1x1 struct
14	1x1 struct	1x1 struct	1x1 struct	1x1 struct	1x1 struct	1x1 struct
15	1x1 struct	1x1 struct	1x1 struct	1x1 struct	1x1 struct	1x1 struct
16	1x1 struct	1x1 struct	1x1 struct	1x1 struct	1x1 struct	1x1 struct
17	1x1 struct	1x1 struct	1x1 struct	1x1 struct	1x1 struct	1x1 struct
18	1x1 struct	1x1 struct	1x1 struct	1x1 struct	1x1 struct	1x1 struct
19	1x1 struct	1x1 struct	1x1 struct	1x1 struct	1x1 struct	1x1 struct
20	1x1 struct	1x1 struct	1x1 struct	1x1 struct	1x1 struct	1x1 struct

Figure 16: Structure representing all dataset cleaned and loaded on MATLAB after the first two steps of pre-processing phase.

In particular, the clean_dataset structure was made by (43x6) substructures with their own fields (Figure 17). The major fields of interest are: 'nbchan' and 'chanlocs' indicating respectively the number and name of channels left after cleaning, 'srate' denoting the sampling rate of the data, 'pnts' showing the number of points sampled and 'xmax' indicating the number of seconds left for each audio after the automatic cleaning phase. In fact, these fields vary in each dataset due to Spectral Thresholding and ASR algorithms action.

The screenshot shows a MATLAB Variables window titled 'Variables - clean_dataset{42, 3}'. It displays a list of fields and their corresponding values for the variable 'clean_dataset{42, 3}'. The fields include metadata like 'setname', 'filename', 'filepath', 'subject', 'group', 'condition', 'session', 'comments', and 'nbchan'. It also lists recording parameters such as 'trials', 'pnts', 'srate', 'xmin', and 'xmax'. The 'data' field is a 4x9105 single matrix. Other fields include 'icaact', 'icawinv', 'icasphere', 'icaweights', 'icachansind', 'chanlocs', 'urchanlocs', 'chaninfo', 'ref', 'event', 'urevent', 'eventdescription', 'epoch', 'epochdescription', 'reject', 'stats', 'specdata', and 'specinfo'.

Field	Value
setname	"
filename	"
filepath	"
subject	"
group	"
condition	"
session	[]
comments	"
nbchan	4
trials	1
pnts	9105
srate	256
xmin	0
xmax	35.5641
times	1x9105 double
data	4x9105 single
icaact	[]
icawinv	[]
icasphere	[]
icaweights	[]
icachansind	[]
chanlocs	1x4 struct
urchanlocs	[]
chaninfo	1x1 struct
ref	'common'
event	1x17 struct
urevent	[]
eventdescription	1x3 cell
epoch	[]
epochdescription	0x0 cell
reject	1x1 struct
stats	1x1 struct
specdata	[]
specinfo	[]

Figure 17: Example of structure fields of audio 3 of volunteer number 42.

The third and final step of pre-processing accomplished with the EEGLAB approach consists of filtering the datasets. This is required after a quick manual inspection of the structures. First, it could be seen that the automatic cleaning failed for 3 of the 258 datasets, leading us to decide to exclude the entire subject if at least one of the six audios was corrupted. This process thus reduced the number of subjects in the study from 43 to 40. After that we noticed that many datasets did not contain all four channels recorded via Muse Headband, especially most datasets did not report at least one of the two front channels AF7 and AF8. This led us to decide to conduct the study carried out with the EEGLAB approach with TP9 and TP10 channels only, since the temporal lobe is mostly responsible for brain responses to sound stimuli as well. For this reason, we dedicated a small part of the script to verify the presence of both temporal channels in each dataset. If the latter condition was not met, we decided to remove all datasets of that

particular subject from the study. This resulted in the reduction of subjects from 40 to 37, for a total of 222 datasets (33 subjects x 6 audios) (Figure 18).

```

%% Check Dataset with TP9-TP10 %%

count = 1;
for ii = 1:size(clean_dataset,1)
    for jj = 1:size(clean_dataset,2)
        app = length(clean_dataset{ii, jj}.chanlocs);
        for hh = 1:app
            b.elem{count, hh} = clean_dataset{ii, jj}.chanlocs(hh).labels; %creazione struttura%
        end
        count = count+1;
    end
end

for jj=1:size(b.elem,1)
    for ii=1:size(b.elem,2)
        TP9(jj,ii)=strcmp('TP9',b.elem{jj,ii});
        AF7(jj,ii)=strcmp('TP10',b.elem{jj,ii});
        AF8(jj,ii)=strcmp('AF8',b.elem{jj,ii});
        TP10(jj,ii)=strcmp('TP10',b.elem{jj,ii});
    end
end

GOOD_TP9=sum(sum(TP9==1)); % Numero di TP9 totali presenti %
GOOD_TP10=sum(sum(TP10==1)); % Numero di TP10 totali presenti %
sommacolonne_TP9=sum(TP9,2);
BAD_TP9=find(sommacolonne_TP9==0); % Per sapere i dataset senza TP9 %
sommacolonne_TP10=sum(TP10,2);
BAD_TP10=find(sommacolonne_TP10==0); % Per sapere i dataset senza TP10 %
SUB_TO_REMOVE_TP9= unique(ceil(BAD_TP9/6)); % Per capire quali soggetti (riga) eliminare %
SUB_TO_REMOVE_TP10= unique(ceil(BAD_TP10/6)); % Per capire quali soggetti (riga) eliminare %
SUB_TO_REMOVE= unique(horzcat(SUB_TO_REMOVE_TP9', SUB_TO_REMOVE_TP10'));

%% Filtration Dataset Without TP9 or TP10 %%

for zz=1:length(SUB_TO_REMOVE)
    clean_dataset(SUB_TO_REMOVE(zz),:)=[];
    SUB_TO_REMOVE=SUB_TO_REMOVE-1;
end

```

Figure 18: Script devoted to dataset filtration.

2.2.2. AUTOREJECT

The second approach proposed by our study requires the use, at least in a first part, of Python. Python is a popular high-level programming language known for its simplicity and readability. It was created by Guido van Rossum and first released in 1991. Python's design philosophy emphasizes code readability, making it easy to write and understand. Python has gained significant popularity due to its versatility and broad range of applications. It is used in web development, data analysis, scientific computing, artificial intelligence, automation, and more. The language provides a comprehensive standard library

and a vast ecosystem of third-party libraries and frameworks that extend its capabilities for various tasks.

M. Jas et al. present an automated algorithm for unified rejection and repair of bad trials in magnetoencephalography (MEG) and electroencephalography (EEG) signals [50]. This method capitalizes on cross-validation in conjunction with a robust evaluation metric to estimate the optimal peak-to-peak threshold, a quantity commonly used for identifying bad trials in M/EEG. This approach is then extended to a more sophisticated algorithm which estimates this threshold for each sensor yielding trial-wise bad sensors. Depending on the number of bad sensors, the trial is then repaired by interpolation or by excluding it from subsequent analysis. Figure 19 shows a typical repair action of signals using autoreject algorithm.

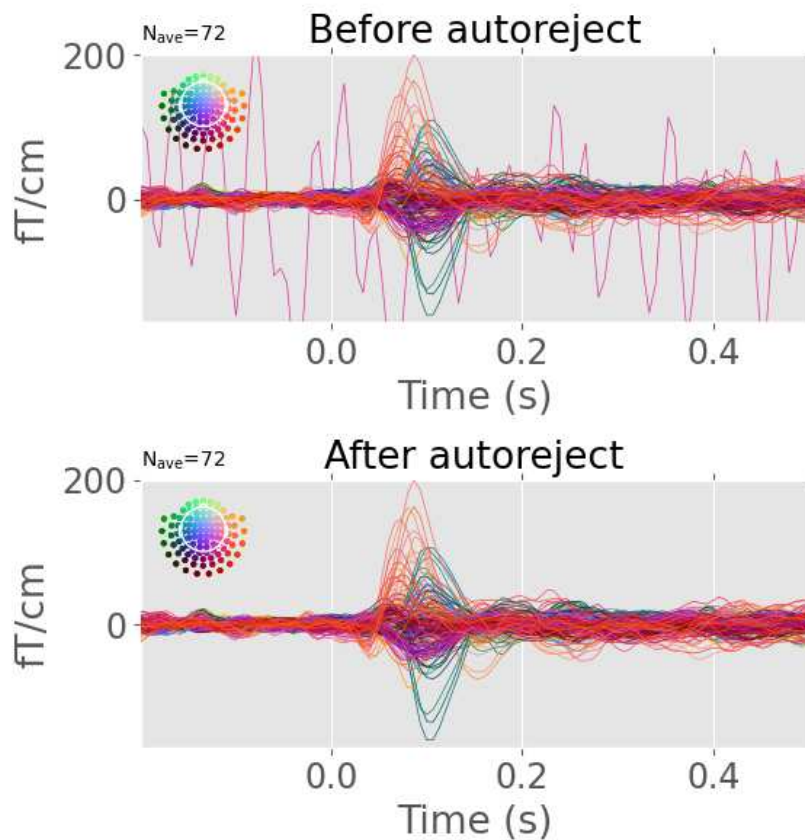


Figure 19: Example of signals repaired with Autoreject Method [51].

Autoreject is a Python library designed to automatically reject or exclude noisy or artifactual segments from electroencephalography (EEG) or magnetoencephalography (MEG) data. It provides a data-driven approach to identify and discard such segments, improving the quality of the recorded neural signals. The autoreject algorithm works by utilizing machine learning techniques to estimate the quality of individual segments or epochs of EEG/MEG data. It leverages the concept of "bad channels" and "bad segments" to identify and exclude the problematic data. The algorithm learns from the data itself to determine the criteria for identifying bad segments, rather than relying on pre-defined thresholds or rules [50]. The autoreject algorithm typically consists of the following steps:

- Estimation of channel-wise and segment-wise quality measures: Autoreject computes quality measures, such as the root mean square (RMS) of the signal, for each channel and segment of the data. These measures provide an indication of the presence of artifacts.
- Dimensionality reduction: The algorithm performs dimensionality reduction techniques, such as principal component analysis (PCA), to reduce the dimensionality of the data while retaining important information. This step helps in capturing the dominant variability in the data and identifying the presence of artifacts.
- Model fitting: Autoreject fits a model, such as a support vector machine (SVM), to the reduced-dimensional data. The model learns the relationship between the extracted features and the presence of artifacts.
- Cross-validation and rejection threshold estimation: Autoreject uses cross-validation techniques to estimate optimal thresholds for rejecting segments based on the learned model. It finds the threshold that maximizes the trade-off between retaining valid data and excluding artifacts.
- Artifact rejection: Once the rejection thresholds are determined, autoreject applies them to the full dataset. It marks and excludes segments that exceed the thresholds, effectively rejecting artifacts from the data.

By automatically identifying and rejecting artifacts, the autoreject library helps researchers and practitioners pre-process EEG/MEG data more efficiently. It reduces the manual effort required for artifact detection and improves the reliability of subsequent analyses performed on the cleaned data [52].

Thus, the first phase of this second approach involved importing the data captured with Muse Headband into Python v3.8. As in the approach with EEGLAB, the utilization of a notch filter to eliminate power line noise (50 Hz), a high-pass filter set at 0.2 Hz to eliminate DC offset and low-frequency skin potential artifacts, as well as a low-pass filter set at 47 Hz to eliminate high-frequency noise was used. Then the second phase could be performed. The Autoreject algorithm was used in order to divide the signal into epochs of 2 seconds, to clean (epochs_clean) and repair the raw data (epochs_rec). In particular, Figure 20 shows several parameters were set on Python in order to perform the automatic data cleaning.

```
epochs = mne.Epochs(raw, new_events, tmin=-1.0, tmax=1.0, reject=None, preload=True)
reject_criteria = dict(eeg=100e-6) # 200  $\mu$ V
flat_criteria = dict(eeg=1e-6) # 1  $\mu$ V
epochs_clean = mne.Epochs(raw, new_events, tmin=-1.0, tmax=1.0,
                          reject=reject_criteria, flat=flat_criteria, reject_by_annotation=False, preload=True)
epochs_clean.plot(n_epochs=10)
ar = AutoReject()
epochs_rec = ar.fit_transform(epochs)
```

Figure 20: Autoreject algorithm used to clean, remove and repair the raw data.

Finally, the processed data was exported in .mat format so that it could be simply loaded into MATLAB and proceeded with the last pre-processing step. Once the second pre-processing phase was completed, the data based on the two different approaches were examined and analysed in data processing. The autoreject approach allow us to proceed with the study with all the subject (43) and datasets (258) recorded with Muse Headband.

2.3. Data Processing

Once the pre-processing phase was finished, we entered the data processing phase. The latter was conducted totally on MATLAB v2020a. As a first step the power spectral density (PSD) of the cleaned data were calculated using MATLAB's pwelch

function on 1-s hamming tapered windows (42.5 dB sidelobe attenuation) with 50% overlap [53]. The pwelch method smooths over non-systematic noise and is more robust compared to the more popular FFT method that is more sensitive to noise and non-stationarities. Figure 21 shows the code for PSD calculation.

```
%% PSD Calculator %%

df = 0.5;
fmin = 0.2;
fmax = 47;
fs = 256;
nfft = fs/df-1;
noverlap = (nfft-1)/2;
window = hanning(nfft);

for k = 1 : size(clean_dataset,1)
    for l=1:6

        data{k,l} = clean_dataset{k,l}.data';
        tempo{k,l} = clean_dataset{k,l}.times';
        [pxx1,f] = pwelch(data{k,l}(:,1),window,noverlap,nfft,fs);
        if size(clean_dataset{k,l}.data,1) == 3
            [pxx2,f] = pwelch(data{k,l}(:,3),window,noverlap,nfft,fs);
        elseif size(clean_dataset{k,l}.data,1) == 4
            [pxx2,f] = pwelch(data{k,l}(:,4),window,noverlap,nfft,fs);
        else
            [pxx2,f] = pwelch(data{k,l}(:,2),window,noverlap,nfft,fs);
        end

        li = f>=fmin & f<=fmax;
        f = f(li);
        pxx_1(k,l,:) = pxx1(li);
        pxx_2(k,l,:) = pxx2(li);

    end
end
```

Figure 21: MATLAB code for PSD calculation.

The next step performed in our study was the rejection of outliers signals. Outliers are data points that significantly deviate from the general pattern or behavior of a dataset. Outlier removal refers to the process of identifying and eliminating these extreme values from a group of data. In statistical analysis, outliers can have a significant impact on the results and interpretations. They can distort statistical estimation such as the mean (average) and standard deviation, leading to misleading conclusions. Outliers may arise due to various reasons, including measurement errors, data entry mistakes, or genuine extreme observations. In order to remove outliers we decided to use the MATLAB function *'rmoutliers.m'*, as depicted in Figure 22.

```
%% Outliers Removal %%  
  
for tt = 1:6  
    psdAudio1 = squeeze(pxx_1(:,tt,:));  
    out_rem_dataAudio1{tt} = rmoutliers(psdAudio1);  
    psdAudio2 = squeeze(pxx_2(:,tt,:));  
    out_rem_dataAudio2{tt} = rmoutliers(psdAudio2);  
end
```

Figure 22: Script section in which the outliers were removed.

Once we removed the outliers from our data, we ended up with statistically meaningful datasets. We then checked whether our data were Gaussian, thus normally distributed, or non-Gaussian. To do this we performed one parametric test called the Shapiro-Wilk Test.

The Shapiro-Wilk test is a statistical test used to assess whether a given dataset follows a normal distribution. It was developed by Samuel Shapiro and Martin Wilk in 1965. The test is based on the null hypothesis that the population from which the sample is drawn follows a normal distribution. The alternative hypothesis is that the population does not follow a normal distribution. The Shapiro-Wilk test provides a p-value that indicates the strength of evidence against the null hypothesis. Here's how the Shapiro-Wilk test works:

- Hypotheses:
 - Null Hypothesis (H_0): The data are normally distributed.
 - Alternative Hypothesis (H_1): The data are not normally distributed.
- Calculation: The test involves calculating the Shapiro-Wilk test statistic, denoted by W . The test statistic is computed using the observed data values and their corresponding expected values under the assumption of normality. The expected values are obtained by sorting the data in ascending order and calculating the expected cumulative proportions assuming a normal distribution.
- P-value interpretation: The test statistic W is compared to critical values from the Shapiro-Wilk distribution. If the p-value is less than a predetermined significance level ($\alpha = 0.05$), the null hypothesis is rejected, suggesting that

the data do not follow a normal distribution. Conversely, if the p-value is greater than the significance level, there is insufficient evidence to reject the null hypothesis, implying that the data may be normally distributed.

It's important to note that the Shapiro-Wilk test is most effective for moderate to large sample sizes (typically recommended for sample sizes up to around 5,000 observations). Figure 23 shows how it was used within our code. This test is performed for each of the two-approach proposed in the thesis with the difference that for Autoreject Method also the Gaussian check for the frontal electrode has been made since the availability of the data recorded by those electrodes. The 'ind_gauss1' and 'ind_gauss2' vectors output of the created code will indicate the number of Gaussian spectral lines on TP9 and TP10 electrodes compared to the total 93 spectral lines. This will let us know how normally our data are distributed along the 0.2-47 Hz frequency range.

```
%% Shapiro Test %%  
  
alfa = 0.05;  
  
for jj = 1:6  
    app1 = out_rem_dataAudio1{jj};  
    app2 = out_rem_dataAudio2{jj};  
    for pp=1:size(app1,2)  
        shapiro_test_1{jj}(pp) = swtest(app1(:,pp),alfa);  
        shapiro_test_2{jj}(pp) = swtest(app2(:,pp),alfa);  
    end  
    ind_gauss1{jj}(:)=find(~shapiro_test_1{jj});  
    ind_gauss2{jj}(:)=find(~shapiro_test_2{jj});  
end
```

Figure 23: Statistical Shapiro-Wilk Test performed on TP9 and TP10 electrodes.

2.4 Statistical Analysis

After the normality of our data was verified, a statistical test was performed, the One-Way ANOVA. This is a particular hypothesis test used to determine whether there is a statistically significant difference between the averages of three or more continuous data groups with respect to a category that differentiates them. In this type of situation, the category that differentiates the data groups is the independent variable

while the continuous data represent the dependent variable. The One-Way ANOVA test is a hypothesis test that accepts or rejects the null hypothesis:

$$H_0: \text{all averages are equal or } \mu_1 = \mu_2 = \mu_3 = \dots = \mu_n$$

and where the alternative hypothesis H_1 the averages are not all statistically equal. Given n sets of data, the ANOVA test allows us to determine whether at least one of the n averages is statistically different from the others. However, the ANOVA test does not say which of the averages is statistically different from the others. It only allows you to determine whether all of the averages are statistically the same or not. To figure out which averages are statistically different from the others, one could proceed with multiple t-tests. However, each t-test carries with it an uncertainty defined by the type 1 and type 2 errors that can occur in testing two averages. In performing a number of consecutive tests, the possibility of error accumulates making the multiple-test mechanism prone to non-negligible errors. In the One-Way ANOVA test, on the other hand, while comparing multiple data sets at the same time, the test error is kept low based on the significance level α chosen. This test is based on F-Statistic which is built on the homonym distribution. This distribution introduced by Fischer Snedecor is given by the ratio of two mutually independent distributions normalized with respect to their own number of degrees of freedom. In the specific case of a One-Way ANOVA test, the two functions express, respectively, the variability between groups of data and the variability of the entire data set at hand. These variabilities are expressed in terms of the quadratic sums SSB and SSW . SSW (squared sum within groups) is the sum of variations existing between individual groups (eq. 2.1). Given n groups of data:

$$SSW = SS_1 + SS_2 + SS_3 + \dots + SS_n \quad (2.1)$$

where each squared sum SS is given by (eq. 2.2):

$$SS_n = \sum_{i=1}^m (y_i - \bar{y}_n)^2 \quad (2.2)$$

Therefore, SSW is given by (eq. 2.3):

$$SSW = SS1 + SS2 + \dots + SSn = \sum_{i=1}^m (y_i - \bar{y}_1)^2 + \sum_{i=1}^m (y_i - \bar{y}_2)^2 + \dots -$$

$$\sum_{i=1}^m (y_i - \bar{y}_n)^2 = \sum_{i=1, k=1}^{m, n} (y_{i,k} - \bar{y}_k)^2 \quad (2.3)$$

The SSW is an indicative function of how much variation there is within the available data sets. An SSW that is too large is indicative of one or more extremely dispersed groups. This function is characterized by a number of degrees of freedom. As N observations on n mean values are compared, the number of degrees of freedom will be given by N-n. If we were dealing with n groups all of the same size m, then the number of degrees of freedom N-n would coincide with n(m-1).

The SSB (squared sum between groups), on the other hand, is the quadratic sum of the differences of the mean of each group with the mean of the averages of the groups. It is indicative of the dispersion of the averages of the groups from the total average (eq. 2.4):

$$SSB = \sum_{i=1}^n m(\bar{y}_i - \bar{y})^2 \quad (2.4)$$

As SSB is defined, its degrees of freedom are n-1 where n are the groups available and independent of each other and 1 is the total mean. SSB and SSW both contribute to the TSS, total sum of squared, (eq. 2.5):

$$TSS = SSW + SSB \quad (2.5)$$

The TSS thus takes into account both types of dispersion: dispersion between groups and dispersion within groups. F statistics is based on the ratio of two chi-square functions, and that a chi-square function is given by the ratio of a quadratic function such as SSW and SSB with respect to its degrees of freedom. In the case of a One-Way ANOVA test, the variable F will be given by (eq. 2.6-2.7):

$$F = \frac{S_B^2}{S_W^2} \quad (2.6)$$

where:

$$\begin{aligned} S_B^2 &= \frac{SSB}{n-1} \\ S_W^2 &= \frac{SSW}{N-n} \end{aligned} \quad (2.7)$$

S_B^2 and S_W^2 are quadratic averages (mean square between samples and mean square within samples). The function F thus defined is a function that increases in value when the variation between groups is greater than the variation within groups. If in performing the hypothesis test the value of the variable F calculated from the ratio of S_B^2 and S_W^2 at a given confidence level exceeds the tabulated values for that confidence level and for the $n(m-1)$ and $n-1$ degrees of freedom then the hypothesis must be rejected. This is because the p-value will be less than the chosen significance level and therefore the probability of obtaining a distribution of groups even more extreme than the one under study is very low. Anyway, the ANOVA test can be used only if certain conditions are met:

- The data sets must be normally distributed. In fact, the ANOVA test can handle even small deviations from normality without having much effect on the possibility of committing type 1 errors. Should the data show large deviations from a Gaussian trend or should it not be possible to transform them as such a different test such as the Kruskal-Wallis H test must be used.
- The data sets must be independent of each other. This condition is necessary to be able to perform the hypothesis test.
- Homogeneity of the variances of the groups tested. This means that the variances of the populations to which the groups belong must be equal to each other. If there is any doubt that the variances may be different from each other,

a test of variances (Levene's test) can be performed. If the variances are different other tests must be used to test the null hypothesis (Tukey HSD test).

By default, 'anoval.m' function returns two figures. One is the standard ANOVA table, and the other one is the box plots of data by group. The ANOVA table captures the variability in the model by source, the F-statistic for testing the significance of this variability, and the p-value for deciding on the significance of this variability. The p-value returned by *anoval* depends on assumptions about the random disturbances ε_{ij} in the model equation. For the p-value to be correct, these disturbances need to be independent, normally distributed, and have constant variance. The standard ANOVA table has this form (Figure 24):

Source	SS	df	MS	F	p-value
Group (Between)	SSR	$k - 1$	$MSR = SSR / (k - 1)$	MSR / MSE	$P(F_{k-1, N-k}) > F$
Error (Within)	SSE	$N - k$	$MSE = SSE / (N - k)$		
Total	SST	$N - 1$			

Figure 24: Standard ANOVA Table [54].

'anoval' returns the standard ANOVA table as a cell array with six columns, as described in Table 2.

COLUMN	DEFINITION
Source	Source of the variability.
SS	Sum of squares due to each source.
df	Degrees of freedom associated with each source. Suppose N is the total number of observation and k is the number of groups. Then, $N - k$ is the within-groups degrees of freedom (Error), $k - 1$ is the between-groups degrees of freedom (Columns), and $N - 1$ is the total degrees of freedom: $N - 1 = (N - k) + (k - 1)$.
MS	Mean Squares for each source, which is the ratio SS/df.
F	F -statistic, which is the ratio of the mean squares.
Prob>F	p -value, which is the probability that the F -statistic can take a value larger than the computed test-statistic value. <i>anoval</i> derives this probability from the cdf of the F -distribution.

Table 2: Columns definition of ANOVA Table.

The rows of the ANOVA table show the variability in the data, divided by the source, Table 3.

ROW (SOURCE)	DEFINITION
Groups or Columns	Variability due to the differences among the group means (variability between groups).
Error	Variability due to the differences between the data in each group and the group mean (variability within groups).
Total	Total variability.

Table 3: Row definition of ANOVA Table.

3. RESULTS

The results found in this thesis will be discussed in this chapter where the differences in the two approaches used for dataset cleaning will be shown. As reported in the previous chapter, the analysis conducted by this study focused on only two of the four channels available for recording EEG signals using Muse Headband (AF7, AF8, TP9, TP10). This is because during data processing with EEGLAB, many datasets did not contain the frontal electrodes (AF7, AF8). Thus, in order to proceed with the study and comparison between the two proposed approaches, only channels TP9 and TP10 were considered.

3.1. Outliers Removal

Data in Table 4 were derived only after expressing PSD values in decibels. The initial dataset, i.e. the total number of subjects, consisted of 43 people. The EEGLAB approach brought it down to 37 subjects because of the parameters selected while the approach that used the AUTOREJECT algorithm was able to retain all 43 subjects. After the step of removing outliers we ended up with the values expressed in Table 4.

	EEGLAB						AUTOREJECT					
	S1	A1	S2	A2	S3	A3	S1	A1	S2	A2	S3	A3
TP9	21	19	22	14	17	15	19	19	23	19	24	23
TP10	21	19	17	16	18	17	22	23	21	18	20	20

Table 4: Number of subjects (datasets) remained after the outliers removal. Left part concerns the EEGLAB method while right part refers to AUTOREJECT's algorithm.

The results regarding the number of datasets rejected with the *rmoutliers.m* function in MATLAB shows that with the EEGLAB method there are more subjects discarded than with the AUTOREJECT method considering, of course, the fact that EEGLAB started with 37 datasets versus 43 in AUTOREJECT. To

go into details, EEGLAB method discards 228 of the 444 total PSDs (51.35%) while AUTOREJECT algorithm removes 265 of the 516 total PSDs (51.36%). In order to further notice this difference, it is important to show the graphs of the various PSDs for each subject before and after the application of the *rmoutliers.m* function. Now the results obtained by the first method, the EEGLAB method, will be displayed. Figure 25 and Figure 26 show plots of the PSDs of the subjects during the minute of Silence 2 (S2) stimuli before and after the outliers removal. It can be seen that datasets that deviate greatly from the normal curve of the subjects are removed and especially it is possible to appreciate how the Y-axis scale changes from initial values around 30 dB to initial values of 15 dB.

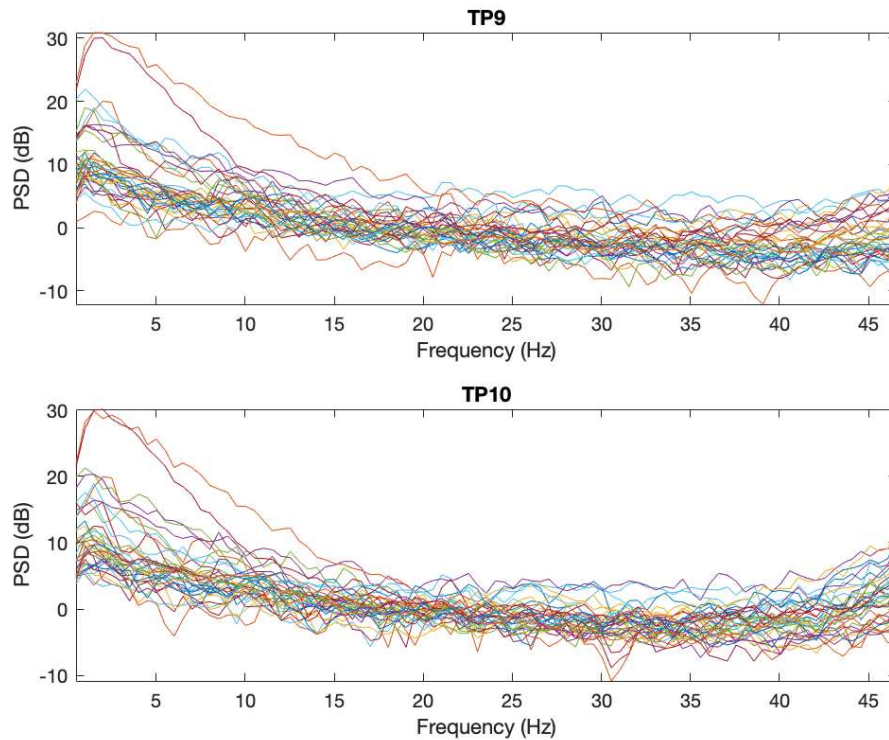


Figure 25: PSD expressed in dB of Silence 2 (S2) before Outliers Removal (EEGLAB method).

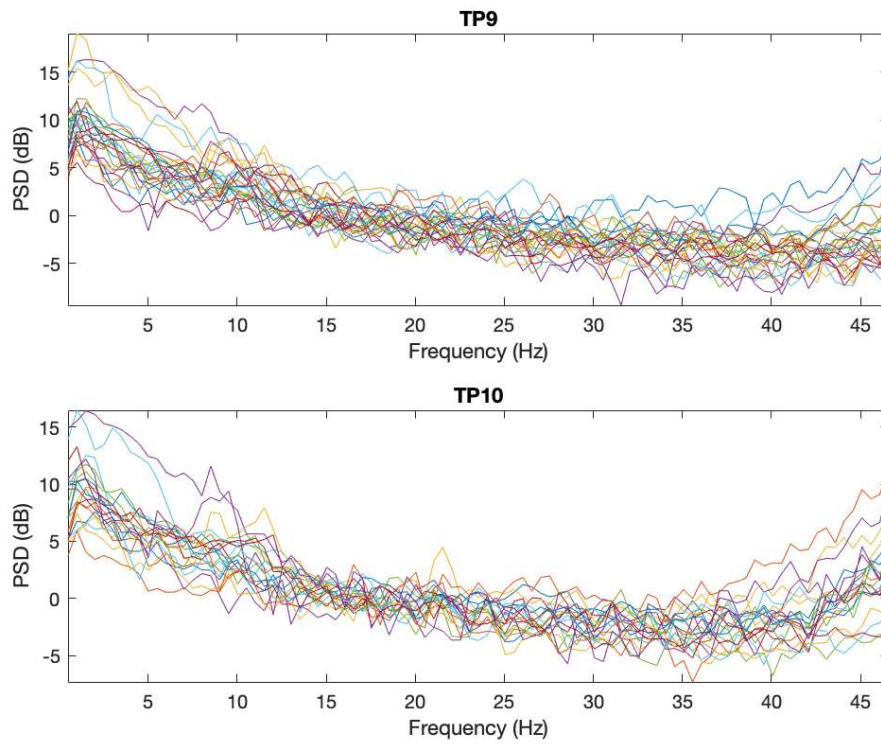


Figure 26: PSD expressed in dB of Silence 2 (S2) after Outliers Removal (EEGLAB method).

This trend is obviously repeated, although less visibly, even when we plot the averages over all subjects of the PSDs concerning the six proposed stimuli, Figure 27 and Figure 28 below.

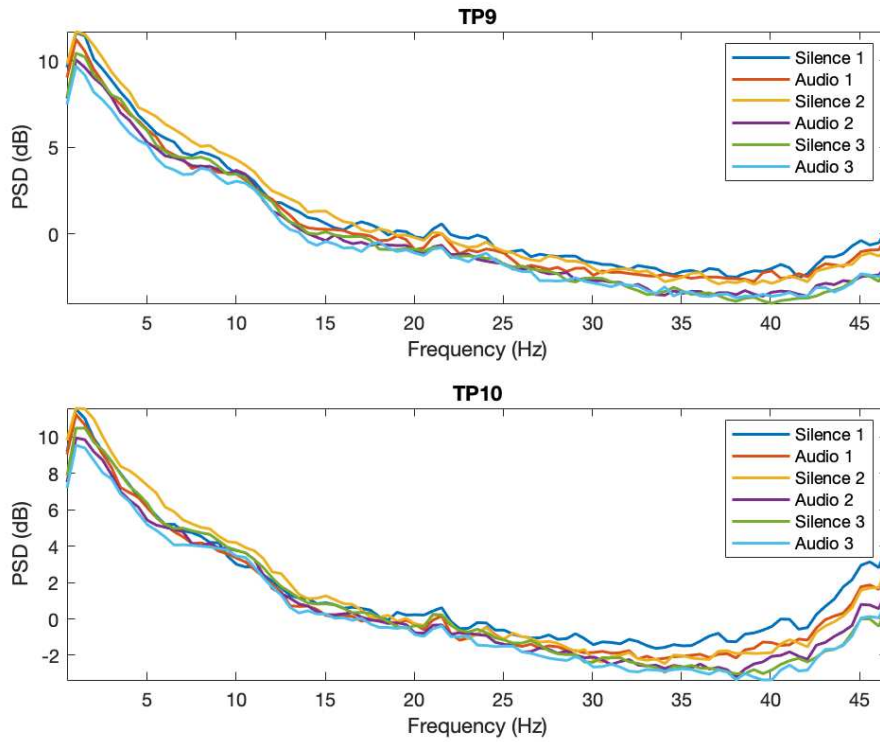


Figure 27: Mean PSD expressed in dB of all stimuli before Outliers Removal (EEGLAB method).

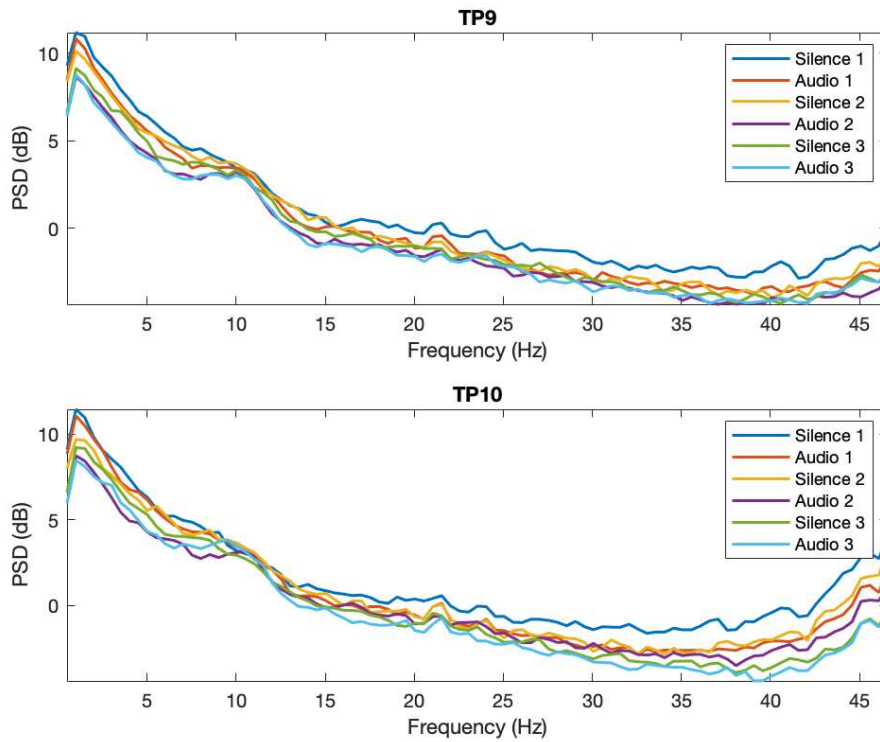


Figure 28: Mean PSD expressed in dB of all stimuli after Outliers Removal (EEGLAB method).

For a better visualization of the effect of outliers removal, reporting the graph of average PSDs on a linear scale may also be helpful. For this reason, Figure 29 and Figure 30 shows the effect of outliers removal, with better results on earlier frequency range.

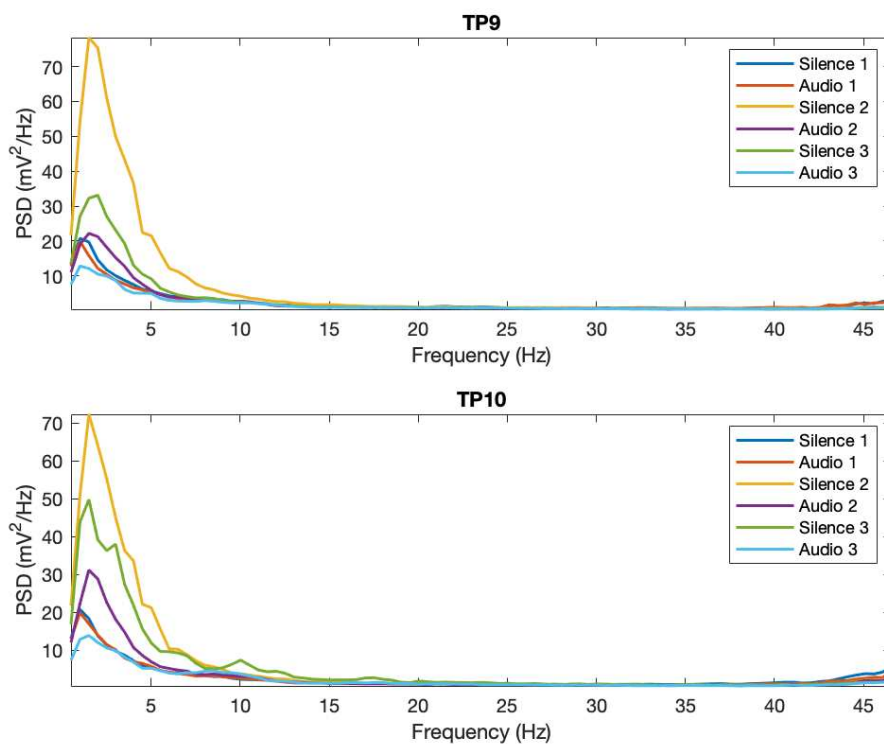


Figure 29: Mean PSD expressed in Linear Scale of all stimuli before Outliers Removal (EEGLAB method).

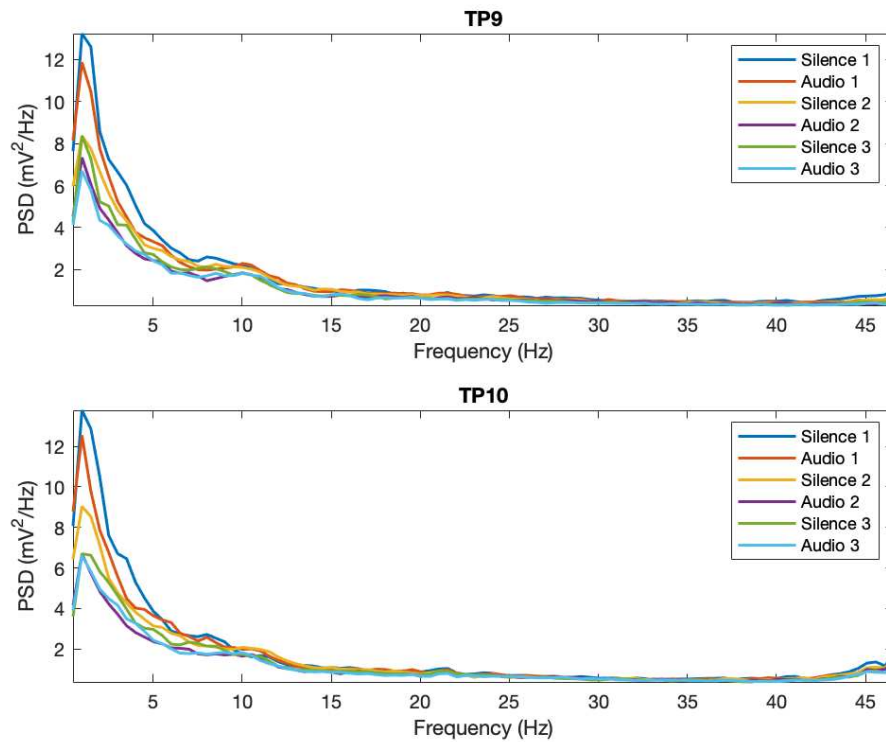


Figure 30: Mean PSD expressed in Linear Scale of all stimuli after Outliers Removal (EEGLAB method).

In this case it is possible to observe how the application of the *rmoutliers.m* function had its effects. In particular, it can be seen that in the first 0-10 Hz frequency range the PSD values go from peaks around 70 mV^2/Hz to values that are in the 2-12 mV^2/Hz range.

All the graphs shown so far are those concerning the first approach, that is, the EEGLAB approach. Now those concerning the AUTOREJECT algorithm will be reported. Figure 31 and Figure 32 display plots illustrating the Power Spectral Densities (PSDs) of the subjects' data during the Audio 3 (A3) stimuli, respectively before and after the removal of outliers.

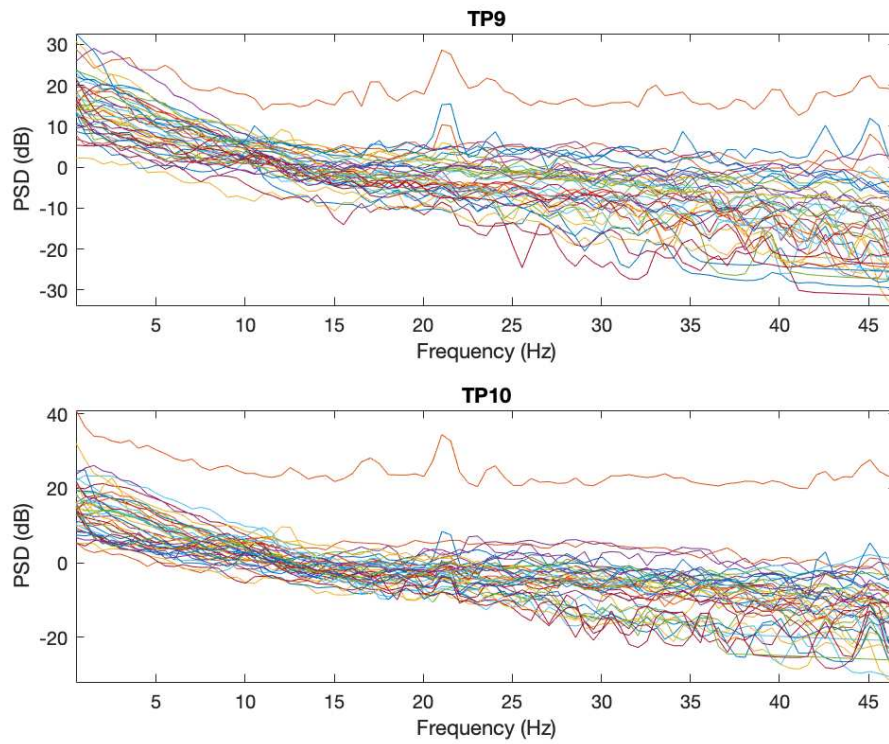


Figure 31: PSD expressed in dB of Audio 3 (A3) before Outliers Removal (AUTOREJECT method.)

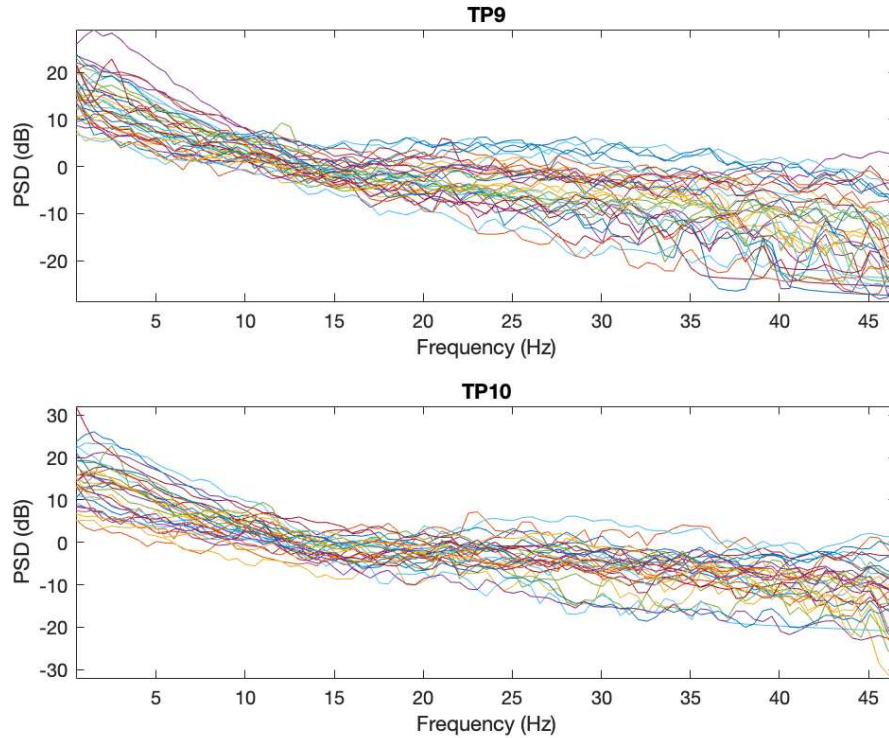


Figure 32: PSD expressed in dB of Audio 3 (A3) after Outliers Removal (AUTOREJECT method.)

These figures clearly demonstrate the exclusion of datasets that significantly deviate from the normal curve of the subjects. In particular, the 10-decibel decrease in the remaining curves can be seen. Even for the AUTOREJECT method, differences using the decibel scale to plot averages over subjects are not too remarkable, Figure 33 and Figure 34.

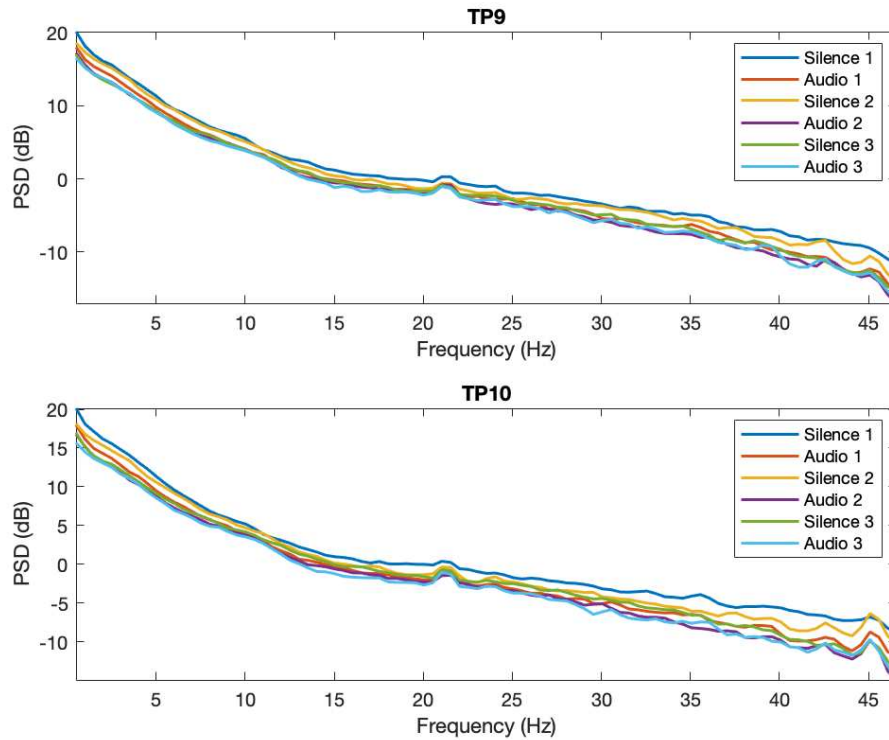


Figure 33: Mean PSD expressed in dB of all stimuli before Outliers Removal (AUTOREJECT method).

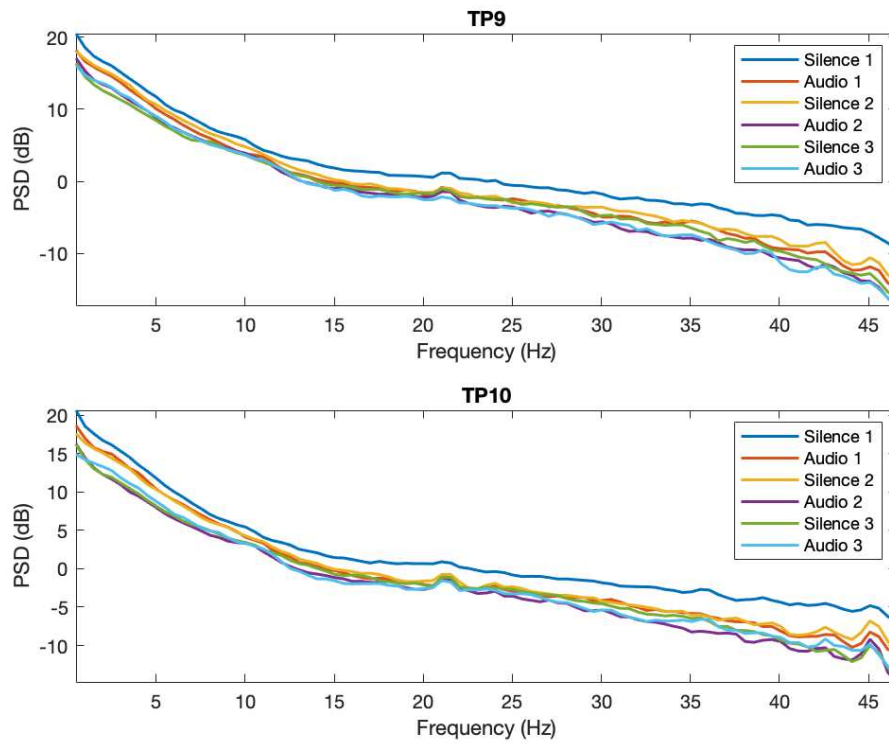


Figure 34: Mean PSD expressed in dB of all stimuli after Outliers Removal (AUTOREJECT method).

Therefore, we considered even with this method to report the same types of data but on a linear scale in order to better appreciate differences between graphs, Figure 35 and Figure 36 below.

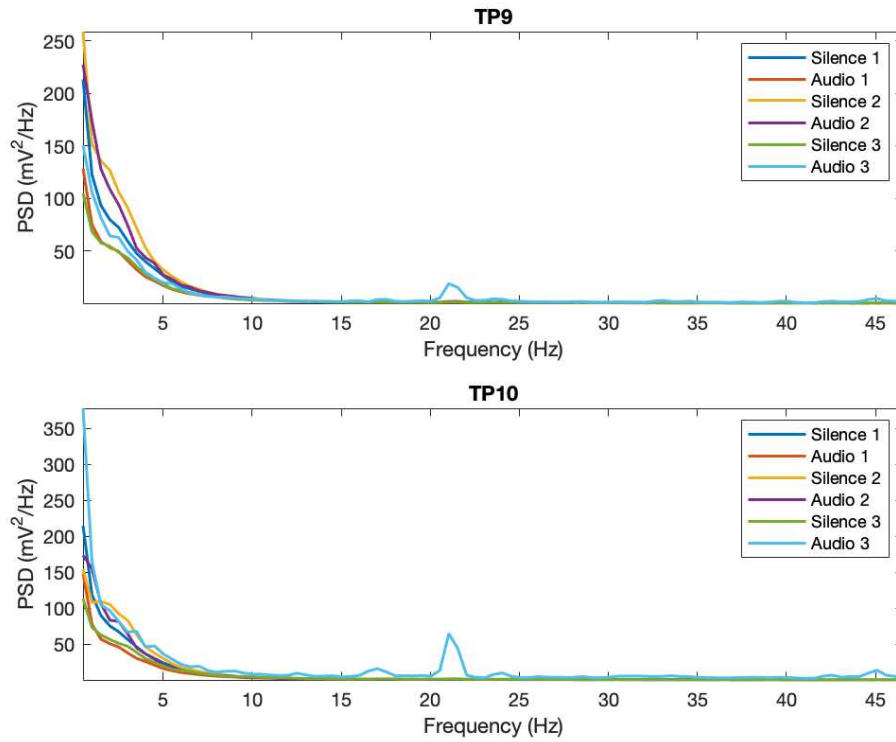


Figure 35: Mean PSD expressed in Linear Scale of all stimuli before Outliers Removal (AUTOREJECT method).

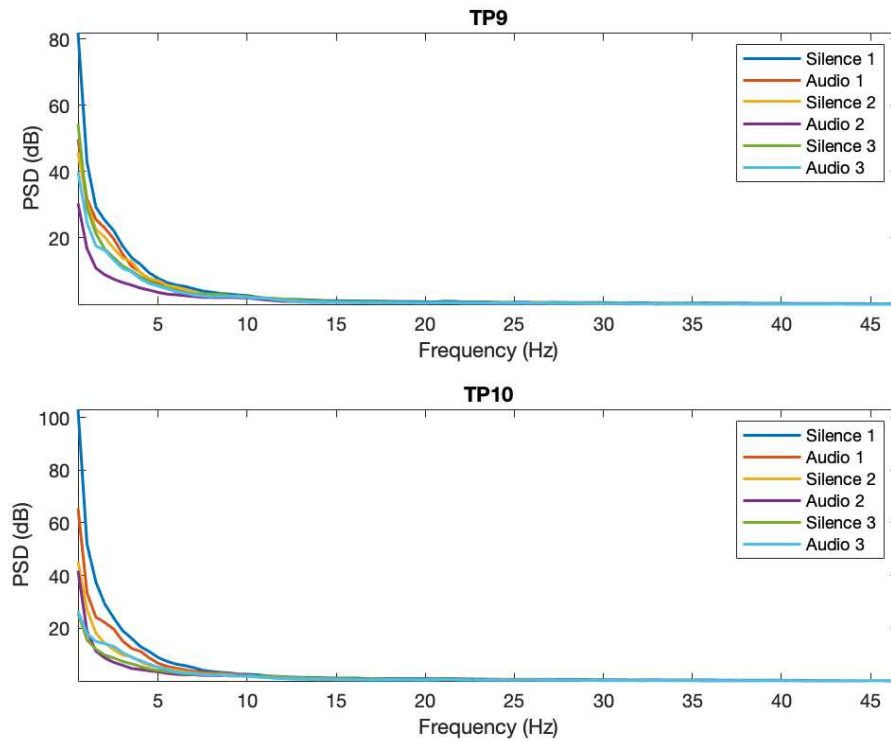


Figure 36: Mean PSD expressed in Linear Scale of all stimuli after Outliers Removal (AUTOREJECT method).

On a linear scale, it is possible to appreciate how the curves after outliers removal start from values around 80-100 mV²/Hz while without using outliers removal they would have started from values around 250-300 mV²/Hz.

3.2. Gaussian Data Analysis

In this section, we have summarized the results of the Gaussian Analysis performed both in the entire frequency range and in the alpha frequency range. The test performed to obtain this kind of information is the Shapiro-Wilk test, a parametric type test. The Shapiro-Wilk test is a statistical test used to assess whether a given dataset follows a normal distribution.

3.2.1. All Frequency Band

The data represented in Table 5 show the number of Gaussian Spectral Lines in a total of 93 for the Temporal Channels (TP9-TP10) by both the EEGLAB and AUTOREJECT methods.

	EEGLAB						AUTOREJECT					
	S1	A1	S2	A2	S3	A3	S1	A1	S2	A2	S3	A3
TP9	88	88	75	87	88	84	55	84	90	85	79	82
TP10	88	85	86	88	89	88	68	75	72	91	80	90

Table 5: Number of Gaussian Spectral Lines of data.

Starting with 93 spectral lines, it can be noticed that using EEGLAB method, 1034 on 1116 total spectral lines are of Gaussian type (92.65%). For what concern AUTOREJECT, 951 on 1116 total lines representing data with normal distribution (85.22%). The worst result for the EEGLAB method is obtained for stimulus S2 recorded from channel TP9, while the best one is stimulus S3 with 89 Gaussian spectral lines. Regarding AUTOREJECT, it is easy to see that the worst results

are obtained at stimulus S1 even though many of the spectral lines turn out to be in very high frequency bands and therefore not important for the purpose of our study, while the best results are obtained for Audio number 2. Thanks to the plots in Figure 37 and Figure 38, it is possible to see both the average accomplished over all subjects for each individual stimulus (S1, A1, S2, A2, S3, A3) by Temporal Channels and the spectral lines reflecting a normal distribution of the data for that frequency (red lines).

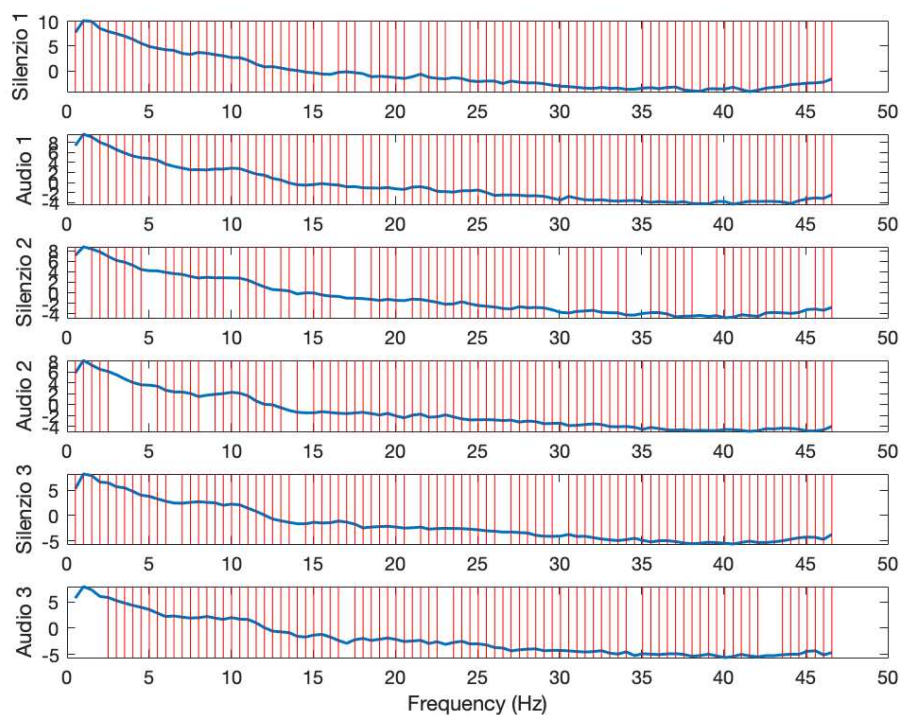


Figure 37: Mean PSD of the six stimuli with Gaussian Spectral Line (red lines) of TP9 channel (EEGLAB method.)

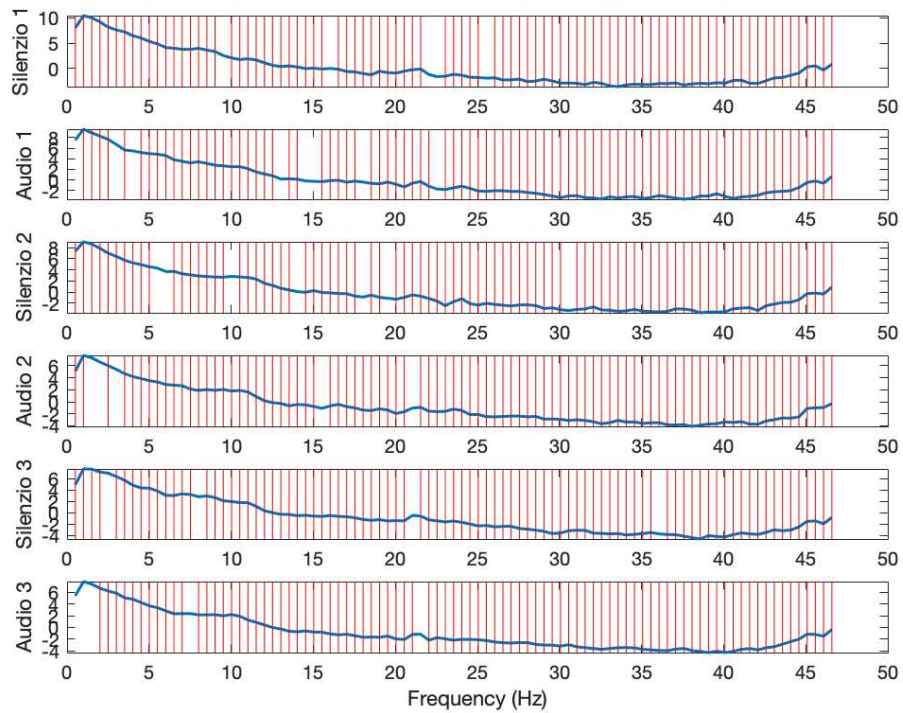


Figure 38: Mean PSD of the six stimuli with Gaussian Spectral Line (red lines) of TP10 channel (EEGLAB method).

These plots allow us to see that all frequency bands are generally Gaussian, and thus also the alpha band, which is the main frequency band for what concerns the physiological response on acoustic stimuli. The same will be conducted for Autoreject Method in Figure 39 and Figure 40 below.

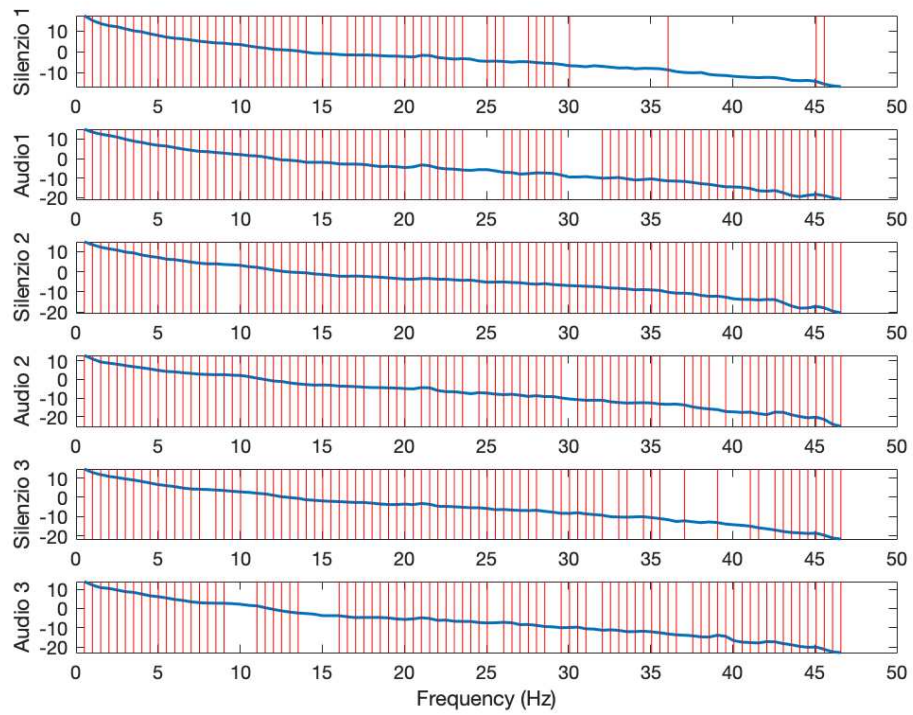


Figure 39: Mean PSD of the six stimuli with Gaussian Spectral Line (red lines) of TP9 channel (AUTOREJECT method).

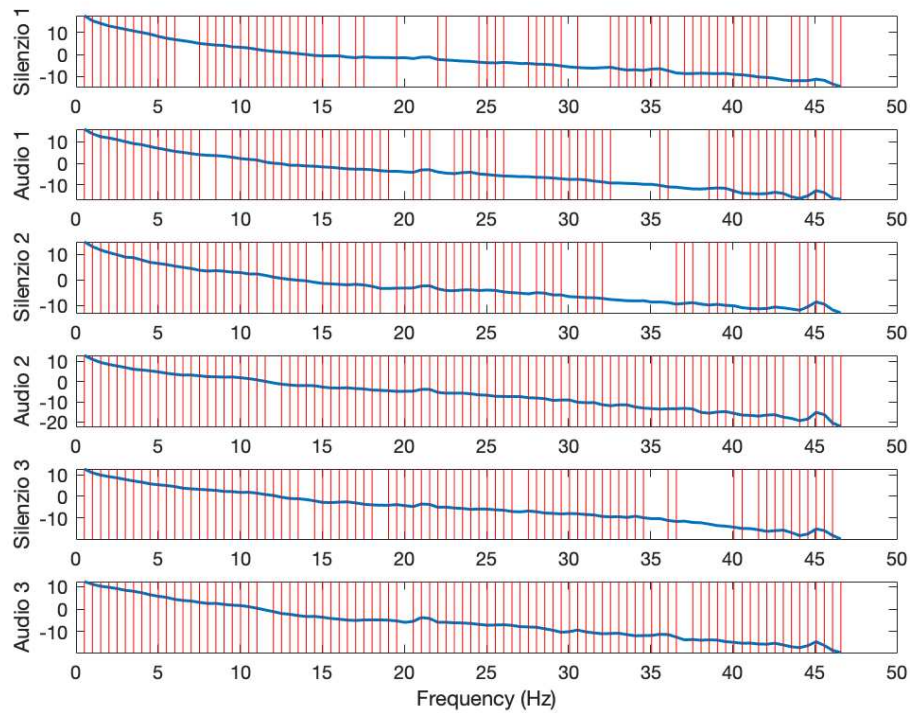


Figure 40: Mean PSD of the six stimuli with Gaussian Spectral Line (red lines) of TP10 channel (AUTOREJECT method).

Again, most spectral lines are retained after the Gaussianity test. This means that most of the data follow a normal distribution across the various frequencies.

3.2.2. Alpha Frequency Band

Since we are considering only the alpha frequency range, the number of total spectral line drops from 93 to only 11, as the frequency resolution is 0.5 Hz. So, the data represented in Table 6 show the number of Gaussian Spectral Lines for the Temporal Channels (TP9-TP10) by both the EEGLAB and AUTOREJECT methods.

	EEGLAB						AUTOREJECT					
	S1	A1	S2	A2	S3	A3	S1	A1	S2	A2	S3	A3
TP9	11	11	9	10	11	11	11	11	9	11	9	8
TP10	10	10	10	11	10	11	11	9	10	10	11	10

Table 6: Number of Gaussian Spectral Lines of data on Alpha Frequency Range.

Starting with 11 spectral lines, it can be seen in the table above that generally the data are Gaussian for both methods. In particular 125 on the total 132 line for EEGLAB Method (94.70%) and 120 on 132 total line for AUTOREJECT Algorithm (90.91%). The worst result for the EEGLAB method is the 9-line obtained for stimulus S2 recorded from TP9 channel, while the best are all stimuli that maintain the total 11-line on TP9 and TP10 electrodes. The worst result for the AUTOREJECT method is the only 8 Gaussian Spectral Lines available for A3 stimulus recorded with TP9 electrode. Thanks to the plots in Figure 41 and Figure 42, it is possible to see both the average accomplished over all subjects for each individual stimulus (S1, A1, S2, A2, S3, A3) by Temporal Channels and the spectral lines reflecting a normal distribution of the data for that frequency (red lines).

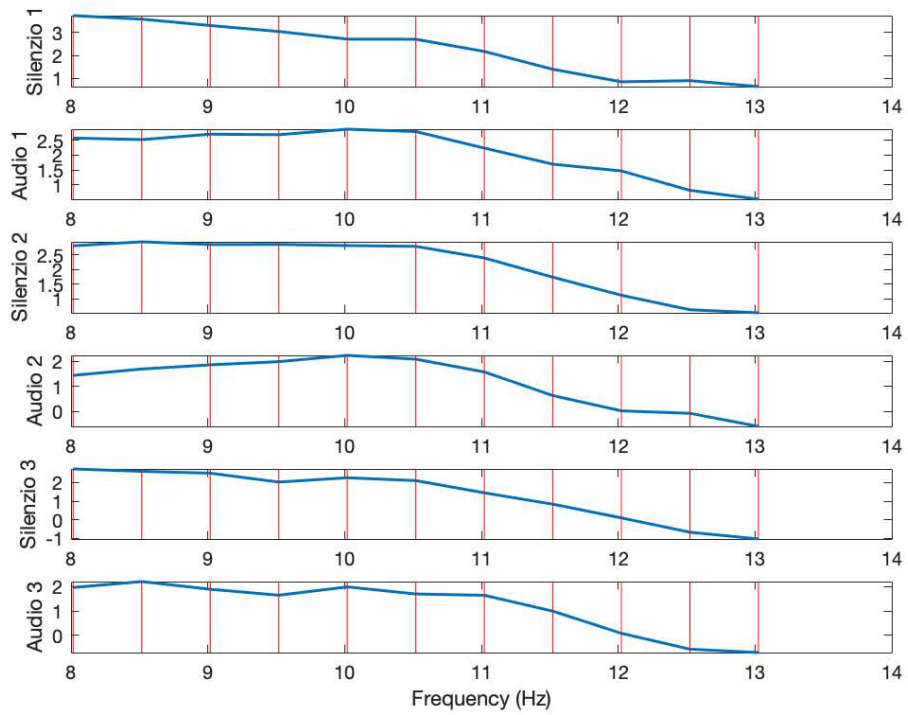


Figure 41: Mean PSD of the six stimuli with Gaussian Spectral Line (red lines) of TP9 channel on Alpha Band (EEGLAB method.)

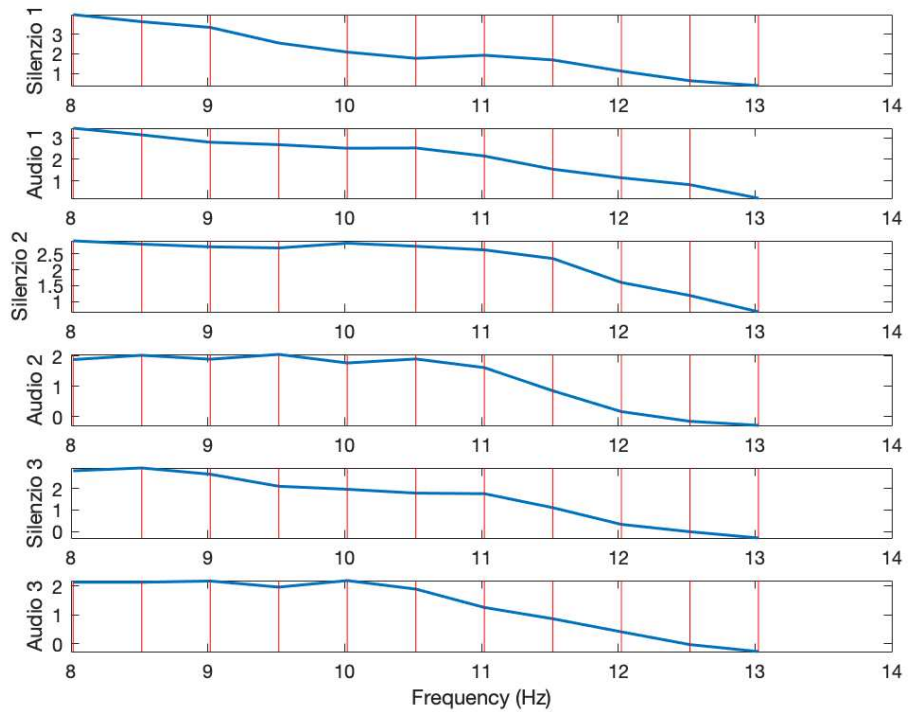


Figure 42: Mean PSD of the six stimuli with Gaussian Spectral Line (red lines) of TP10 channel on Alpha Band (EEGLAB method.)

These plots allow us to see that all frequency bands are generally Gaussian (94.70%), and thus also the alpha band, which is the main frequency band for what concerns the physiological response on acoustic stimuli. The same will be conducted for AUTOREJECT Method in Figure 43 and Figure 44 below.

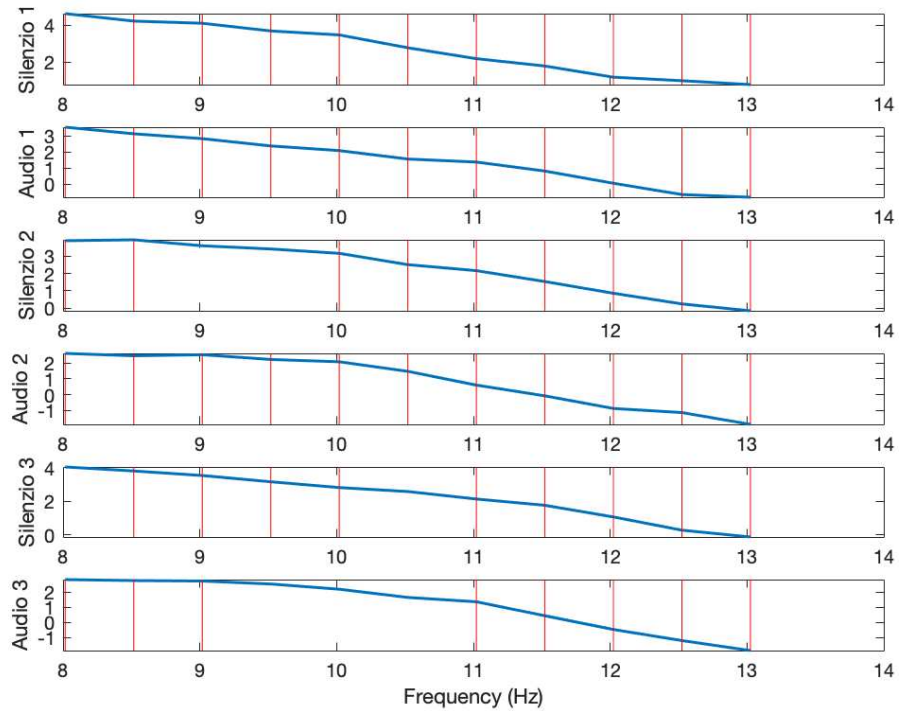


Figure 43: Mean PSD of the six stimuli with Gaussian Spectral Line (red lines) of TP9 channel on Alpha Band (AUTOREJECT method).

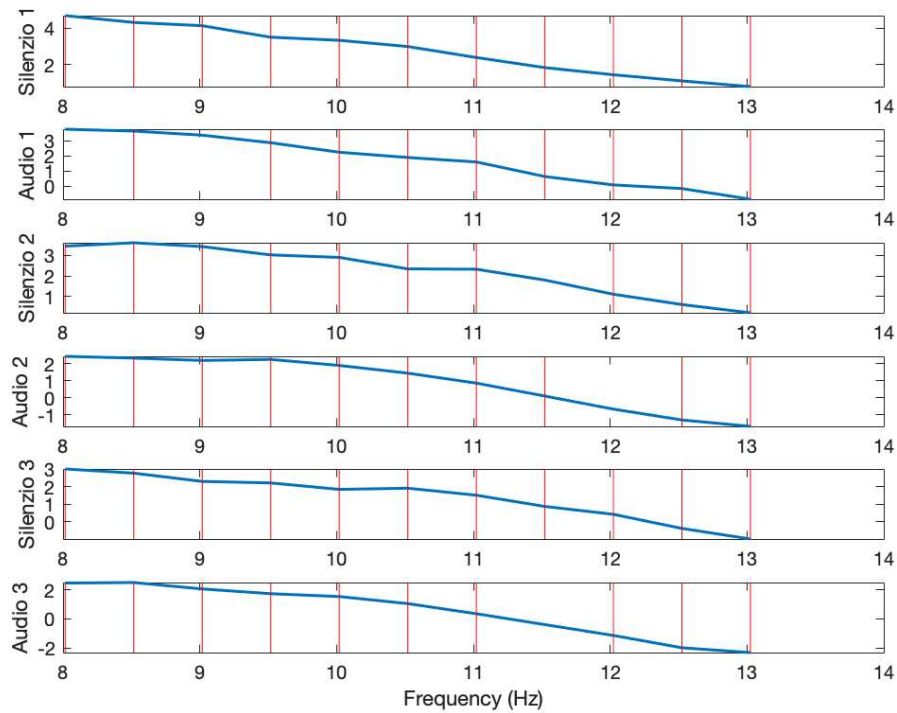


Figure 44: Mean PSD of the six stimuli with Gaussian Spectral Line (red lines) of TP10 channel on Alpha Band (AUTOREJECT method).

Again, most spectral lines are retained after the Gaussianity test. This means that most of the data (90.91%) follow a normal distribution across the various alpha frequencies.

3.3. Statistical Test: One-Way ANOVA

This section reports the results after applying the parametric One-Way ANOVA test. 2 images are shown for each method and electrode used. The first represents a box plot of the observations for each group in y . Box plot provide a visual comparison of the group location parameters. On each box the central red mark is the median and the edge of the box are the 25th and 75th percentiles. The whiskers extend to the most extreme data points that are not considered outliers. The second image is the standard ANOVA table. The test was conducted in the whole frequency band, in the alpha frequency band and also the relative alpha power.

3.3.1. All Frequency Band

Figure 45 shows the box plot of six stimuli proposed to volunteers recorded from TP9 electrode using EEGLAB method. Figure 46 exhibit the classical ANOVA Table parameters.

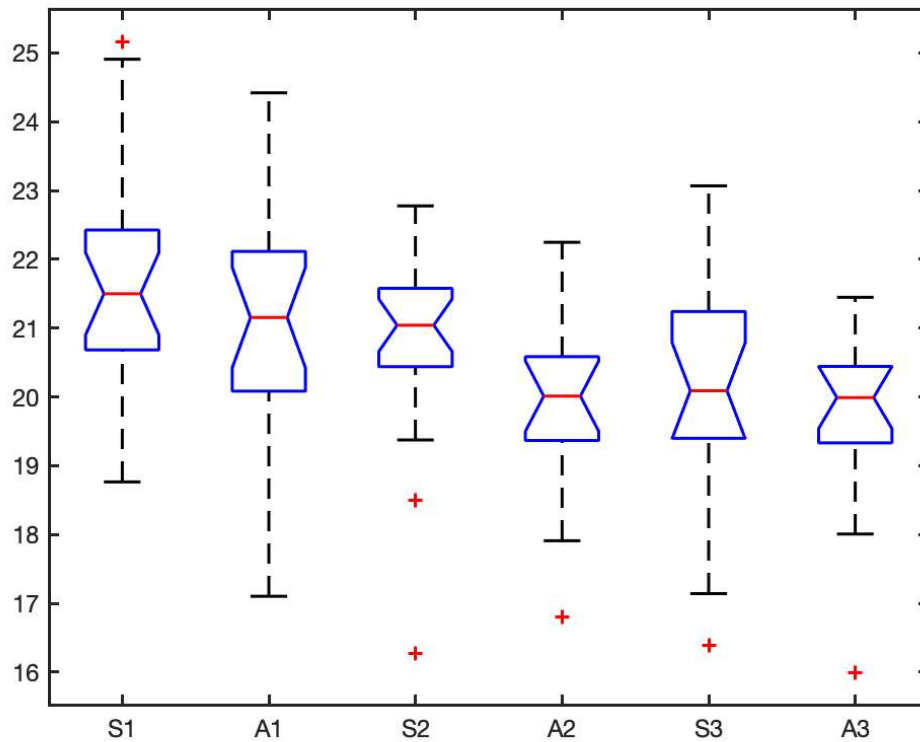


Figure 45: Box Plot of six stimuli on TP9 electrode (EEGLAB Method).

ANOVA Table					
Source	SS	df	MS	F	Prob>F
Groups	51.985	5	10.397	4.07	0.0021
Error	260.704	102	2.5559		
Total	312.689	107			

Figure 46: Standard ANOVA Table on TP9 electrode (EEGLAB Method).

Figure 47 shows the box plot of six stimuli proposed to volunteers recorded from TP10 electrode using EEGLAB method. Figure 48 shows the classical ANOVA Table parameters.

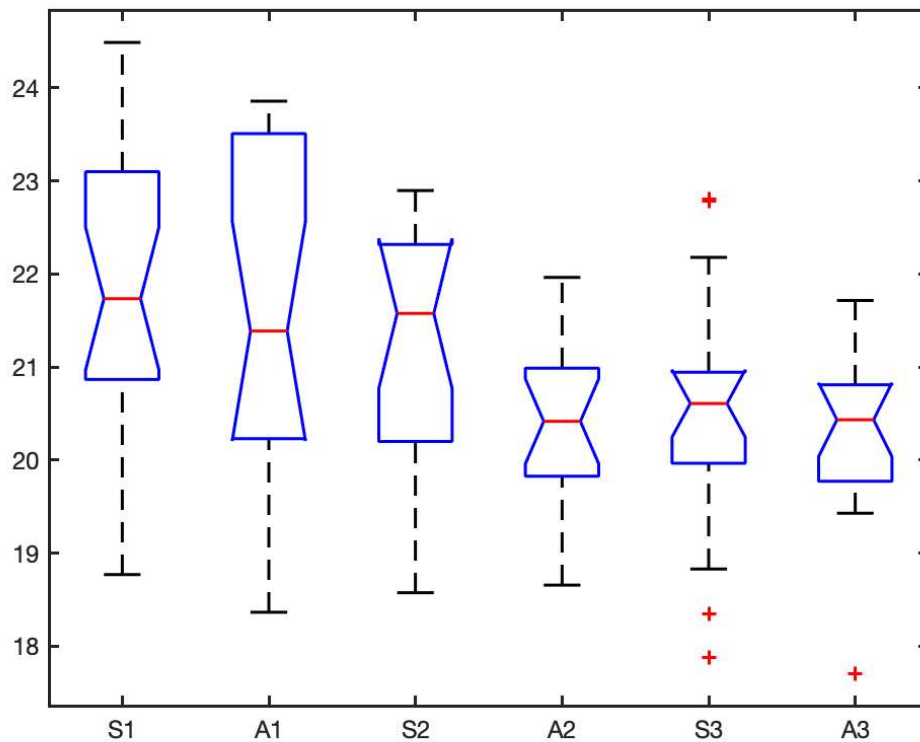


Figure 47: Box Plot of six stimuli on TP10 electrode (EEGLAB Method).

ANOVA Table					
Source	SS	df	MS	F	Prob>F
Groups	42.188	5	8.43757	4.4	0.0011
Error	195.699	102	1.91862		
Total	237.887	107			

Figure 48: Standard ANOVA Table on TP10 electrode (EEGLAB Method).

Figure 49 illustrate the box plot of six stimuli proposed to subjects recorded from TP9 electrode using AUTOREJECT method. Figure 50 exhibit the classical ANOVA Table parameters.

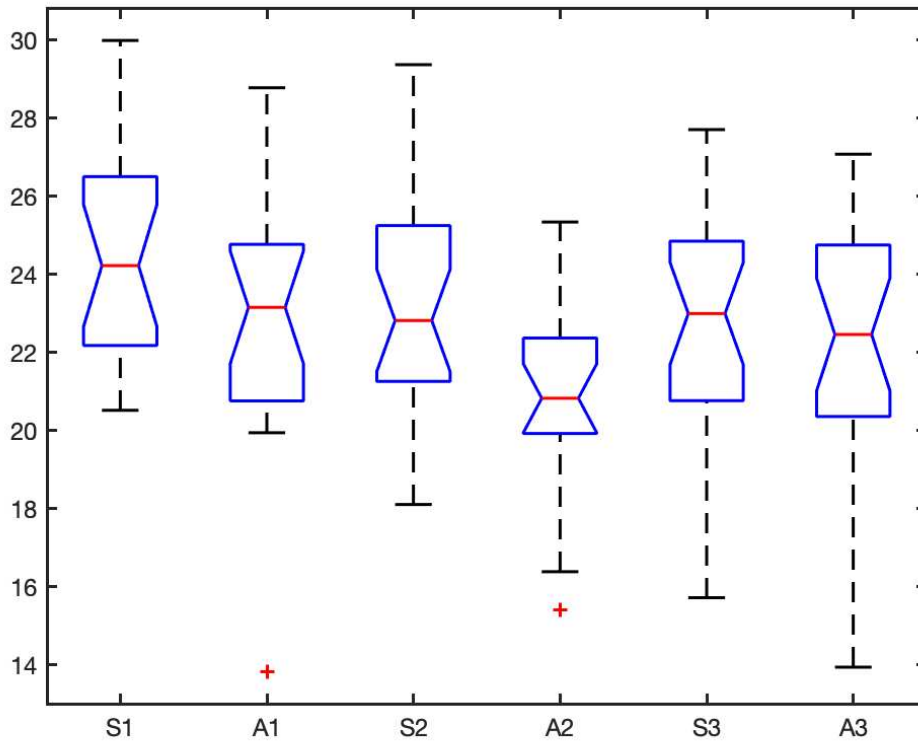


Figure 49: Box Plot of six stimuli on TP9 electrode (AUTOREJECT Method).

ANOVA Table					
Source	SS	df	MS	F	Prob>F
Groups	138.51	5	27.7026	2.91	0.0163
Error	1153.49	121	9.533		
Total	1292	126			

Figure 50: Standard ANOVA Table on TP9 electrode (AUTOREJECT Method).

Figure 51 shows the box plot of six stimuli proposed to volunteers recorded from TP10 electrode using AUTOREJECT method. Figure 52 explains the classical ANOVA Table parameters.

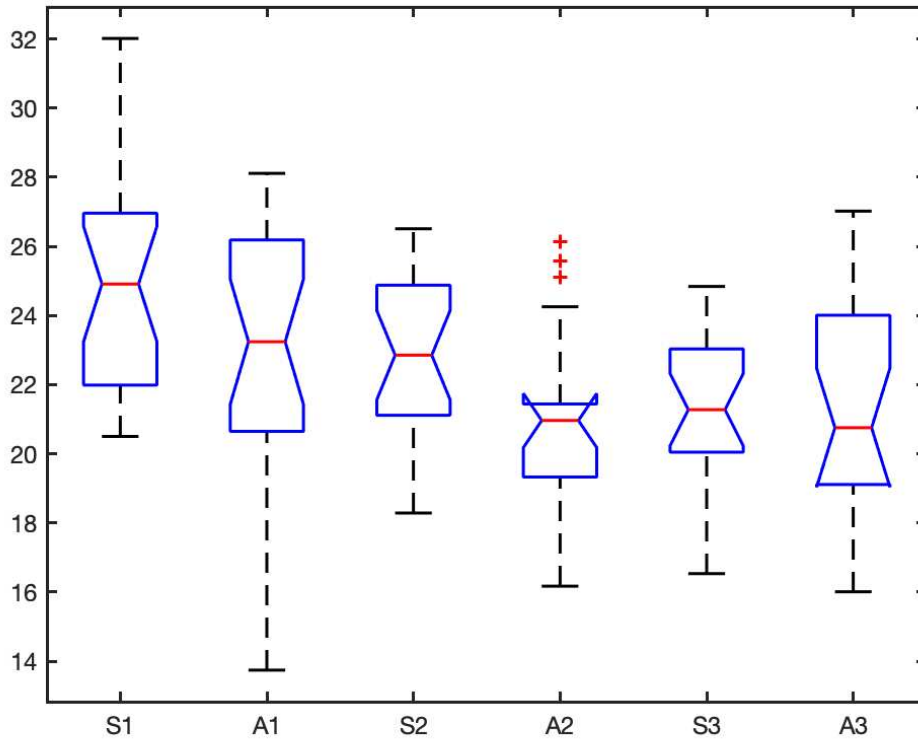


Figure 51: Box Plot of six stimuli on TP10 electrode (AUTOREJECT Method).

ANOVA Table					
Source	SS	df	MS	F	Prob>F
Groups	246.85	5	49.3693	5.76	8.641e-05
Error	1012.14	118	8.5775		
Total	1258.99	123			

Figure 52: Standard ANOVA Table on TP10 electrode (AUTOREJECT Method).

3.3.2. Alpha Frequency Band

Figure 53 displays the box plot illustrating the six stimuli presented to volunteers only in the Alpha Band, recorded specifically from the TP9 electrode using the EEGLAB method. On the other hand, Figure 54 presents the classical ANOVA Table parameters.

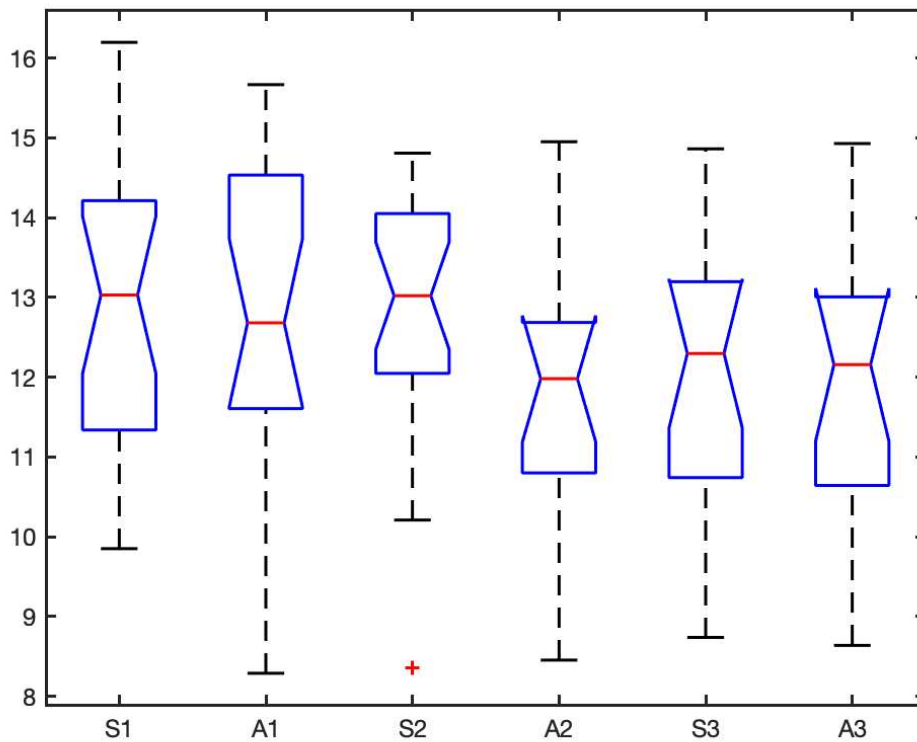


Figure 53: Box Plot of six stimuli on TP9 electrode Alpha Band (EEGLAB Method).

ANOVA Table					
Source	SS	df	MS	F	Prob>F
Groups	22.425	5	4.4849	1.44	0.2155
Error	317.137	102	3.10918		
Total	339.561	107			

Figure 54: Standard ANOVA Table on TP9 electrode Alpha Band (EEGLAB Method).

Figure 55 depicts a box plot representing six stimuli that were presented to volunteers. The data was recorded from the TP10 electrode only for Alpha frequency band using the EEGLAB method. Additionally, Figure 56 displays the classical ANOVA Table parameters.

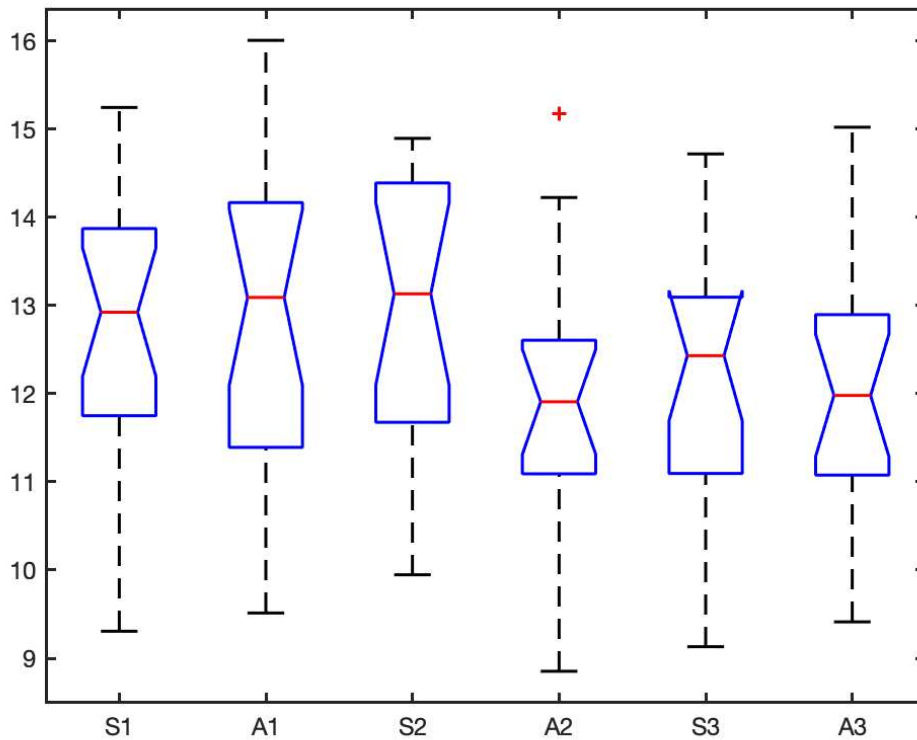


Figure 55: Box Plot of six stimuli on TP10 electrode Alpha Band (EEGLAB Method).

ANOVA Table					
Source	SS	df	MS	F	Prob>F
Groups	18.506	5	3.70129	1.46	0.2109
Error	259.332	102	2.54247		
Total	277.839	107			

Figure 56: Standard ANOVA Table on TP10 electrode Alpha Band (EEGLAB Method).

Figure 57 illustrate the box plot of six stimuli proposed to subjects recorded from TP9 electrode using AUTOREJECT method. Figure 58 exhibit the classical ANOVA Table parameters. Both graphs represent only frequencies included in Alpha range.

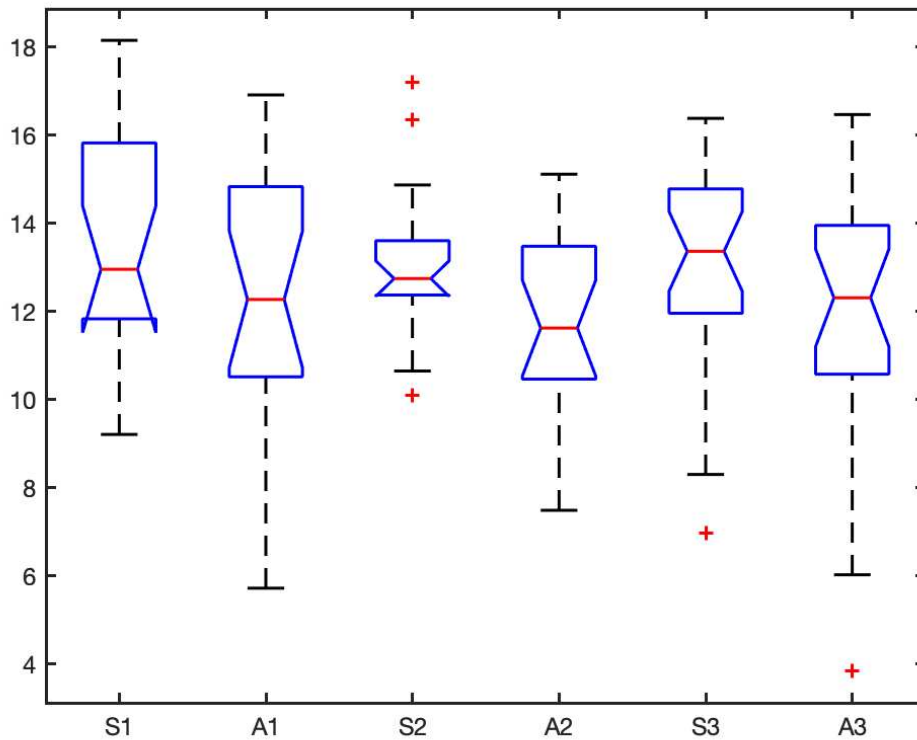


Figure 57: Box Plot of six stimuli on TP9 electrode Alpha Band (AUTOREJECT Method).

ANOVA Table					
Source	SS	df	MS	F	Prob>F
Groups	47.144	5	9.42886	1.58	0.1697
Error	720.447	121	5.95411		
Total	767.592	126			

Figure 58: Standard ANOVA Table on TP9 electrode Alpha Band (AUTOREJECT Method).

Figure 59 shows the box plot of six stimuli listened from subjects and recorded from TP10 electrode using AUTOREJECT method. Figure 60 explains the classical ANOVA Table parameters. All data represent only the contents on 8-13 Hz frequency range.

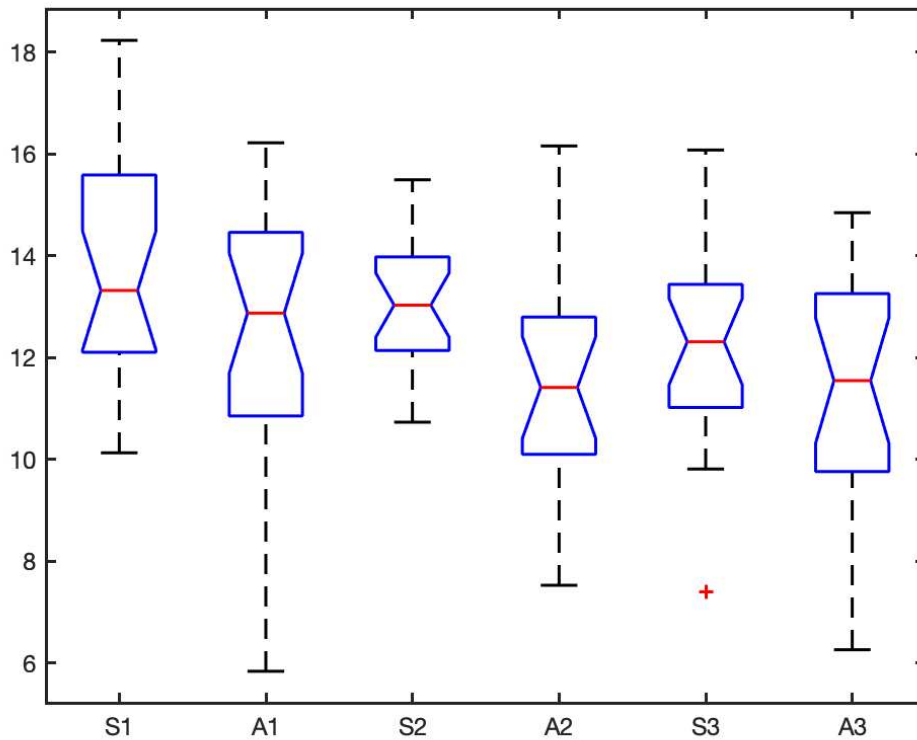


Figure 59: Box Plot of six stimuli on TP10 electrode Alpha Band (AUTOREJECT Method).

ANOVA Table					
Source	SS	df	MS	F	Prob>F
Groups	61.684	5	12.3369	2.43	0.0388
Error	598.406	118	5.0712		
Total	660.09	123			

Figure 60: Standard ANOVA Table on TP10 electrode Alpha Band (AUTOREJECT Method).

3.3.3. Relative Alpha Frequency Band

In this chapter, results about the Relative Alpha Power, calculated as illustrated in chapter 1.3.4, will be shown. Figure 61 displays the box plot illustrating the six stimuli presented to volunteers only in the Relative Alpha Band, recorded specifically from the TP9 electrode using the EEGLAB method. On the other hand, Figure 62 presents the classical ANOVA Table parameters.

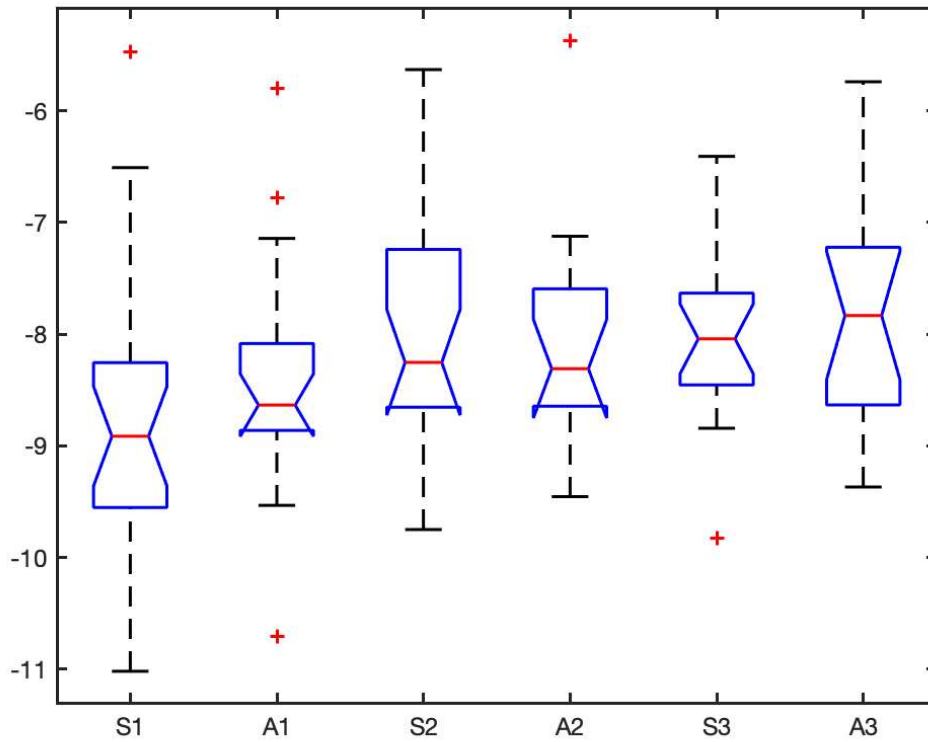


Figure 61: Box Plot of six stimuli on TP9 electrode Relative Alpha Band (EEGLAB Method).

ANOVA Table					
Source	SS	df	MS	F	Prob>F
Groups	9.365	5	1.87307	1.66	0.1518
Error	115.301	102	1.1304		
Total	124.666	107			

Figure 62: Standard ANOVA Table on TP9 electrode Relative Alpha Band (EEGLAB Method).

Figure 63 depicts a box plot representing six stimuli that were presented to volunteers. The data was recorded from the TP10 electrode only for the normalized alpha frequency band using the EEGLAB method. Additionally, Figure 64 displays the classical ANOVA Table parameters.

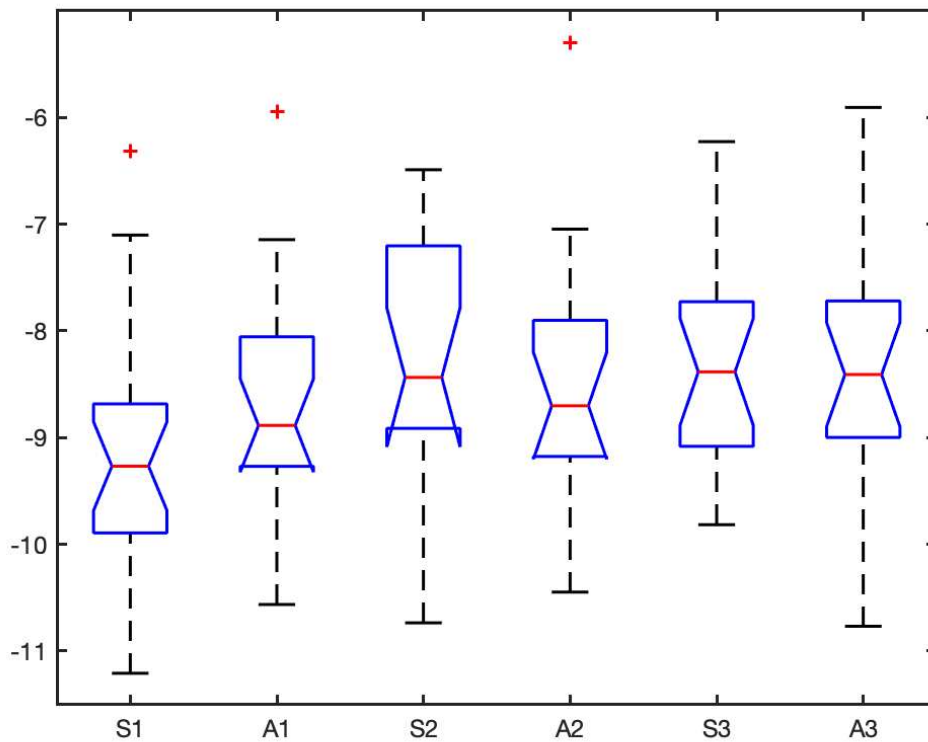


Figure 63: Box Plot of six stimuli on TP10 electrode Relative Alpha Band (EEGLAB Method).

ANOVA Table					
Source	SS	df	MS	F	Prob>F
Groups	10.932	5	2.1864	1.58	0.1733
Error	141.452	102	1.38678		
Total	152.384	107			

Figure 64: Standard ANOVA Table on TP10 electrode Relative Alpha Band (EEGLAB Method).

Figure 65 illustrate the box plot of six stimuli proposed to subjects recorded from TP9 electrode using AUTOREJECT method. Figure 66 exhibit the classical ANOVA Table parameters. Both graphs represent only frequencies included in Alpha range.

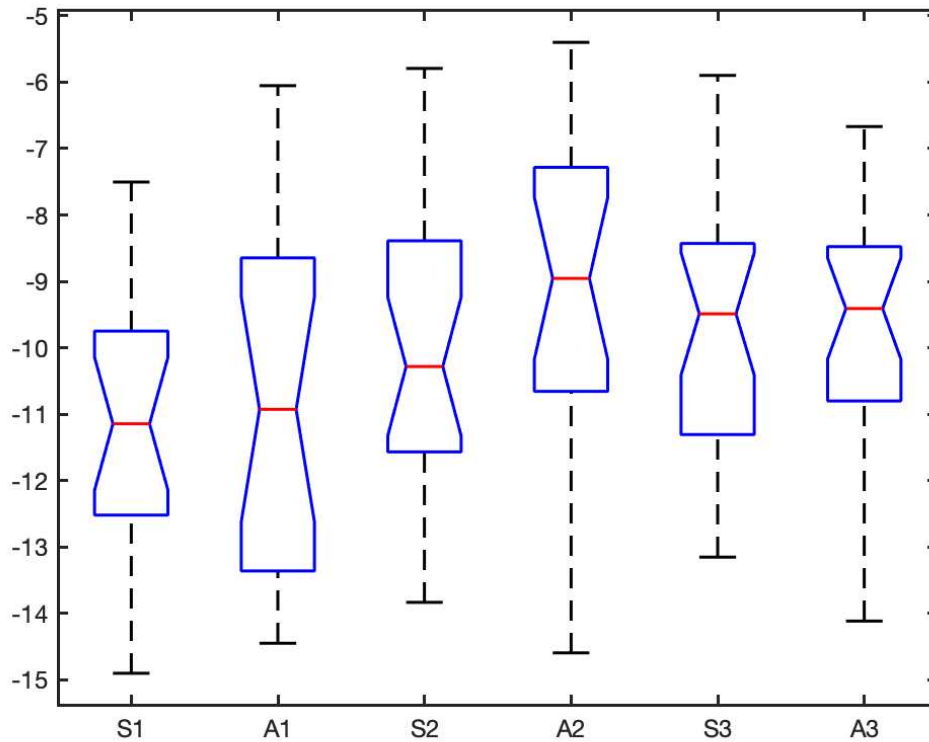


Figure 65: Box Plot of six stimuli on TP9 electrode Relative Alpha Band (AUTOREJECT Method).

ANOVA Table					
Source	SS	df	MS	F	Prob>F
Groups	46.083	5	9.21664	2.01	0.0813
Error	553.58	121	4.57504		
Total	599.663	126			

Figure 66: Standard ANOVA Table on TP9 electrode Relative Alpha Band (AUTOREJECT Method).

Figure 67 shows the box plot of six stimuli listened from subjects and recorded from TP10 electrode using AUTOREJECT method. Figure 68 explains the classical ANOVA Table parameters. All data represent only the contents on 8-13 Hz frequency range.

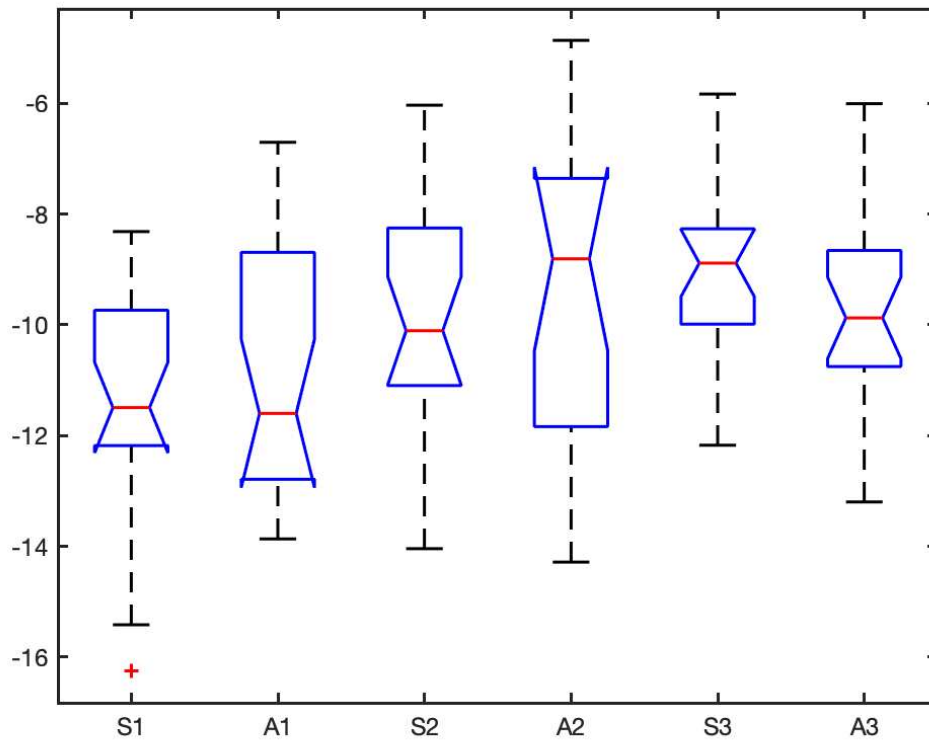


Figure 67: Box Plot of six stimuli on TP10 electrode Relative Alpha Band (AUTOREJECT Method).

ANOVA Table					
Source	SS	df	MS	F	Prob>F
Groups	84.725	5	16.9451	3.89	0.0027
Error	513.764	118	4.3539		
Total	598.49	123			

Figure 68: Standard ANOVA Table on TP10 electrode Relative Alpha Band (AUTOREJECT Method).

4. CONCLUSIONS AND FUTURE DEVELOPMENTS

In this work we have focused our attention on developing a procedure for sound quality evaluation comparing two methodologies which are the EEGLAB method used on MATLAB and the AUTOREJECT algorithm first used in Python for pre-processing and then also on MATLAB for post-processing. A study involving forty-three participants (22 males, 21 females) was conducted in order to collect EEG data while exposing them to three different acoustic stimulation of luxury car engine, classical music and noisy road. The test took place at “Università Politecnica delle Marche” of Industrial Engineering and Mathematical Science Department and a total of 258 datasets were recorded.

After an initial pre-processing phase in which the raw data were filtered in a band ranging from 0.2 to 47 hertz and a removal of electrical noise by means of a notch filter, an initial difference in the two methods could begin to be seen. In fact, EEGLAB set with the parameters discussed above (thresholds for bad channel removal and bad data removal to 25 and 11, respectively) results in the removal of 6 of the total 43 subjects, stands for a reduction of the total datasets from 258 to 222 (13.95%). This elimination was done because it was decided that even if 1 of the 6 datasets for each volunteer was defective, i.e., did not have at least one of the two TP9-TP10 temporal channels, it should be discarded. On the other hand, the approach in which we used AUTOREJECT set up as described in the corresponding chapter allowed us to proceed with the analysis of EEG signals with the totality of subjects and thus datasets (100%). All the data were converted into a power spectral density and managed in dB scale.

In our study, the subsequent step in order to try to understand which of the two methods prosed are the best involved identifying and removing outlier signals, which are data points that exhibit significant deviations from the overall pattern or behaviour observed in the dataset. So that, we decided to use the MATLAB function *'rmoutliers.m'*.

Results in Table 4 shows that EEGLAB method excludes 228 out of the total 444 power spectral densities (PSDs), which accounts for 51.35% of the dataset. On the other hand, the AUTOREJECT algorithm eliminates 265 out of the total 516 power spectral densities,

representing 51.36% of the dataset. This first result does not give us a very good indication of which of the two methods is better since the rejection rate of the 'rmoutliers.m' function is almost identical. It should be noted, however, that AUTOREJECT started with more initial data, so after the removal of the outliers it certainly finds itself with more data to handle.

After this phase, a test was conducted to verify that our data were distributed normally. In particular, the Shapiro-Wilk test was used to obtain this kind of information. In general, both methods yielded good results. AUTOREJECT showed to have 85.22% of the data normally distributed compared with the EEGLAB method, which showed 92.65% Gaussian data. The same type of test was then conducted only on the alpha frequency range, this being, in agreement with the literature, the frequency range most sensitive to acoustic stimuli. This study again resulted in a better percentage for EEGLAB method, which is seen to have 94.70% Gaussian data as opposed to 90.91% for AUTOREJECT. Thus, this phase shows us that both methods are robust for the determination of Gaussianity of the data, with a slight advantage for the EEGLAB approach.

The last step conducted in this thesis was a statistical analysis. Especially, because the data are normally distributed, it was possible to perform One-Way ANOVA, a parametric statistical test. We focused on two specific values in the ANOVA Table: F-statistic and p-value. The F-statistic is the ratio of the mean squares' treatment to the mean squares error, in other words a ratio between variation between sample means and variation within samples. So, larger the F-statistic, the greater the variation between sample means relative to the variation within the samples. Additionally, the larger the F-statistic, the greater the evidence that there is a difference between the group means. Results reported on ANOVA Tables reported on results (3.3) prove how data processed with the two approach for TP9-TP10 channels have a relatively high F-statistic, standing for a gap between the groups means (4.29 ± 1.17).

An absolute difference can be found in the analysis of alpha frequencies. In fact, the F-statistic values decrease, standing for little statistical difference between the averages of the groups examined (1.73 ± 0.47). In particular, the only value that would deviate slightly would be that concerning the TP10 channel with the AUTOREJECT method as it assumes an F-statistic value of 2.43 and simultaneously an alpha value close to 0.05 while the others are clearly above this alpha value. For what concern p-value, if it is less than $\alpha = 0.05$, we reject the null hypothesis of the ANOVA and conclude that there is a statistically

significant difference between the means of the three groups. Otherwise, if the p-value is not less than $\alpha = 0.05$ then we fail to reject the null hypothesis and conclude that we do not have sufficient evidence to say that there is a statistically significant difference between the means of the three groups. To go into details, results reported on the ANOVA tables are consistent. Indeed, considering the whole frequency range both EEGLAB and AUTOREJECT behave the same way, with p-values much less than 0.05 ($4.9e-3 \pm 7.6e-3$). In this way we reject the null hypothesis of the ANOVA and conclude that there is a statistically significant difference between the means of the three groups. Instead, in the alpha frequency range we can see a change in trend, with alpha values much greater than 0.05, which thus leads us to say that the variance of the averages between the 3 silences and the 3 proposed audios is not so pronounced (0.16 ± 0.08). As mentioned earlier, in this frequency range, the only data that deviates from the others is that concerning the TP10 electrode examined by the AUTOREJECT method. In fact, the value of this channel is the only one to remain below the threshold of 0.05, in particular it takes the value of $3.9e-2$. So that we could best characterize the responses to the different stimuli proposed to our volunteers, we decided to go even deeper by conducting another ANOVA test but this time in the Relative Alpha Band, calculated as the energy in the alpha band divided by the total energy. What we expected was to see different reactions for A1 being a stimulus that could both like and dislike. Therefore, we gave little weight to the data obtained for this stimulus. Differently, having proposed a classical song as the second stimulus and noisy road as the third, we expected greater activation of alpha power at the second stimulus than at the third. Therefore, we believe that the results shown in Figure 65 and Figure 67 are excellent in this aspect. In fact, the values obtained by the AUTOREJECT method on the mean of A2 is clearly greater than the mean obtained for A3, with the values of S3 that can be interpreted as an intermediate between the differentiation of the two sounds heard. Another validation of this assumption can be found in the F-statistic and alpha values between the two approaches used. In particular, it is possible to point out that the values obtained in Relative Alpha Band Power with the AUTOREJECT (F-statistic = 2.95 ± 1.33 , $\alpha = 0.042 \pm 0.056$) method reflect a greater characterization of the proposed stimuli than the values analyzed with the EEGLAB method (F-statistic = 1.62 ± 0.06 , $\alpha = 0.16 \pm 0.02$).

Obviously, this thesis was only a preliminary study. In fact, many limitations were found throughout and more may be done in the future. Some of the difficulties experienced were:

- **Data Integrity:** The presence of ocular and muscular artifacts is the probable cause for the unfavorable outcomes observed. Particularly in EEG recordings, it is advisable to employ advanced equipment featuring an increased number of channels, higher sample rate, and low-impedance electrodes. This approach aims to capture data with a higher signal-to-noise ratio (SNR).
- **Data Quantity:** Having only 43 subjects certainly limited the study and data analysis. Conducting studies with as many subjects as possible, and thus with the possibility of discarding more data that would be outdated, would certainly lead to more precise and accurate conclusions.
- **Devices:** To facilitate effective independent component analysis (ICA) for blind source separation and reliable artifact removal, a greater number of channels is necessary. Consideration should also be given to utilizing manual epoch rejection instead of relying solely on automatic rejection algorithms, as it can yield more precise and accurate results. Implementing the use of better performing headphones could also lead to better results by having to study physiological responses to acoustic stimuli.
- **Data Integration:** Combining EEG data with other kinds of data that can detect for example heart rate, muscle stimuli or attention level could definitely improve the results by making them more reliable.
- **Auditory Stimuli:** To enhance the ability to manipulate individual psychoacoustic parameters, it could prove beneficial to decrease the complexity and variability of the stimuli under examination. One potential approach is to replace real-world sounds with varying degrees of sharpness with white noise. This would allow for a more controlled experimentation environment and enable targeted investigation of specific psychoacoustic factors.

In conclusion, we can say that due to the three analyses conducted in this thesis, the EEGLAB method and the AUTOREJECT method are very similar in terms of outliers

removal and normality analysis of the data. While with regard to the ANOVA statistical test, nothing statistically significant could be stated in the characterization between one sound and another. Differently, we noticed how the AUTOREJECT method seems to perform better in the range of relative alpha power than the EEGLAB approach.

FIGURE LIST

Figure 1: Graphic representations of a sound wave: (A) air at equilibrium, in the absence of a sound wave; (B) compressions and rarefactions that constitute a sound wave; and (C) transverse representation of the wave, showing amplitude (A) and wavelength (λ) [3].	6
Figure 2: Structure of the brain [18].	13
Figure 3: Typical structure of a neuron cell [19].	15
Figure 4: Classification of neurons [22].	16
Figure 5: Structure of the auditory system [25].	19
Figure 6: Origin of EEG Signal [29].	22
Figure 7: Brodmann Areas: The auditory cortex is highlighted in pink and interacts with the other areas highlighted [29].	23
Figure 8: EEG signals processing steps [31].	24
Figure 9: Hans Berger achieved the first-ever recording of human electroencephalography (EEG) in 1924. In his ground-breaking experiment, Berger captured the upper signal representing EEG activity, while the lower signal served as a 10 Hz timing reference [35].	26
Figure 10: Characteristic PSD of EEG Signals. Data taken from our study. The plots show the averaged PSD across all subject measured both for TP9-TP10 electrodes.	34
Figure 11: The 2016 Muse EEG system made by InterAxon Inc [40].	36
Figure 12: Top-down view of the 10-20 system EEG electrode positions on the subject's head [41].	37
Figure 13: Experimental setup of a volunteer during a test.	39
Figure 14: GUI window in EEGLAB Toolbox that allow to import .CSV file recorded with Muse Headband Device.	43
Figure 15: pop_musemonitor function parameter adjustment.	44
Figure 16: Structure representing all dataset cleaned and loaded on MATLAB after the first two steps of pre-processing phase.	45
Figure 17: Example of structure fields of audio 3 of volunteer number 42.	46
Figure 18: Script devoted to dataset filtration.	47
Figure 19: Example of signals repaired with Autoreject Method [51].	48
Figure 20: Autoreject algorithm used to clean, remove and repair the raw data.	50

Figure 21: MATLAB code for PSD calculation.	51
Figure 22: Script section in which the outliers were removed.	52
Figure 23: Statistical Shapiro-Wilk Test performed on TP9 and TP10 electrodes.	53
Figure 24: Standard ANOVA Table [54].	57
Figure 25: PSD expressed in dB of Silence 2 (S2) before Outliers Removal (EEGLAB method).	60
Figure 26: PSD expressed in dB of Silence 2 (S2) after Outliers Removal (EEGLAB method).	61
Figure 27: Mean PSD expressed in dB of all stimuli before Outliers Removal (EEGLAB method).	62
Figure 28: Mean PSD expressed in dB of all stimuli after Outliers Removal (EEGLAB method).	62
Figure 29: Mean PSD expressed in Linear Scale of all stimuli before Outliers Removal (EEGLAB method).	63
Figure 30: Mean PSD expressed in Linear Scale of all stimuli after Outliers Removal (EEGLAB method).	64
Figure 31: PSD expressed in dB of Audio 3 (A3) before Outliers Removal (AUTOREJECT method.)	65
Figure 32: PSD expressed in dB of Audio 3 (A3) after Outliers Removal (AUTOREJECT method).	65
Figure 33: Mean PSD expressed in dB of all stimuli before Outliers Removal (AUTOREJECT method).	66
Figure 34: Mean PSD expressed in dB of all stimuli after Outliers Removal (AUTOREJECT method).	67
Figure 35: Mean PSD expressed in Linear Scale of all stimuli before Outliers Removal (AUTOREJECT method).	68
Figure 36: Mean PSD expressed in Linear Scale of all stimuli after Outliers Removal (AUTOREJECT method).	68
Figure 37: Mean PSD of the six stimuli with Gaussian Spectral Line (red lines) of TP9 channel (EEGLAB method.)	70
Figure 38: Mean PSD of the six stimuli with Gaussian Spectral Line (red lines) of TP10 channel (EEGLAB method).	71

Figure 39: Mean PSD of the six stimuli with Gaussian Spectral Line (red lines) of TP9 channel (AUTOREJECT method).	72
Figure 40: Mean PSD of the six stimuli with Gaussian Spectral Line (red lines) of TP10 channel (AUTOREJECT method).	73
Figure 41: Mean PSD of the six stimuli with Gaussian Spectral Line (red lines) of TP9 channel on Alpha Band (EEGLAB method.).....	75
Figure 42: Mean PSD of the six stimuli with Gaussian Spectral Line (red lines) of TP10 channel on Alpha Band (EEGLAB method).....	75
Figure 43: Mean PSD of the six stimuli with Gaussian Spectral Line (red lines) of TP9 channel on Alpha Band (AUTOREJECT method).	76
Figure 44: Mean PSD of the six stimuli with Gaussian Spectral Line (red lines) of TP10 channel on Alpha Band (AUTOREJECT method).	77
Figure 45: Box Plot of six stimuli on TP9 electrode (EEGLAB Method).....	78
Figure 46: Standard ANOVA Table on TP9 electrode (EEGLAB Method).	78
Figure 47: Box Plot of six stimuli on TP10 electrode (EEGLAB Method).....	79
Figure 48: Standard ANOVA Table on TP10 electrode (EEGLAB Method).	79
Figure 49: Box Plot of six stimuli on TP9 electrode (AUTOREJECT Method).	80
Figure 50: Standard ANOVA Table on TP9 electrode (AUTOREJECT Method).....	80
Figure 51: Box Plot of six stimuli on TP10 electrode (AUTOREJECT Method).	81
Figure 52: Standard ANOVA Table on TP10 electrode (AUTOREJECT Method).....	81
Figure 53: Box Plot of six stimuli on TP9 electrode Alpha Band (EEGLAB Method)..	82
Figure 54: Standard ANOVA Table on TP9 electrode Alpha Band (EEGLAB Method).	82
Figure 55: Box Plot of six stimuli on TP10 electrode Alpha Band (EEGLAB Method).	83
Figure 56: Standard ANOVA Table on TP10 electrode Alpha Band (EEGLAB Method).....	83
Figure 57: Box Plot of six stimuli on TP9 electrode Alpha Band (AUTOREJECT Method).	84
Figure 58: Standard ANOVA Table on TP9 electrode Alpha Band (AUTOREJECT Method).	84
Figure 59: Box Plot of six stimuli on TP10 electrode Alpha Band (AUTOREJECT Method).....	85

Figure 60: Standard ANOVA Table on TP10 electrode Alpha Band (AUTOREJECT Method).....	85
Figure 61: Box Plot of six stimuli on TP9 electrode Relative Alpha Band (EEGLAB Method).....	86
Figure 62: Standard ANOVA Table on TP9 electrode Relative Alpha Band (EEGLAB Method).....	86
Figure 63: Box Plot of six stimuli on TP10 electrode Relative Alpha Band (EEGLAB Method).....	87
Figure 64: Standard ANOVA Table on TP10 electrode Relative Alpha Band (EEGLAB Method).....	87
Figure 65: Box Plot of six stimuli on TP9 electrode Relative Alpha Band (AUTOREJECT Method).	88
Figure 66: Standard ANOVA Table on TP9 electrode Relative Alpha Band (AUTOREJECT Method).	88
Figure 67: Box Plot of six stimuli on TP10 electrode Relative Alpha Band (AUTOREJECT Method).	89
Figure 68: Standard ANOVA Table on TP10 electrode Relative Alpha Band (AUTOREJECT Method).	89

TABLE LIST

Table 1: EEG frequency bands.....	32
Table 2: Columns definition of ANOVA Table.....	57
Table 3: Row definition of ANOVA Table.....	58
Table 4: Number of subjects (datasets) remained after the outliers remotion. Left part concerns the EEGLAB method while right part refers to AUTOREJECT's algorithm.	59
Table 5: Number of Gaussian Spectral Lines of data.....	69
Table 6: Number of Gaussian Spectral Lines of data on Alpha Frequency Range.....	74

BIBLIOGRAPHY

- [1] “<https://hub.salford.ac.uk/sirc-acoustics/psychoacoustics/sound-quality-making-products-sound-better/an-introduction-to-sound-quality-testing/defining-sound-quality/>.”
- [2] “Fundamentals of Telephone Communication Systems,” Western Electrical Company, 1969.
- [3] Richard E. Berg, “<https://www.britannica.com/science/sound-physics>,” *Britannica*. 2023.
- [4] “<https://pages.jh.edu/virtlab/ray/acoustic.htm>.”
- [5] “<https://en.wikipedia.org/wiki/Sound>.”
- [6] G. Pulvirenti, N. Totaro, and E. Parizet, “A perceptual evaluation of numerical errors in acoustic FEM simulation for sound quality applications,” *Applied Acoustics*, vol. 207, p. 109295, May 2023, doi: 10.1016/j.apacoust.2023.109295.
- [7] I. B. Mauss and M. D. Robinson, “Measures of emotion: A review,” *Cogn Emot*, vol. 23, no. 2, pp. 209–237, Feb. 2009, doi: 10.1080/02699930802204677.
- [8] S. Denjean, V. Roussarie, R. Kronland-Martinet, S. Ystad, and J.-L. Velay, “How does interior car noise alter driver’s perception of motion? Multisensory integration in speed perception,” *Acoustics 2012*. Nantes, France, 2012.
- [9] R. WESTERMANN, K. SPIES, G. STAHL, and F. W. HESSE, “Relative effectiveness and validity of mood induction procedures: a meta-analysis,” *Eur J Soc Psychol*, vol. 26, no. 4, pp. 557–580, Jul. 1996, doi: 10.1002/(SICI)1099-0992(199607)26:4<557::AID-EJSP769>3.0.CO;2-4.
- [10] J. I. Alpert and M. I. Alpert, “Music influences on mood and purchase intentions,” *Psychol Mark*, vol. 7, no. 2, pp. 109–133, 1990, doi: 10.1002/mar.4220070204.
- [11] G. C. B. II, “Music, Mood, and Marketing,” *J Mark*, vol. 54, no. 4, p. 94, Oct. 1990, doi: 10.2307/1251762.
- [12] “Burden of disease from environmental noise: quantification of healthy life years lost in Europe,” *World Health Organization*. 2011.
- [13] J. Blauert and U. Jekosch, “Sound-quality evaluation - a multi-layered problem,” *Acustica*, vol. 83, pp. 747–753, 1997.
- [14] Y. Huang and Q. Zheng, “Sound quality modelling of hairdryer noise,” *Applied Acoustics*, vol. 197, p. 108904, Aug. 2022, doi: 10.1016/j.apacoust.2022.108904.

- [15] K. A. Maldonado and K. Alsayouri, “Physiology, Brain,” *StatPearls*. StatPearls Publishing.
- [16] “<https://mayfieldclinic.com/pe-anatbrain.htm>.”
- [17] V. Straticiu, I. E. Nicolae, R. Strungaru, T. M. Vasile, O. A. Bajenaru, and G. M. Ungureanu, “A preliminary study on the effects of music on human brainwaves,” in *2016 8th International Conference on Electronics, Computers and Artificial Intelligence (ECAI)*, IEEE, Jun. 2016, pp. 1–4. doi: 10.1109/ECAI.2016.7861196.
- [18] “<https://www.atlantabrainandspine.com/brain-anatomy/>.”
- [19] “<https://owlcation.com/stem/Structure-of-a-Neuron>.”
- [20] P. E. Ludwig, V. Reddy, and M. Varacallo, “Neuroanatomy, Neurons,” *StatPearls*. StatPearls Publishing, 2022.
- [21] “<https://www.ninds.nih.gov/health-information/public-education/brain-basics/brain-basics-life-and-death-neuron>.”
- [22] “<https://www.vedantu.com/question-answer/name-different-types-of-neurons-and-give-one-class-12-biology-cbse-5f8377fea6aa52304a65a35d>.”
- [23] D. C. Peterson, V. Reddy, and R. N. Hamel, *Neuroanatomy, Auditory Pathway*. 2023.
- [24] “https://en.wikipedia.org/wiki/Auditory_system.”
- [25] “<https://www.svtaudiology.com/the-auditory-system>.”
- [26] Purves Dale, Augustine George J, and Fitzpatrick David, Eds., *Neuroscience, 2nd edition*.
- [27] J. P. Rauschecker, “Early Auditory Processing,” in *Brain Mapping*, Elsevier, 2015, pp. 537–542. doi: 10.1016/B978-0-12-397025-1.00042-7.
- [28] I. Velasco, A. Sipols, C. S. De Blas, L. Pastor, and S. Bayona, “Motor imagery EEG signal classification with a multivariate time series approach,” *Biomed Eng Online*, vol. 22, no. 1, p. 29, Mar. 2023, doi: 10.1186/s12938-023-01079-x.
- [29] J. Egeler, “Physiological correlates of psychoacoustic annoyance, a deep learning approach,” Technische Hochschule Ingolstadt, Ingolstadt, 2021.
- [30] Y. Tran, “EEG Signal Processing for Biomedical Applications,” *Sensors*, vol. 22, no. 24, p. 9754, Dec. 2022, doi: 10.3390/s22249754.
- [31] “<https://www.neuroelectrics.com/blog/2014/12/18/eeg-signal-processing-for-dummies/>.”

- [32] J. S. Kumar and P. Bhuvaneshwari, “Analysis of Electroencephalography (EEG) Signals and Its Categorization—A Study,” *Procedia Eng*, vol. 38, pp. 2525–2536, 2012, doi: 10.1016/j.proeng.2012.06.298.
- [33] “<https://www.emotiv.com/eeg-guide/>.”
- [34] J. W. Britton, L. C. Frey, and J. L. Hopp, *Electroencephalography (EEG): An Introductory Text and Atlas of Normal and Abnormal Findings in Adults, Children, and Infants*. Chicago: American Epilepsy Society, 2016.
- [35] “<https://brainclinics.com/history-of-the-eeg-and-qeeg/>.”
- [36] “<https://en.wikipedia.org/wiki/Electroencephalography>.”
- [37] M. Soufineyestani, D. Dowling, and A. Khan, “Electroencephalography (EEG) Technology Applications and Available Devices,” *Applied Sciences*, vol. 10, no. 21, p. 7453, Oct. 2020, doi: 10.3390/app10217453.
- [38] J. W. Y. Kam *et al.*, “Systematic comparison between a wireless EEG system with dry electrodes and a wired EEG system with wet electrodes,” *Neuroimage*, vol. 184, pp. 119–129, Jan. 2019, doi: 10.1016/j.neuroimage.2018.09.012.
- [39] H. Hinrichs, M. Scholz, A. K. Baum, J. W. Y. Kam, R. T. Knight, and H.-J. Heinze, “Comparison between a wireless dry electrode EEG system with a conventional wired wet electrode EEG system for clinical applications,” *Sci Rep*, vol. 10, no. 1, p. 5218, Mar. 2020, doi: 10.1038/s41598-020-62154-0.
- [40] “https://www.researchgate.net/figure/Muse-Headband-Sensors_fig3_329909772.”
- [41] N. Phutela, D. Relan, G. Gabrani, P. Kumaraguru, and M. Samuel, “Stress Classification Using Brain Signals Based on LSTM Network,” *Comput Intell Neurosci*, vol. 2022, pp. 1–13, Apr. 2022, doi: 10.1155/2022/7607592.
- [42] S. A. Mansi *et al.*, “Measuring human physiological indices for thermal comfort assessment through wearable devices: A review,” *Measurement*, vol. 183, p. 109872, Oct. 2021, doi: 10.1016/j.measurement.2021.109872.
- [43] E. S. Kappenman and S. J. Luck, “The effects of electrode impedance on data quality and statistical significance in ERP recordings,” *Psychophysiology*, Mar. 2010, doi: 10.1111/j.1469-8986.2010.01009.x.
- [44] X. Wang, D. Li, C. C. Menassa, and V. R. Kamat, “Investigating the effect of indoor thermal environment on occupants’ mental workload and task performance

- using electroencephalogram,” *Build Environ*, vol. 158, pp. 120–132, Jul. 2019, doi: 10.1016/j.buildenv.2019.05.012.
- [45] O. E. Krigolson, C. C. Williams, A. Norton, C. D. Hassall, and F. L. Colino, “Choosing MUSE: Validation of a Low-Cost, Portable EEG System for ERP Research,” *Front Neurosci*, vol. 11, Mar. 2017, doi: 10.3389/fnins.2017.00109.
- [46] A. E. Youssef, H. T. Ouda, and M. Azab, “MUSE: A Portable Cost-efficient Lie Detector,” in *2018 IEEE 9th Annual Information Technology, Electronics and Mobile Communication Conference (IEMCON)*, IEEE, Nov. 2018, pp. 242–246. doi: 10.1109/IEMCON.2018.8614795.
- [47] E. Ratti, S. Waninger, C. Berka, G. Ruffini, and A. Verma, “Comparison of Medical and Consumer Wireless EEG Systems for Use in Clinical Trials,” *Front Hum Neurosci*, vol. 11, Aug. 2017, doi: 10.3389/fnhum.2017.00398.
- [48] “<https://sccn.ucsd.edu/eeglab/index.php>.”
- [49] A. Delorme and J. A. Martin, “Automated Data Cleaning for the Muse EEG,” in *2021 IEEE International Conference on Bioinformatics and Biomedicine (BIBM)*, IEEE, Dec. 2021, pp. 1–5. doi: 10.1109/BIBM52615.2021.9669415.
- [50] M. Jas, D. A. Engemann, Y. Bekhti, F. Raimondo, and A. Gramfort, “Autoreject: Automated artifact rejection for MEG and EEG data,” *Neuroimage*, vol. 159, pp. 417–429, Oct. 2017, doi: 10.1016/j.neuroimage.2017.06.030.
- [51] “<https://pypi.org/project/autoreject/>.”
- [52] M. Jas, D. Engemann, F. Raimondo, Y. Bekhti, and A. Gramfort, “Automated rejection and repair of bad trials in MEG/EEG,” in *2016 International Workshop on Pattern Recognition in Neuroimaging (PRNI)*, IEEE, Jun. 2016, pp. 1–4. doi: 10.1109/PRNI.2016.7552336.
- [53] C. Cannard, H. Wahbeh, and A. Delorme, “Electroencephalography Correlates of Well-Being Using a Low-Cost Wearable System,” *Front Hum Neurosci*, vol. 15, Dec. 2021, doi: 10.3389/fnhum.2021.745135.
- [54] “<https://it.mathworks.com/help/stats/one-way-anova.html>.”

APPENDIX 1

The information sheet and informed consent statement that have been given to the participants before the beginning of the survey procedure are reported hereafter.

INFORMATION SHEET

ECO DRIVE - Noise and vibration in eco-efficient powertrains

You have been invited to take part in a research project called “ECO DRIVE”. In order that you are able to take an informed decision as to whether to take part or not, it is important that you understand:

- (a) What the project is about;
- (b) Why the project is important;
- (c) What your participation would involve.

This Information Sheet is designed to explain these things.

Please read this Information Sheet carefully. If you have any questions about this document, the accompanying “Statement of Informed Consent” form, or the project in general, please ask **Milena Martarelli** (contact details below).

1. WHAT IS ECO DRIVE?

ECO DRIVE is a research project to develop new technologies for the testing and simulation of eco-powertrains. The project offers a multi-disciplinary research-training program to Early-Stage-Researchers, with the ultimate aim being to create a new generation of NVH professionals for the transport sector.

ECO DRIVE deals with the complex challenges related to combustion noise, the irritating sound from electric motors, transmission-induced NVH (Noise, Vibration and Harshness) and driveline torsional vibrations, leading to new designs with improved eco-efficiency and NVH performance.

More detailed info can be find also here (<http://www.ECO DRIVE.eu/>)

2. HOW YOU CAN HELP

You have been invited to contribute to ECO DRIVE. Your contribution to ECO DRIVE would involve psychoacoustical listening tests focusing on the acoustical behavior of different e-motors/downsized IC engines. The test involves the use of a headset to perform Electroencephalography (EEG) analysis. This headset will record the electrical activity of your brain during the psychoacoustical test. With the gathered Information, a new test-based method for an acoustic evaluation of e-motors/downsized IC engines designs by means of psychoacoustic metrics and rating algorithms will be developed. Moreover, the test involves also the use of a video camera storing a video of your face during the test. This video will be used to extrapolate the facial expression of the subject that can be correlated to the sensation related to the submitted audios.

3. WHAT ARE THE POSSIBLE BENEFITS AND DISADVANTAGES OF TAKING PART?

There are no costs apart from your time, and the cost for attending in the study. The listening test will be conducted at reasonable Loudness levels. Annoying sounds and noise can occur throughout the listening test. Please inform the study leader if you are wearing hearing aids, so the levels can be set to comfortable levels. The EEG headset will record the electrical activity of your brain through electrodes distributed on the headset, but there is no risk of pain nor electrical shock.

Unfortunately, it is not possible for us to compensate you for the time and effort involved. If you are a student, no advantages (grades etc.) will result from a participation in the study. No disadvantage will follow your decision to withdraw from the study.

4. CONFIDENTIALITY

During the psychoacoustic test you will be asked to listen to given sounds and provide rates and opinions based on specific questions raised on a computer. Sounds are being provided to you through over-ear headphones. In case EEG signals are recorded, you will be asked to wear an EEG headset. The research will take place in a dedicated room. A preliminary trial will be performed to make you comfortable in running the real test, which will be performed afterwards. Tests will not last more than 30 minutes, including your preparation, your test and your dismissal.

All data concerning your person will be stored separately from the collected data so that your anonymity is preserved. This also includes film recordings that are taken of you during the test. The data will only be accessible to the scientific staff involved in the project. It is planned to publish the data collected during the experiment in a doctoral thesis, a bachelor thesis and in articles in scientific journals. **You retain the right to withdraw yourself and your data from the study, at no disadvantage. You have the right to know what data is held concerning yourself, and have it rectified if necessary.**

5. IF YOU WOULD LIKE TO TAKE PART...

Please understand that participation is entirely voluntary: you are under no obligation whatsoever to take part in this study. No disadvantage or stigma will arise should you decide not to participate.

If, after consideration, you decide that you wish to take part in the study you will be asked to sign a "*Statement of Informed Consent*". This document records your agreement to take part, but it in no way obliges you to take part. You may decide not to take part at any time before or during your involvement with ECO DRIVE, even if you have signed the Statement of Informed Consent. **You always retain the right to withdraw from the study for any reason at all (or even for no reason at all).** You may be asked why you have decided to withdraw, but you are under no obligation to give a reason.

You should retain both this document and your copy of the Statement of Informed Consent for your records and information.

6. FURTHER INFORMATION

Thank you for taking the time to read this Information Sheet. If you have any questions about any aspect of the ECO DRIVE project, or your prospective involvement in it, please contact:

Prof. MILENA MARTARELLI

***Email:* m.martarelli@staff.univpm.it**

Telephone: 0039 071 22 0 4976

Address: Via Brezze Bianche 12, Ancona, 60100, ITALY

You may also contact **Milena Martarelli's** colleague:

Prof. PAOLO CASTELLINI

Email: p.castellini@staff.univpm.it

Telephone: 0039 071 22 0 4976

Address: Via Brezze Bianche 12, Ancona, 60100, ITALY

STATEMENT OF INFORMED CONSENT

Project Full Title: Noise and vibration in eco-efficient powertrains

Project Acronym: ECO DRIVE (<https://h2020-ecodrive.eu/>)

Contact: Milena Martarelli

Email: m.martarelli@staff.univpm.it

Telephone: 0039 071 22 0 4976

By signing this form, you agree to take part in the ECO DRIVE project. The nature of the project, your involvement in it, and your rights regarding your participation in the project, are explained in the Information Sheet accompany this form.

Before signing:

- Be aware that you are under no obligation whatsoever to sign this form or to take part in the project.
- Even if you do sign this form, you may withdraw yourself, and any data relating to you, from the project at any time, for any (or no) reason. You need give no explanation.
- If anything on this form, or on the accompanying Information Sheet, is unclear, ask **Prof. Milena Martarelli** for clarification.
- If you have questions which are not answered by this form or the accompanying Information Sheet, ask **Prof. Milena Martarelli**
- You may wish to take some time to consider whether to take part in the project. You are absolutely free to do so.

Please place an "X" in the boxes below to indicate agreement with the following statements (leave them blank if you do not agree).

- 1.) I confirm that I have read and understood both this form and the accompanying Information Sheet.
- 2.) I have had the opportunity to ask questions regarding (a) the nature of the project, (b) my potential involvement in it, and (c) this form and the accompanying Information Sheet.
- 3.) I understand that my participation in the project is entirely voluntary, and that I may withdraw from the project at any time for any (or no) reason.
- 4.) I understand and agree that the data gathered during my participation in the project may be used, stored, and shared in the ways described on the accompanying Information Sheet.

Participant Name
Signature
Date

Researcher Name
Signature
Date

Statement by the researcher/person taking consent

I have accurately provided the information sheet to the potential participant, and to the best of my ability made sure that the participant understands it.

I confirm that the participant was given an opportunity to ask questions about the research Project, and the research activity he/she will be involved in, and all the questions asked by the participant have been answered correctly and to the best of my ability. I confirm that the individual has not been coerced into giving consent, and the consent has been given freely and voluntarily.

A copy of this Informed consent form has been provided to the participant.

Print Name of Researcher/person taking the consent _____

Signature of Researcher /person taking the consent _____

Date _____

Day/month/year